2024-08-01

Zebra Limestone From The Gypsum Valley Salt Diapir, Colorado

Rebecca Navarrette
University of Texas at El Paso

ZEBRA LIMESTONE FROM THE GYPSUM VALLEY SALT DIAPIR, COLORADO

REBECCA D. NAVARRETTE

Master's Program in Geological Sciences

APPROVED:

Benjamin Brunner, Ph.D., Chair

Katherine Giles, Ph.D.

Antonio Arribas, Ph.D.

Evey Gannaway Dalton, Ph.D.

Stephen L. Crites, Jr., Ph.D.
Dean of the Graduate School

ZEBRA LIMESTONE FROM THE GYPSUM VALLEY SALT DIAPIR, COLORADO

by

REBECCA D. NAVARRETTE, B.S.

THESIS

Presented to the Faculty of the Graduate School of

The University of Texas at El Paso

In Partial Fulfillment

of the Requirements

for the Degree of

MASTER OF SCIENCE

Department of Earth, Environmental and Resource Sciences

THE UNIVERSITY OF TEXAS AT EL PASO

August 2024

Acknowledgements

To Cecilia, the best daughter anyone could ask for, my everything. I would not have had the courage and strength to have done this without you. You have been my number one supporter since you learned how to talk. One of my favorite memories is from my undergraduate pre-commencement ceremony when you looked at my mom and said, "You didn't even get my mom flowers???" Raising you has been the greatest joy.

I want to give a special thanks to Dr. Benjamin Brunner the crazy geochemist & dinosaur enthusiast that has been by my side for the last 5 years. You've always encouraged me when I felt this was unattainable and gave me a push when I needed it. On that same note I want to thank Dr. Gail L. Arnold (master of all advisors), when we met, I remember you planning the next few years of my life, and I'm grateful because this journey would have been much harder without you. I also want to thank my committee members, Dr. Kate Giles (salt & carbonate queen), Dr. Antonio Arribas (ore deposits & professional presentation master), Dr. Evey Gannaway Dalton (field guru). I have learned a lot from each of you over my time at UTEP and I am better for it.

To my closest friends Daphne and Yeshey. Thank you for being there with me through all the late nights, ranting sessions, and adventures. I look forward to seeing where life will take us as we branch out into the professional world, and I will cherish all the wonderful memories we have made along the way. Here's to the many more adventures that lie ahead.

Lastly, I couldn't have accomplished this without my incredible support system. To my family – Mague, Oscar, Mayte, Ethan, and Jaedynn – thank you for always being there for us. I couldn't have balanced school, work, and motherhood without you. Los quiero mucho, y sin ustedes esto no sería posible. Thank you from the bottom of my heart for believing in me and standing by my side every step of the way.

Abstract

Zebra rocks displaying alternating light and dark-colored millimeter to centimeter thick bands of crystals have been found at the Gypsum Valley salt diapir, Colorado in the Paradox Basin where they are associated with gypsic diapiric caprock. Elucidating their origin may provide crucial information about intermittent fluid flow at the margin of salt diapirs and about Zebra rock formation, which often is associated with carbonate-hosted lead-zinc mineralization (Mississippi Valley Type, MVT) and hydrothermal dolomite -hosted hydrocarbon reservoirs.

The Gypsum Valley Zebra rocks consist of calcite, i.e., it is a Zebra limestone. It shows a finely crystalline light banding and coarsely crystalline dark color banding which is inverse to the often dolomitic Zebra rocks in the literature. It also exhibits a wide variety of crystal fabrics from regular banding to chaotic distribution of bands and vugs with sedimentary infill. Combining field observations, petrographic and geochemical analyses with new insights into the impacts of anhydrite-gypsum transformation, I conclude that Zebra limestone at Gypsum Valley originates from the replacement of a petroliferous microcrystalline dolostone. Conversion of anhydrite to gypsum in the cap of the salt diapir is both the driver and benefactor of a process that cyclically results in compression and extension of the lithologies overlying the anhydrite/gypsum cap.

This study documents numerous fluid flow events at the margin of the Gypsum Valley salt wall, offers a model to reconcile opposing explanations for Zebra rock formation by integrating cyclic extension and compression, and proposes a so far unrecognized geochemical transformation that induces replacement of dolomite by calcite while potentially releasing carbon dioxide to the atmosphere.

Table of Contents

List of Tables

List of Figures

Introduction

Zebra rocks are characterized by alternating color bands ranging in size from millimeters to centimeters, which can result from differences in abundance in impurities, mineralogy, and/or crystal size. Rocks with such features are often associated with carbonate-hosted lead-zinc mineralization (Mississippi Valley Type, MVT deposits) and hydrothermal dolomite hydrocarbon reservoirs but have been reported from a wide range of geologic settings (Wallace and Hood, 2018; for examples of Zebra rocks, see Figure 1). Despite their eye-catching patterns and association with mineral resources, the processes that lead to formation of Zebra rocks remains unclear (Wallace and Hood, 2018). Zebra limestone, composed mainly of calcite, has been discovered at the Gypsum Valley salt diapir in the Paradox Basin, Utah and Colorado (Lerer, 2017). This discovery presents a unique opportunity to gain insights into Zebra rock formation processes due to several distinguishing characteristics: i) unlike typical Zebra rocks, the Gypsum Valley example is solely composed of calcite, ii) exhibits an unusual color banding pattern, iii) displays a variety of fabric types, and iv) is located in a geologically well-studied area. This thesis investigates the Zebra limestone at Gypsum Valley, aiming to document its distinct characteristics and unravel its origins.

BACKGROUND

Interest in Zebra rocks is driven by both scientific curiosity as well as considerable economic significance because they often occur in association with carbonate-hosted lead-zinc mineralization (Mississippi Valley Type, MVT deposits) and hydrothermal dolomite hydrocarbon reservoirs (Sass-Gustkiewicz and Mochnacka, 1994; Morrow, 2014). Despite decades of research, there is no clear consensus on the processes that cause the formation of Zebra rocks (Ramsay,

1980; Merino et al., 2006; Morrow, 2014; Dill et al., 2014; Quijada et al., 2014; Kelka et al., 2017; Wallace and Hood, 2018; Anikina and Bortnikov, 2020; Kawahara et al., 2022; Coward et al., 2023). Researchers generally agree that the dark-colored bands form through the replacement of a host rock, typically presumed to be a sedimentary carbonate rock and more rarely, evaporite rocks such as gypsum or anhydrite (Wallace and Hood, 2018).

The dark color bands in these rocks are postulated to be caused by the presence of detrital material/inclusions from a depositional precursor (i.e., siliciclastic material or organic matter; Wallace and Hood, 2018). The origin of the light bands is debated more fiercely, with the dominant view that these are mineral-filled cavities (e.g., Morrow, 2014; Wallace and Hood, 2018), while others think that recrystallization is the answer (e.g., Merino et al., 2006; Kelka et al., 2017). In a nutshell, the debate is if: a) the minerals that constitute the white bands grow into a cavity which implies the existence of a process that drives the opening of such cavities; or if b) white bands are constituted by minerals that cannibalize smaller-grained minerals from the dark-colored bands, which implies some self-driven/organized process that may take place in a stress field.

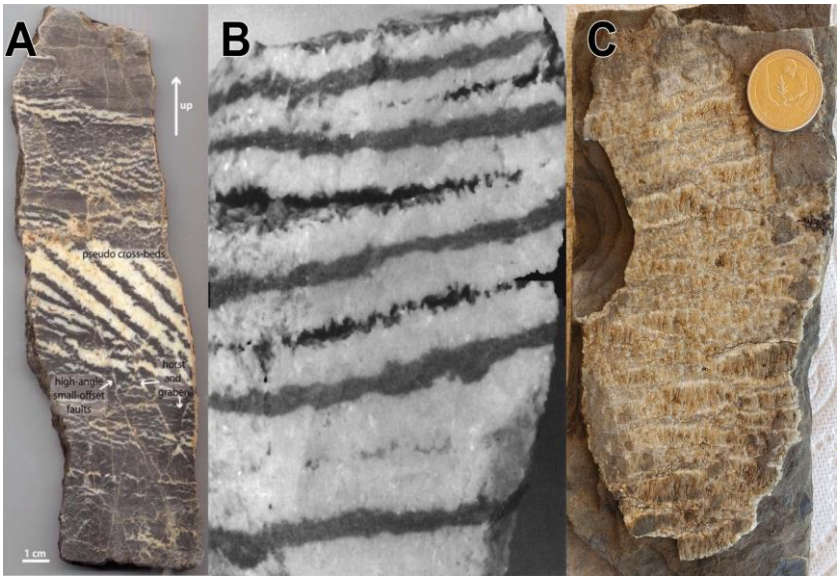

Figure 1: Examples for Zebra rocks

A) Picture from Diehl et al. (2010), Zebra Dolomite. B) Picture from Beales and Hardy (1980), interbedded pale brown (dark) early diagenetic finely sucrosic dolomite and white sparry dolomite (band thickness from mm to cm size, width of sample ~5 cm). C) Example of a Zebra rock consisting of quartz (white) and calcite fibers (beige), arranged parallel

to extension veins found in a Liassic unit located in the core of the Morcles fold nappe, Valais, Switzerland (diameter of coin is 15 mm; photo: Hermann Lebit).

ZEBRA LIMESTONE AND ASSOCIATION WITH SALT DIAPIRS

The most commonly observed examples of Zebra rocks are Zebra dolostones, which have been recorded across the globe (Diehl et al., 2010). Zebra limestone has been documented fare less frequently and the expression is used in two different contexts. Most commonly 'Zebra limestone' is used in the literature for fabrics similar to Zebra rocks, but in limestone of biogenic origin and remnants. These are commonly associated with stromatactis structures, often found in reefs and mounds (Ross Jr et al., 1975; Flügel, 2004). Less commonly, 'Zebra limestone' has been used in the context of carbonate caprock on salt diapirs from the coastal region of the Gulf of Mexico, with a Zebra/banded limestone above the anhydrite/gypsum caprock, followed by a variegated/disrupted carbonate caprock (Posey and Kyle, 1988; Brunner et al., 2019), displaying an entirely diagenetic origin. This association of Zebra limestone with caprock on salt diapirs resonates with the finding of Zebra limestone at the Gypsum Valley salt diapir, and with reports of Zebra textures found in MVT deposits from the Eastern Maghreb salt diapir province, north Africa. Notably, zebra calcite consisting of mm- to cm-scale alternations of dark and white calcite has been documented in a peridiapiric-type Pb-Zn deposit at Fedj el Adoum, Tunisia (Bouhlel et al., 2007) and zebra fabrics in celestite (a strontium sulfate mineral also known as celestine) have been found associated with dolomitic cap rock also in Tunisia at the Oued Jebs Pb-Zn-Sr deposit, (Bejaoui et al., 2014) and Bougrine, (also referred to as Bou Grine) Zn-Pb deposit (Bouhlel et al., 2024).

Zebra limestone from Gypsum Valley, Colorado

Zebra limestone was discovered at the Bridge Canyon location on the northeast margin of Little Gypsum Valley, Colorado in the framework of a Master's thesis on the generation of carbonate caprock at salt diapirs (Lerer, 2017; Figure 2). The valley is located on a breached salt wall that has its origins in the late Paleozoic with the deposition of a layered evaporite sequence (Paradox Formation) in the Paradox Basin. The Paradox Basin is a flexural foreland basin that formed in response to the genesis of an uplift referred to as the Uncompahgre uplift (Stevenson and Baars, 1986; Nuccio and Condon, 1996; Trudgill and Arbuckle, 2009; Trudgill, 2011). The layered evaporite sequence – referred to as the Paradox Formation – was formed because the basin went through phases of restriction and desiccation, with deposition of evaporite minerals, that alternated with phases of connection to the global ocean during which carbonate rocks and shales were deposited (Hite and Buckner, 1981). Prograding clastic sediments derived from the Uncompahgre uplift caused differential loading of the layered evaporite sequence and drove salt displacement, initiating a series of salt walls flanked by mini basins, and creating the geological and geographical features seen today (Trudgill, 2011; Brunner et al., 2019; Escosa et al., 2019; Thompson Jobe et al., 2020).

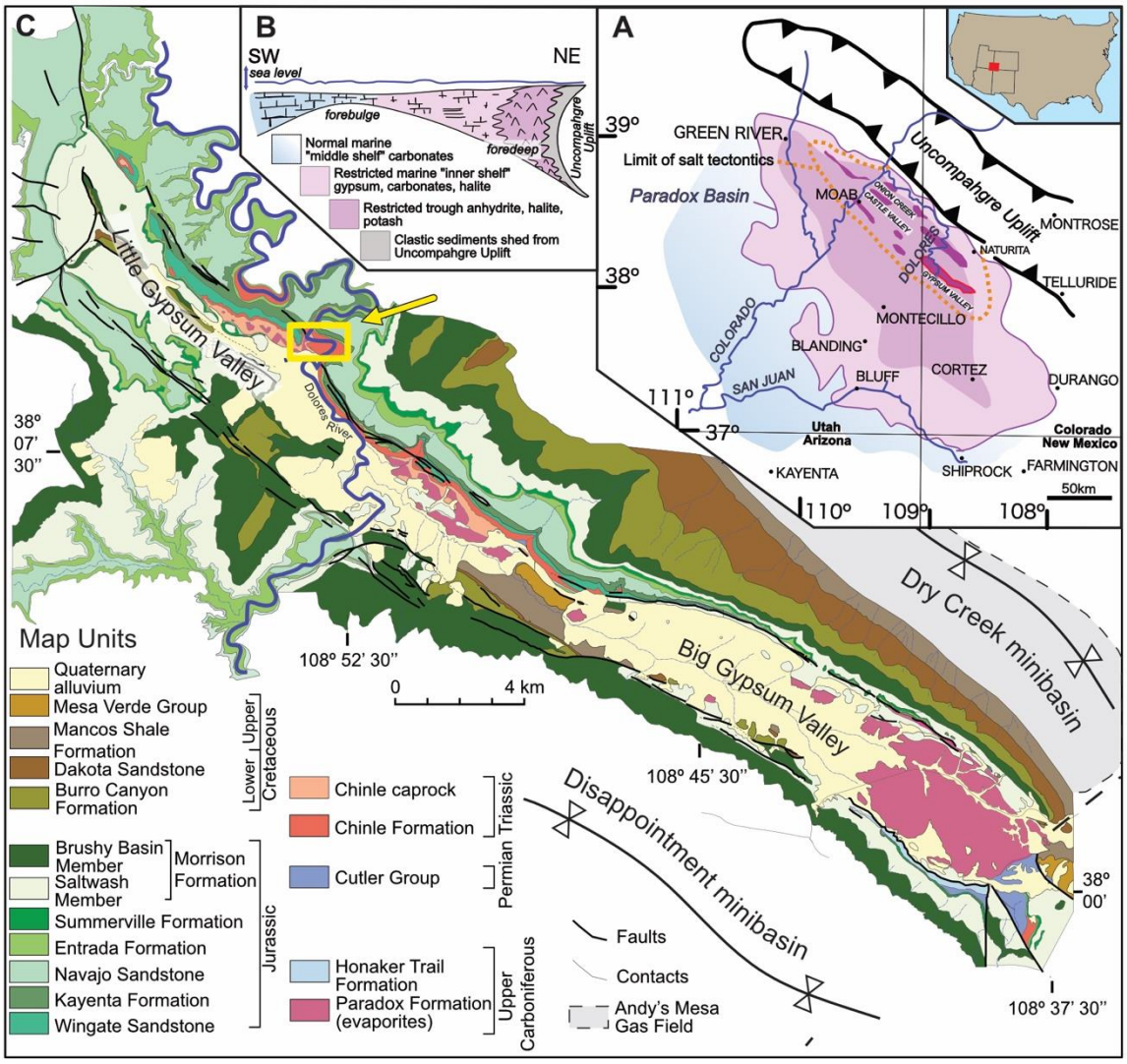

Figure 2: Paradox Basin, Location of Gypsum Valley and Zebra Limestone outcrop
(modified from Escosa et al., 2019 and Brunner et al., 2019)

A) Geological setting of Paradox Basin in Four Corners Region with Gypsum Valley highlighted in red and other breached salt walls in dark purple. B) Schematic depiction of flexural foreland basin and deposition of layered evaporite sequence (Paradox Formation). C) Geological map of Gypsum Valley, yellow arrow indicates location of Zebra Limestone outcrop.

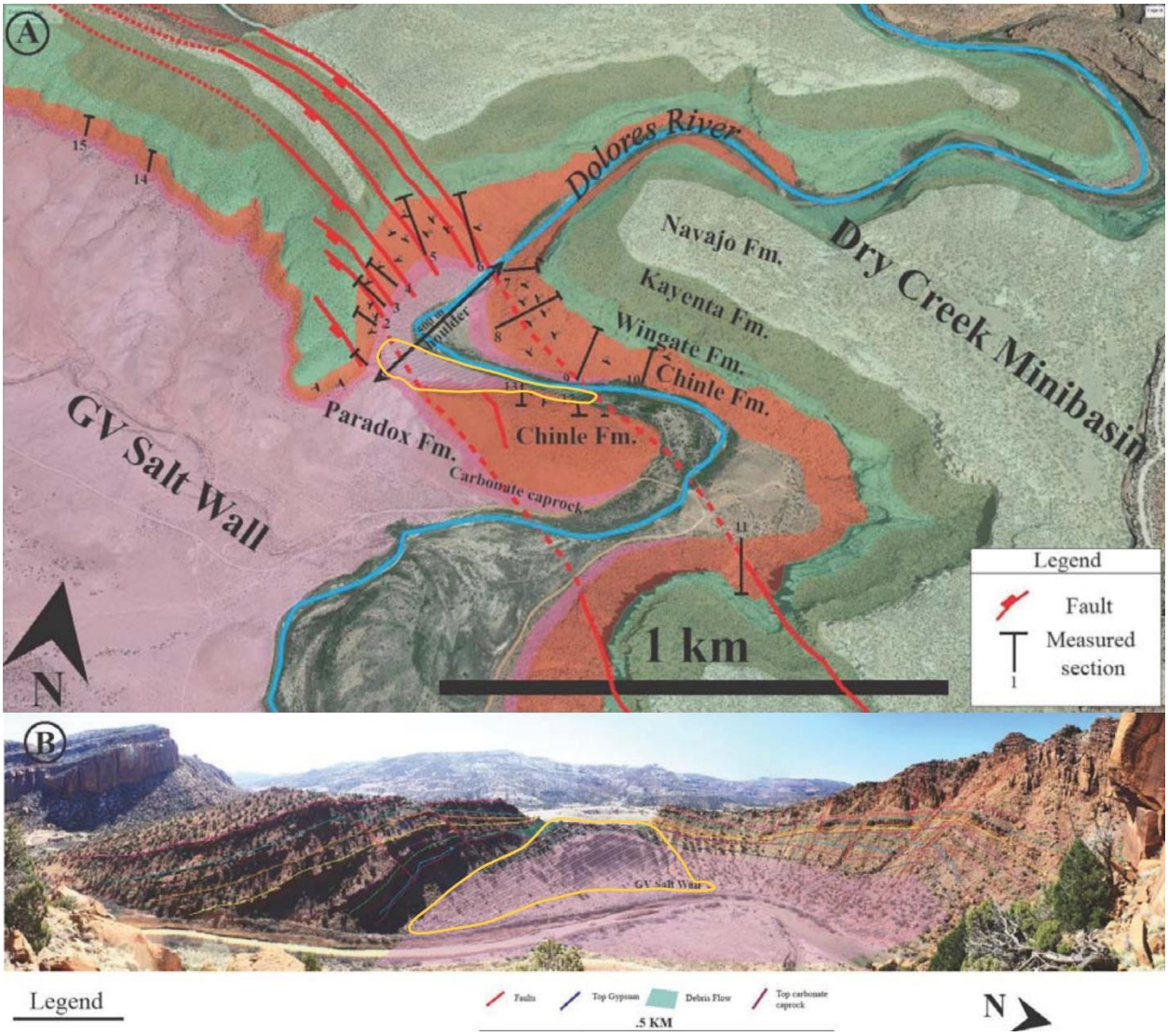

Figure 3: Location of study area (modified from McFarland, 2017)
A) Geological setting of Bridge Canyon site with study area outlined in yellow, indicated measured sections and geological interpretation by McFarland (2017). B) Drone image of Bridge Canyon with study area outlined in yellow (McFarland, 2017).

The Zebra limestone is located close to a bridge crossing the Dolores River in Little Gypsum Valley. It is in proximity to gypsum, presumably gypsic caprock derived from the Pennsylvanian-aged Paradox Formation, and a poorly outcropping zone with carbonates that transitions into sandstone and conglomerates of the Triassic-aged Chinle Formation, which forms a burial wedge on top of the diapir (Figures 3, 4; Heness, 2016; McFarland, 2016; Langford et al., 2022).

Figure 4: Overview of Zebra limestone outcrops at Bridge Canyon site, Gypsum Valley
Zebra limestone outcrops (red circle) are located in proximity to gypsum caprock and a poorly outcropping zone (hatched area) with carbonate rocks that transitions into sandstone and conglomerates of the Triassic-aged Chinle Formation. Note different colors of outcrops from Chinle Formation: to the east of the domal shape rocks are dark red, which is typical for outcrops from the Chinle Formation in this region, to the west they display a yellow discoloration, presumably caused by bleaching caused by oil migration. Blue arrow indicates flow direction of Dolores River.

Initial studies of the Zebra limestones produced several insights: Lerer (2017) investigated the sulfur chemistry of carbonate rocks at the Gypsum Valley salt wall margin to assess if sulfate was incorporated during the formation of carbonate rocks, including Zebra limestone. He found that in general, there is very little carbonate-associated sulfate (CAS) in those rocks, ranging from 345 to 1345 ppm. This is about one eighth of the average sulfate content found in the Damon Mound salt stock (Labrado, 2021), which has a gypsum and limestone caprock. At Gypsum Valley, the oxygen and sulfur isotope values for limestone CAS range for $\delta^{18}O$ (relative to the VSMOW standard) from +16‰ to +20‰, and for $\delta^{34}S$ (relative to the VCDT standard) from +16‰ to +18‰. In gypsum caprock, the $\delta^{18}O$ ranged from +12‰ to +15‰, and the $\delta^{34}S$ from +13‰ to +16‰. Thus, oxygen and sulfur isotope values of sulfate in CAS are only slightly enriched in ^{18}O and ^{34}S over the sulfate from gypsum. Lerer (2017) and Brunner et al. (2019) interpreted these findings as indication that either microbial sulfate reduction played a negligible role in the formation of carbonates in the caprock of the Gypsum Valley salt wall or that fluid flow during the conversion of gypsum caprock to carbonate caprock would have been very large, suppressing the recording of an isotope signature typical for microbial activity.

Labrado (2021) analyzed clumped isotope signatures of caprock carbonates, where she referred to the Zebra limestones as 'straight laminated' limestones. The clumped isotope technique allows to not only determine the oxygen and carbon isotope values of the carbonate rocks (relative to the VPDB standard), but also to infer – assuming equilibrium conditions – the temperature conditions under which those rocks formed, and the oxygen isotope composition of the water (relative to the VSMOW standard) in which they precipitated. Two Zebra limestone samples were analyzed in that study. One sample yielded a temperature of 80 ºC, a $\delta^{18}O$ of +5.6‰ (vs. VSMOW) for the fluid in which it was formed, and a $\delta^{18}O$ of –4.2‰ and a $\delta^{13}C$ of –5.6 ‰ (vs. VPDB) for the carbonate. A second, more irregularly banded Zebra limestone sample yielded a temperature of 50 ºC, a $\delta^{18}O$ of +0.3‰ (vs. VSMOW) for the fluid in which it was formed, and a $\delta^{18}O$ of –4.3‰ and a $\delta^{13}C$ of –5.6‰ (vs. VPDB) for the carbonate. Thus, the more regularly banded Zebra limestones recorded a higher temperature and positive oxygen isotope signature of water, the irregularly banded a lower temperature and negative isotope signature of water, indicating overprinting by cold, isotopically light meteoric water (Labrado, 2021).

Significance

Elucidating the origin of Zebra limestone at Gypsum Valley has great potential to contribute new insights to the geological community on a global scale. Zebra limestone is a component of carbonate caprocks in salt diapirs, which serve as an archive of the temperature and fluid history associated with salt tectonics (Brunner et al., 2019). Thus, understanding Zebra limestone formation provides important insight for oil and gas exploration, but also for any other salt-diapir related geological enterprise, such as the storage of hydrogen gas (Małachowska et al., 2022), sequestration of carbon dioxide (Mack and Endemann, 2010) or lithium exploration (Kukla et al., 2019). Understanding the origin of Zebra limestone is also relevant to that of Zebra rocks in general, which may be of considerable economic significance because they often occur in association with carbonate-hosted lead-zinc mineralization (Sass-Gustkiewicz and Mochnacka, 1994; Morrow, 2014). Moreover, the chemical reaction for Zebra limestone genesis I propose indicates potential release of CO_2. Discovering a so far unknown source of CO_2 emissions is important to a better understanding of atmospheric CO_2 concentrations (Masson-Delmotte et al., 2021) and the current climate crisis.

Project Goal, Hypotheses and Objectives

The goal of the study is to contribute key steps that will aid in deciphering the origin of the Zebra limestone at Gypsum Valley and Zebra rocks in general. To do so, I aim to test a number of hypotheses that are driven by a set of underlying questions that scale from details about the specific outcrop at Bridge Canyon in Gypsum Valley to the big picture-questions about Zebra rock formation.

HYPOTHESIS H1: ZEBRA LIMESTONES AT THE BRIDGE CANYON LOCATION IN GYPSUM VALLEY ARE THE RESULT OF A SUCCESSION OF DIAGENETIC ALTERATIONS

The first hypothesis originates from the remarkable variability in rock fabrics and chemical/mineralogical composition within the small outcrop of Zebra limestone at the Bridge Canyon location in at Gypsum Valley. I propose that over time, a succession of diagenetic processes induced different stages of alteration within these Zebra rocks, and that the observed variability is caused by the expression of any particular stage at a specific outcrop (implying highly localized differences). These processes have led to characteristic features such as vugs, discoloration, and cross-cutting relationships.

To test H1, I formulated the following objectives:

O1.1: Establish an inventory of all Zebra limestone outcrops at the Bridge Canyon site, including outcrop data (size, geological context, structure, petrography, mineralogy, fabrics, with particular focus on authigenic minerals such as dolomite, calcite, doubly terminated quartz and quartz rosettes).

O1.2: Extract accessory minerals from gypsum and Zebra limestone samples to assess if Zebra limestone inherited accessory minerals from gypsum (i.e., replaced gypsum) and if Zebra

limestone incorporated additional materials (e.g., detrital material from the Chinle Formation or Paradox Formation of non-evaporite inclusions?).

O1.3: Develop a paragenetic sequence that encompasses all major steps of Zebra limestone formation at the Bridge Canyon site that is compatible with the observations from O1.1.

HYPOTHESIS H2: THE INVERSE DARK-LIGHT COLOR BANDING OF THE BRIDGE CANYON ZEBRA LIMESTONE IS CAUSED BY 'SELF-CLEANING' DURING REMINERALIZATION.

My second hypothesis ties into the paradigm that dark layers in Zebra rocks reflect original impurities inherited in replacement minerals. While it is not explicitly stated in the literature reviewing the mechanisms of Zebra rock formation (e.g., Wallace and Hood, 2018), a review of photographs and text documenting Zebra rocks brings us to the conclusion that the 'dark bands' in the literature correspond to finer-crystalline and typically more uniformly sized fabric, whereas 'white bands' correspond to coarser-crystalline fabrics, with size of minerals increasing away from the finer-crystalline (dark bands) fabric (Beales and Hardy, 1980; Merino et al., 2006; Diehl et al., 2010; Morrow, 2014) – often appearing to show syntaxial growth on grains from the dark bands (for a discussion of syntaxial growth, see Wallace and Hood, 2018). The Paradox Basin Zebra limestones at Gypsum Valley show the same pattern, but with reverse color patterns: white bands correspond to a finer-crystalline and more uniformly sized fabric, darker bands to coarser-crystalline fabrics, with size of minerals increasing away from the finer-crystalline, white fabric. If the darker color described in the literature is indeed due to detrital material from a depositional precursor (i.e., siliciclastic material; Diehl et al., 2010; Wallace and Hood, 2018; Coward et al., 2023), it could be argued that the precursor material for the Zebra limestone must have been low in detrital material.

I propose that the Bridge Canyon Zebra limestone originates from a precursor that only contained minimal amounts of mineral-grain impurities but significant dead oil. Such oil would be more mobile than actual crystals, allowing for the displacement and concentration of the oil outside of the growing replacement crystals, instead of entrapment in the crystal lattice, explaining the 'finely crystalline light' vs. 'coarsely-crystalline dark' pattern of banding that is inverse to what is generally observed.

To test H2, I formulated the following objectives:

O2.1: Investigate in detail (optical microscopy, XRF) the fate of impurities of Bridge Canyon Zebra limestone. This is facilitated because the zebra patterns are not established everywhere, and yet there are changes in calcite crystal sizes.

O2.2.: Discuss options to explain the apparent cleanness of the fine-crystalline light bands based on O2.1:

The 'self-cleaning' process is a two-stage process in which first impurities get trapped, and then later, in a second recrystallization process, excluded.

The process is a single-stage process in which growing crystals continuously displace impurities to the crystal boundaries.

There were no impurities to start with.

HYPOTHESIS H3: ZEBRA LIMESTONE GENESIS IS LINKED TO THE CONVERSION FROM ANHYDRITE TO GYPSUM CAPROCK.

My third hypothesis aims to address the bigger picture of Zebra rock formation. One of the commonalities in salt-diapir associated MVT deposits is the presence of a caprock which that constitutes a zone with steep chemical gradients (infiltrating meteoric water, ascending brines, and

changes in fluid chemistry due to evaporite dissolution) in a setting that may experience deformation due to salt dissolutional collapse, and halokinetic drape-folding of the caprock from crestal into a diapir-flanking position (Giles et al., 2012). Such conditions are conducive for recrystallization and rock deformation. I hypothesize that a critical driver for the formation of Zebra rocks is the conversion from anhydrite to gypsum, which exerts a major control on the availability of water (chemical activity of $H_2O << 1$) but also induces changes in rock volume and pore water pressure, which has implications for rock deformation (brittle/ductile/compression/expansion).

To test H3, I formulated the following objectives:

O3.1: Assess the field relationship between gypsum caprock and Zebra limestone. In particular, determine if there is a relationship between the presence of Zebra limestone and proximity to gypsum caprock and if the type of Zebra fabric (e.g., chaotic to organized) provides an indication of that relationship. Important in this assessment is also what lithology (if any) separates the gypsum from the limestone, i.e., if there is shale that would limit water exchange between the two rock packages, and that could also accommodate rock deformation.

O3.2.: Establish a qualitative model for how anhydrite-gypsum conversion could facilitate Zebra limestone formation.

Methods

FIELD WORK

In order to decipher the succession of diagenetic processes of the Zebra limestone (H.1), I conducted fieldwork at the Zebra limestone outcrop in Gypsum Valley in November of 2021, and in November of 2023. I collected samples and recorded lithologies in the outcrop to establish field relationships. The field work focused on the description of the known Zebra limestone outcrops and a search for additional Zebra limestone outcrops. Using Strabo Spot to record data and exact locations, I measured sections from (and including) the underlying gypsum caprock, through the Zebra limestone, and into the overlying Chinle Formation. Measuring the outcrops provides valuable information about the sequence and arrangement of rock layers (strata) in a particular area. To accomplish this, I utilized measuring tape, Brunton, GPS, drone images, as well as Strabo Spot, a mapping and documenting software.

PETROGRAPHY

For petrographic analysis, samples collected in the field were cut into slabs and thin section billets using a tile saw. The slabs were studied with a Leica EZ4© stereo microscope (8x to 35x magnification). The thin section billets were sent to petrographic services companies to be made into thin sections. The first batch of samples were fully stained with a ferrous iron stain (ferricyanide, results in a blue color if ferrous iron is available), as well as a "calcite stain" (Alizarin Red S, stains calcium red; Dickson, 1966; Puchtler et al., 1969). Because of the fragile nature of most samples, they also underwent a clear epoxy impregnation to protect their integrity. The second set of samples were only half stained with ferricyanide and Alizarin Red S such that the unstained portion of the thin section could be better used for investigation under cross-polarized

light. Thin section analysis was performed with a petrographic microscope Lecia DM750P©. A selection of gypsum and carbonate samples was used to extract accessory minerals (see below) that were analyzed by X-ray diffraction (XRD). Micro X-ray fluorescence (μXRF) spectroscopy was performed on selected slabs and thin section blocks with assistance from UTEP graduate student Jose Franco (advised by Dr. Arribas) to produce elemental maps.

EXTRACTION OF ACCESSORY MINERALS

Accessory minerals from gypsum and Zebra limestone samples can be used to assess if Zebra limestone inherited accessory minerals from gypsum (i.e., replaced gypsum) and if Zebra limestone incorporated additional materials (e.g., detrital material from the Chinle Formation) as laid out in O1.2.

Extraction techniques are based on the ability of a reactant to dissolve the major components of the investigated sample, which in this case is gypsum ($CaSO_4 \cdot 2H_2O$) and calcite ($CaCO_3$). Acids can dissolve carbonate rocks by converting carbonate into carbon dioxide which degasses from solution (bubbles out). Acids can also form complexes with calcium, which is attracted to conjugate base of acid, such as calcium-chloride complexes in the case of hydrochloric acid or calcium acetate in the case of acetic acid. Strong acidity, i.e., abundant hydrogen cations (H^+) can also convert sulfate ions (SO_4^{2-}) into protonated ions (HSO_4^-) which facilitates gypsum dissolution. A concern with using acids is that they may damage/alter accessory minerals, leading to erroneous interpretations. In the case of gypsum, a sodium chloride solution can be used instead, whereby the sodium forms sulfate complexes ($NaSO_4^-$), enhancing gypsum dissolution. However, that approach does not work for calcium carbonate. For calcite, using a strong chelating agent (chelator) could be an alternative. Diethylenetriaminepentaacetic acid (DTPA, sometimes referred to as pentetic acid), in its conjugate base form (i.e., when kept under a high pH) is a strong chelator

for cations and has been successfully applied for the dissolution of barite (Bao, 2006). Thus, in the addition of a strong acid extraction, I tested the extraction of accessory minerals with DTPA under strongly basic conditions. I hypothesized that under basic conditions, alteration of accessory minerals would be different from acid conditions, allowing me to identify artifacts caused by the dissolution approach. Due to the purity of the samples large amounts needed to be dissolved (>100 g), which turned out to be ineffective for weak acid (acetic acid) but successful for strong acid (hydrochloric acid).

Extraction with DTPA yielded mixed results: whereas gypsum dissolved readily in the same solution, limestone did not. I hypothesize that in a basic solution (e.g., ~pH 11.5), carbonate ions accumulate both by dissolution of calcite and addition of carbon dioxide from the atmosphere. These carbonate ions then compete with DTPA for calcium, stopping further dissolution. To offset this, I added hydrochloric acid (HCl) to the DTPA solution to lower the pH such that DTPA could continue to dissolve the rock. I tested this approach a total of three times, with every pH reduction resulting in the dissolution of approximately 1-2 grams of the sample. Starting with a 50-gram sample, this would require approximately 25-50 acidification steps to fully dissolve it. While this process is time-consuming, it introduces a novel extraction method that avoids exposing accessory minerals to acids. In addition to the extraction of the accessory minerals, the dissolution of Zebra limestone was also employed to determine its sulfate content (for methodology, see Lerer, 2017).

Results

GEOLOGICAL CONTEXT OF ZEBRA LIMESTONES IN THE FIELD

At Bridge Canyon, four Zebra limestone-bearing outcrops located to the east of the gypsum outcrops were identified in the slope below a burial wedge consisting of Triassic Chinle strata (Figure 5). A burial wedge describes deposition of strata on to a diapir that is only partially buried (Langford et al., 2022). Other notable features are deformed strata in the Chinle burial wedge just above the transition to a poorly outcropping area and an outcrop with sandy limestone (Figure 6). The folds at the base of the small cliff that constitutes the Chinle burial wedge change in amplitude, orientation, and shape (open rounded to tight-angular Chevron-folds) and do not propagate into overlying strata (Figure 7). This indicates that they were likely formed as consequence of soft-sediment deformation, such as slumping during sediment deposition (McFarland, 2016). At the Bridge Canyon site, the relationship between the lithologies belonging to the poorly outcropping zone and the overlying rocks in the Chinle Formation has been documented by McFarland (2016) who referred to the poorly outcropping zone as ‘laminated & brecciated caprock.’

Figure 5: Zebra limestone outcrops at Bridge Canyon site, Gypsum Valley

Zebra limestone outcrops (highlighted in purple) located to the east of gypsum caprock which consists of two prominent bands (yellow and light blue coloration). The Zebra limestone outcrops are located at the base a poorly outcropping zone that transitions into the conglomerates and sandstones from the Chinle Formation. Individual units which change in thickness can be identified and followed (red lines and colored area) in the burial wedge of the Chinle Formation. Note above the transition to the poorly outcropping zone deformed beds belonging to the Chinle Formation. Below the level of the Zebra limestone outcrops, an outcropping ledge (referred to as 'Sandy limestone' can be identified).

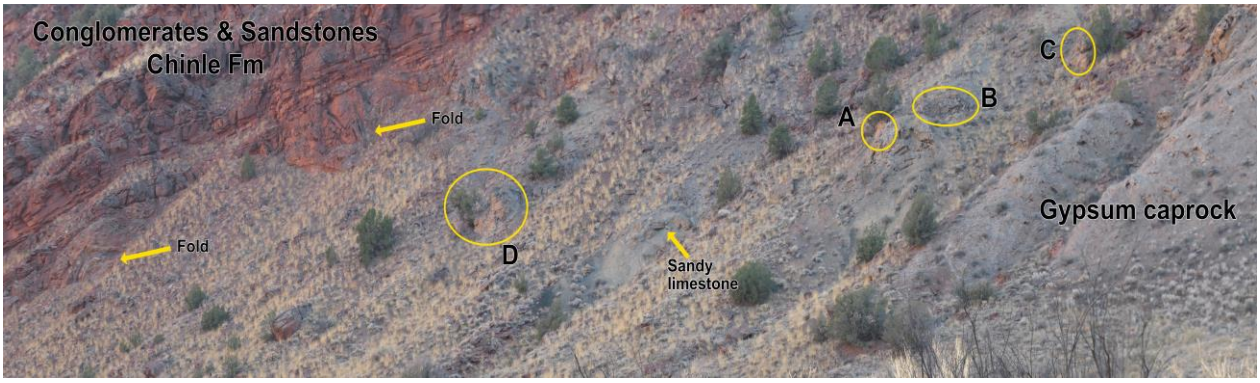

Figure 6: Location of Zebra limestone outcrops relative to landmarks

The Zebra limestone outcrops were named A, B, C, D in order of their discovery. Outcrop D is in proximity to two distinct folds at the base of the cliff formed by the Chinle Formation. Outcrop C and D are located above the east-most gypsum outcrops.

Figure 7: Deformed Chinle strata above transition to poorly outcropping zone

Folds at the base of the small cliff that constitutes the Chinle burial wedge, changing in amplitude, orientation and shape and do not propagate into overlying Chinle strata.

To the west, the group of Zebra limestone-bearing outcrops are adjacent to gypsum outcrops that display a domal shape (Figures 4, 5). The outcrop displays two distinct ledges, with a less competent slope-forming band in between (Figure 8). The ledge-forming gypsum benches are interlayered with dolostones (Figure 9A). The gypsum contains varying amounts of shale, fully transitioning into shale/dolomudstone in the center of the recessive slope (Figure 9B, C, D).

Figure 8: Ledge-forming and recessive beds in gypsum caprock
An upper (purple color) and lower (yellow color) ledge can be easily traced across the entire gypsum caprock outcrop.

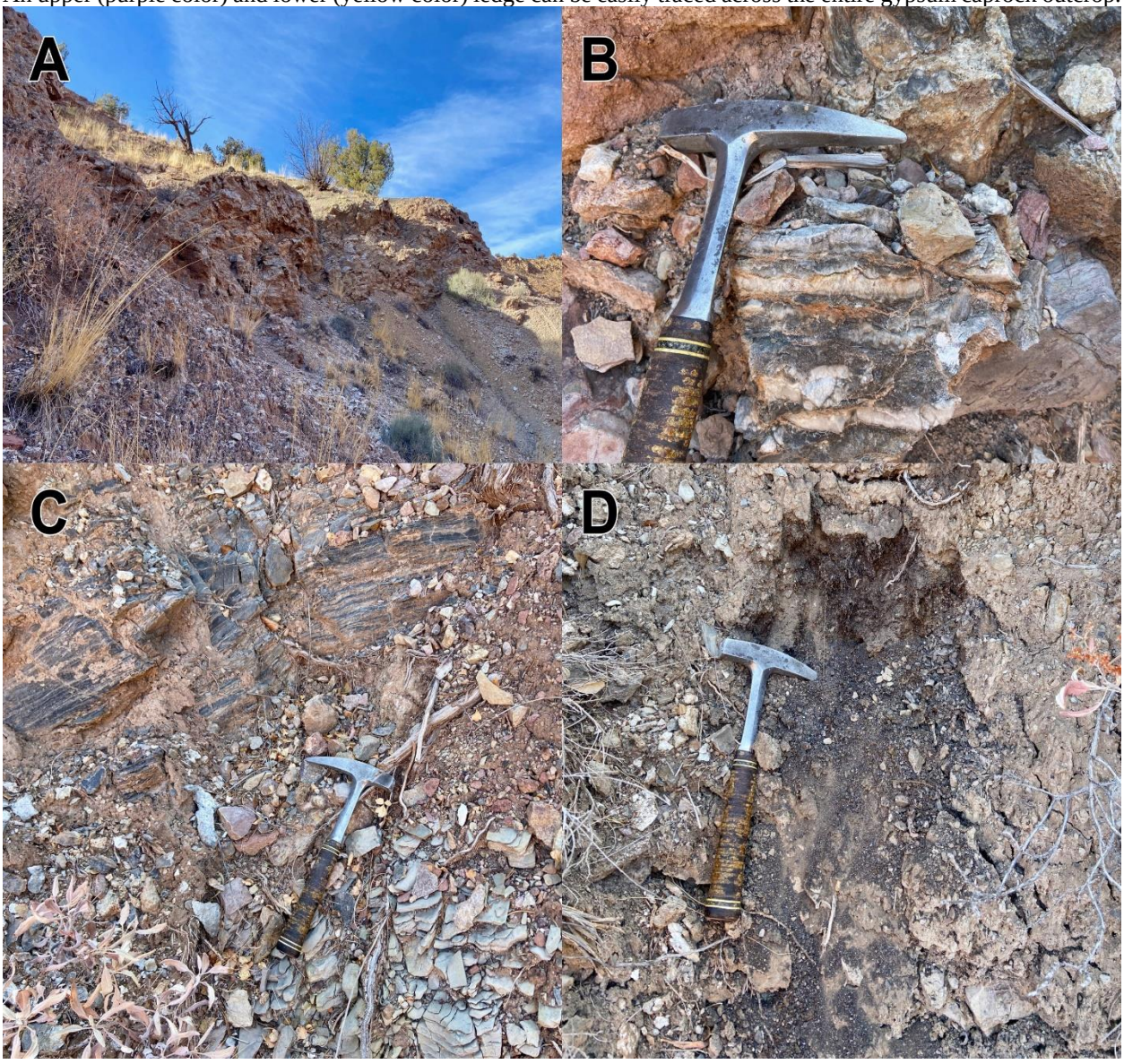

Figure 9: Influence of dolostone and shale components on gypsum caprock
A) The upper ledge consists of gypsum that is interbedded with dolostone. B-D) Increasing content of shale/dolomudstone leads to more fissile and less weathering-resistant rocks.

The zone in between the two more competent gypsum ledges is characterized by intense folding, with high amplitude and short wavelength folds (Figure 10).

Figure 10: High amplitude fold in gypsum/shale interbedded recessive band
Note lighter colored gypsum core vs. darker colored gypsum-dolomudstone-shale interbedded lithology.

Above the upper competent gypsum ledge follows a zone with poor outcrops. Right above the ledge, digging reveals more shale/dolomudstone (Figure 11A). Higher up the slope small outcrops of dolostones and patches of deeply weathered shale/dolomudstone alternate, until a chaotic mixture of dolostones and sandstones from the Chinle Formation form more competent bands, eventually transitioning into regular beds belonging to the Chinle burial wedge (Figure 11B, C).

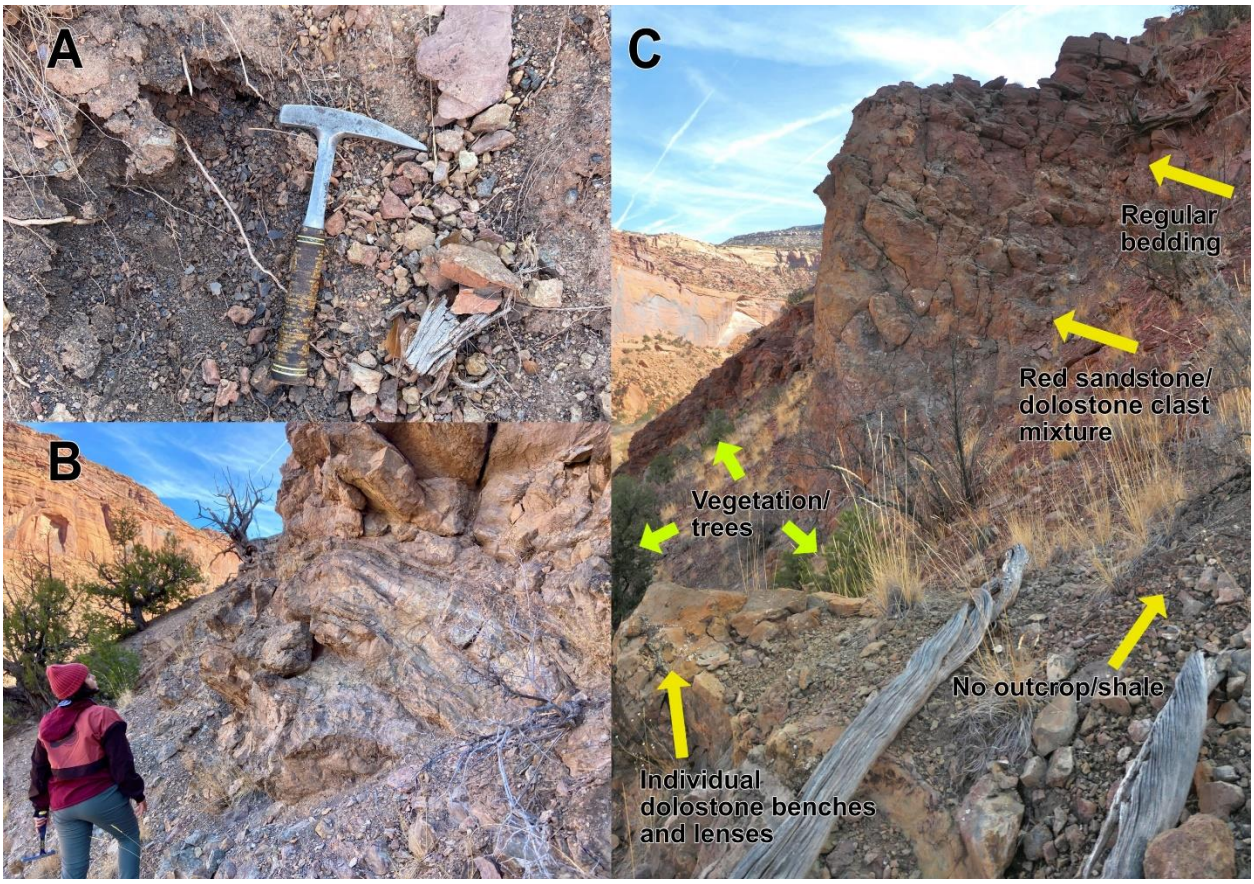

Figure 11: Dolostone/dolomudstone/shale zone
A) Digging reveals shale/dolomudstone with roots. B, C) Small outcrops of dolostones and deeply weathered shale alternate, overlain by a chaotic mixture of dolostones and sandstones from the Chinle Formation, eventually transitioning into normal Chinle sandstone and conglomerate beds.

Laterally, the contact between the uppermost gypsum ledge and the zone with poor outcrops can be followed to the two western-most Zebra limestone outcrops (B and C), placing them within the zone of the poor outcrops and stratigraphically higher than the gypsum caprock, which is corroborated by the finding of a rock package that corresponds to the upper gypsum caprock ledge with shale changing into a competent gypsum ledge, followed by shale, all underlying Zebra limestone outcrop B (Figure 12).

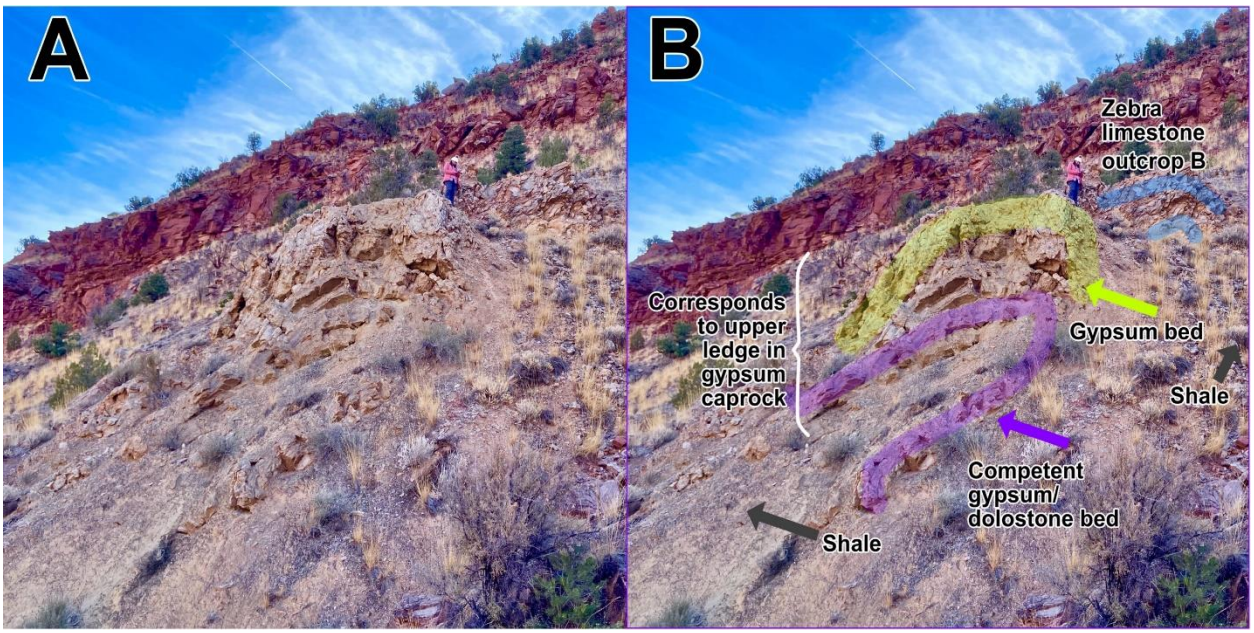

Figure 12: Gypsum caprock ledge underneath of Zebra limestone outcrop B
A) R. Navarrette standing next to Zebra limestone outcrop B, and on top of a gypsum ledge. B) This ledge is interpreted as correlative to the top ledge of the gypsum caprock.

ZEBRA LIMESTONE OUTCROPS AND NEARBY STRATA

At or adjacent to the four Zebra limestone localities (Zebra A-D), seven particular outcrops were studied in detail (Figure 13, Table 1) and a total of 30 samples was collected (Table 2).

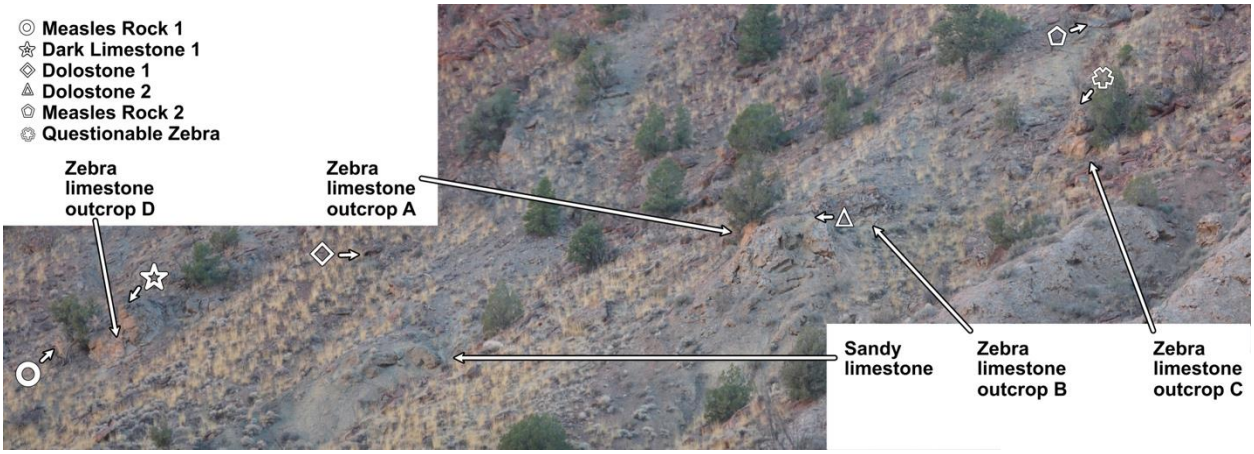

Figure 13: Detailed location of Zebra limestone and other investigated outcrops
Large outcrops are marked with arrows, small outcrops with symbols.

Table 1: Outcrops studied, listed from East to West.

Outcrop Name	**Outcrop dimensions**	**Samples collected**	**Coordinates***
Zebra D	Height: 4.3m Length 4.6m	RNNZ1 RNNZ2 RNNZ3	Latitude: 38.155501 Longitude: -108.888271
Measles Rock 1	Height: 2.6m Length: 4.1m	RNMR1	Latitude: 38.155442 Longitude: -108.88817
Dark Limestone	Height: 1.6m Length: 0.84m	RNDL1 RNDL2	Latitude: 38.1554 Longitude: -108.888289
Dolostone 1	Height 0.4 m Length: 8.2 m	RNSD1	Latitude: 38.155461 Longitude: -108.888505
Sandy limestone	Height: 0.8m Length: 1.6m	RNSC1	Longitude: 38.155683 Latitude: -108.888749
Zebra A	Height: 1.5m Length: 6.1m	KLGP013A	Longitude: 38.1555 Latitude: -108.888803
Zebra B	Height: 2.62m Width: 2.54m Length: 7.1m	RNCL2	Latitude: 38.155506 Longitude: -108.888918
Dolostone 2	Height: 0.15m Length: 1m	RNCZDOLO	Longitude: 38.155522 Latitude: -108.888904
Zebra C	Height: 2.5m Length: 3.2m	BC-VZA BC-VZB BC-VZC	Longitude: 38.155418 Latitude: -108.889033
Questionable Zebra	Height: 0.4m Length 0.6m	RNQZ	Latitude: 38.155348 Longitude: -108.88898
Measles Rock 2	Height: 1.46m Length: 2.2m	RNMR2	Latitude:38.155298 Longitude: -108.888932

*In Figure 13, large outcrops are marked with arrows, small outcrops with symbols.

Table 2: Sample list

Sample	Description
RN-GV-ZEBRACC-GV	Zebra with Red Vugs
KLGVP 041A	Grey limestone with small zebra texture
BC-VZA	Petroliferous Zebra C with Dolomite infill
BC-VZB	Petroliferous Zebra C with Dolomite infill
BC-VZC	Petroliferous Zebra C with Dolomite infill
KLGVP013A	Zebra A
KLGVP013B	Zebra A
ZB-BB056A	Zebra A with small to big banding
ZB-BB056B	Zebra A with small to big banding
RNDL1	Petroliferous Limestone
RNMR1	Spotted carbonate
RNSC1	Sandy limestone
RNZBREC	Brecciated Zebra
RNDL2	Petroliferous Limestone
RNCL1	Zebra B
RNCZCRUD	“Crud” under Classic Zebra
RNCZTM	Tan Limestone at the Classic Zebra base fold
RNSZV	Petroliferous Zebra Vug
RNCZGYP	Gypsum Below Classic Zebra
RNCZGSM	Green Sandy mess below Classic Zebra
RNQZ	Questionable Zebra textured rock
RNML1	Marly Limestone below Petroliferous Limestone
RNDS1	Tan Sandy Dolostone
RNMR2	Spotted carbonate
RNCZDL	Dark Band above Classic Zebra
RNCZDOLO	Dolostone under Classic Zebra
RNCZBAND	Tan Band above RNCZDL
RNNZ1	Zebra D
RNNZ2	Zebra D
RNNZ3	Zebra D

Zebra limestone outcrop A

Zebra limestone outcrop A hosts the most regularly banded zebra rocks identified in this study (Figure 14). This outcrop is located under a small pine tree. The outcrop measures 1.5 meters in length and 6.1 meters in height. This outcrop is isolated due to coverage with soil and loose rock, i.e., no direct contact to other rock units can be found. Soil and pine needle debris coats the entire outcrop red, making its distinctive features difficult to see from a distance. The Zebra banding exhibits continuity across the outcrop length, with banding being thinnest at the base and gradually increasing in thickness towards the top. Band thickness ranges from 0.05 cm alternating bands at the base of the outcrop (Figure 14F) to 0.5 cm dark bands alternating with 2-3 cm white bands at the top (Figure 14H). The thickest dark bands measure up to 1.5 cm, and white bands up to 6 cm (Figure 14C). Upon close examination, the coarse-crystalline dark layers of the Zebra pattern exhibit a dark rim of clay and dead oil along their edges, accompanied by the presence of lighter dogtooth calcite growth in their centers (Figure 14G). The light fine-crystalline layers display discoloration at their centers, characterized by a subtle light yellow or orange hue.

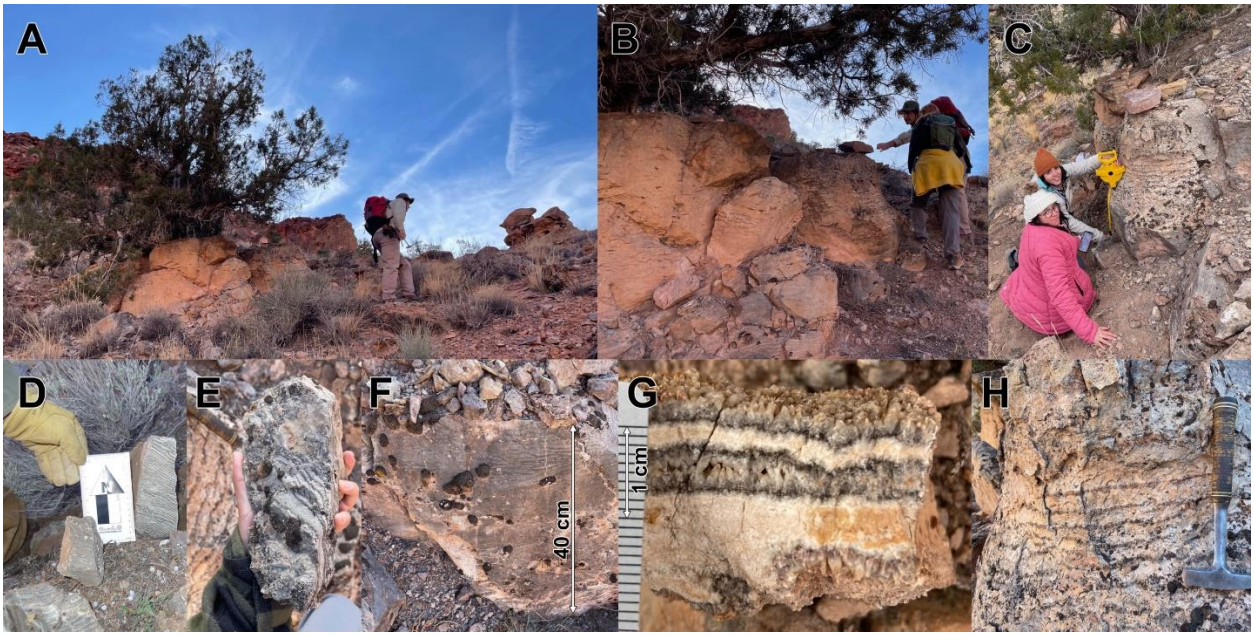

Figure 14: Zebra limestone outcrop A
A) Outcrop overview, below pine tree, stained with red coating from the shale the tree is rooted in. B. Brunner is walking toward Zebra outcrop to the right (west). B and C) Top right of the outcrop with wide banding. D) Pieces of the outcrop broken off near the base with very fine banding. E) Piece of outcrop with fine dark bands with slightly thicker white bands. F) Outcrop displaying thickening of bands. G) Close up look of thick zebra band showing dark rim at contact between band with coarse, tan gray and band with finer, white crystals and discoloration of white crystals. H). Thicker banding up close, outcrop seen in C.

Zebra limestone outcrop B

Zebra limestone outcrop B measures 2.62 meters in height, 2.54 meters width, and 7.1 meters in length (Figure 15). It is approximately 4 meters to the west of Zebra limestone outcrop A, and approximately 1 meter higher in elevation. Of all Zebra limestone outcrops, this outcrop shows the best exposed contact to underlying strata. Approximately 50 cm below the lowest carbonate bench of the Zebra limestone, there is a massive gypsum outcrop (at least 50 cm thick) which is capped by a 15 cm thick dolostone bed, overlain by shale (Figure 16). Digging in the covered portion of the outcrop in between the shale and the carbonate belonging to the Zebra limestone reveals more pieces of shale, indicating that the carbonate is directly in contact with a package or ~40 cm thick shale.

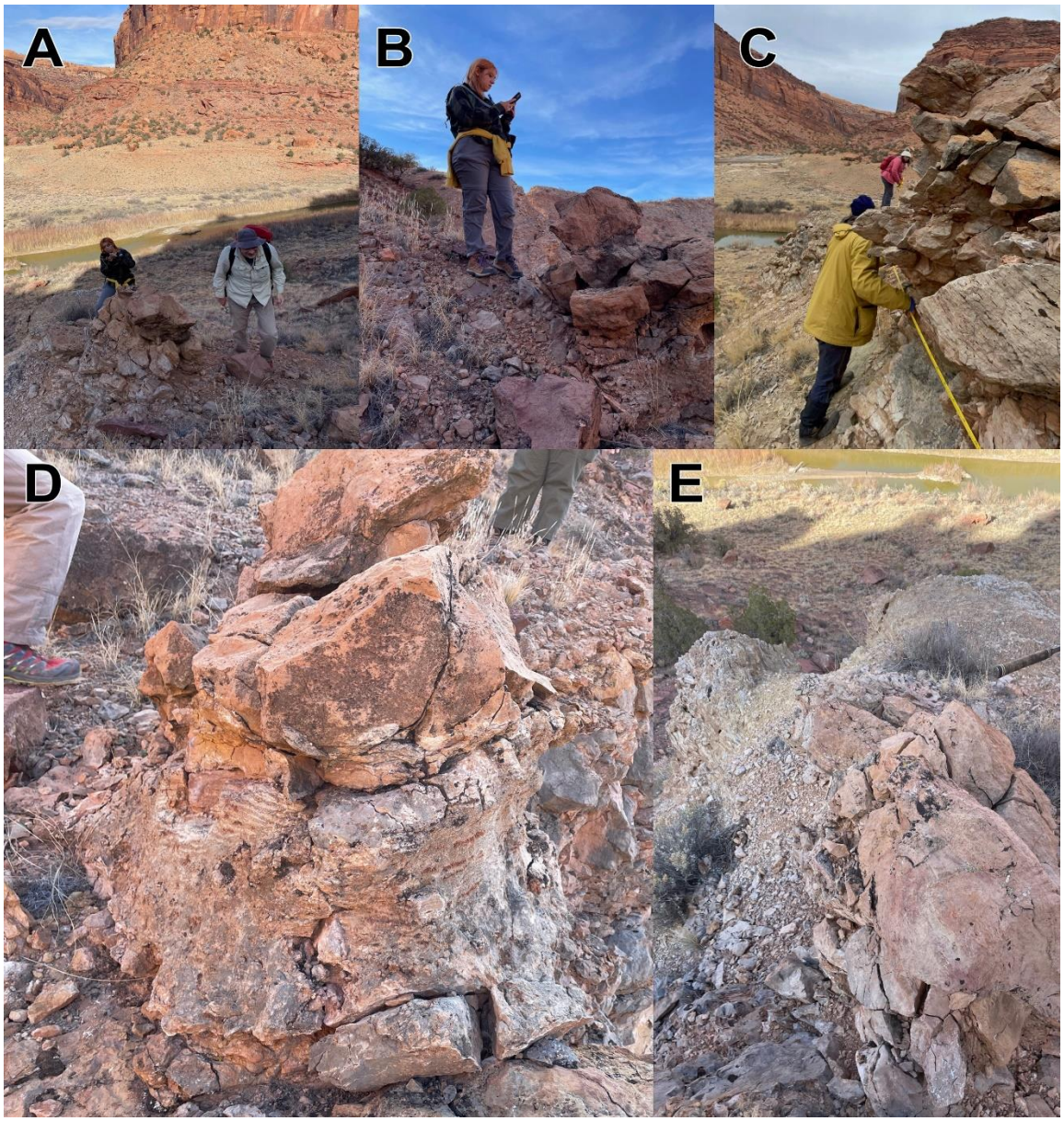

Figure 15: Zebra limestone outcrop B

A) R. Navarrette and B. Brunner standing at the top of the outcrop. Note tan color of top and white color in flank of outcrop. B) R. Navarrette at the top of the outcrop, with large gypsum outcrop in background. C) B. Brunner and R. Navarrette measuring the length of the outcrop at its base. Note Zebra fabric in foreground of picture and dark colored band in foreground, level with white hat of R. Navarrette. D) Zebra banding at top of outcrop. E) Downslope view from top of the outcrop, with yellow band on top of white gypsum outcrop.

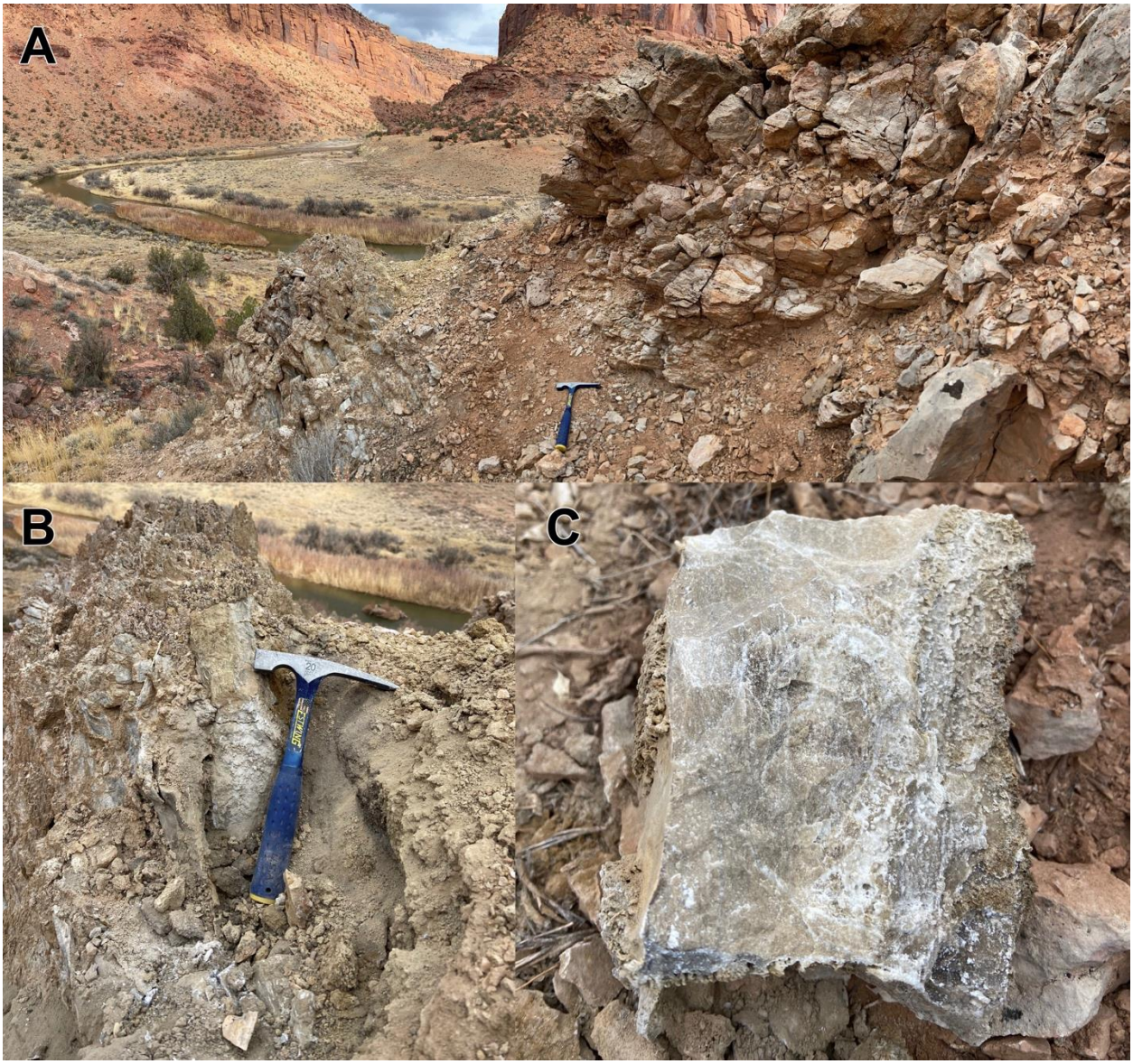

Figure 16: Zebra limestone outcrop B – lower contact
A) Overview of lower contact. B) A small package of gypsum that forms a cliff is overlain by a competent band of dolostone, which is covered by shale. C) Slab of the competent bed (15 cm thick).

The base of Zebra limestone outcrop B hosts a folded package of massive to banded Zebra limestone (Figure 17A), 17 cm thick green massive limestone, and a 30 cm by 30 cm large inclusion of folded shale (Figure 17D, E). At the top of a prominent fold, well-developed Zebra limestone is visible (Figure 17B). A notable characteristic of this fold are the Zebra vugs 1-1.5 mm in size cross-cutting the fold (Figure 17C) which imply that the formation of Zebra texture postdates the fold formation.

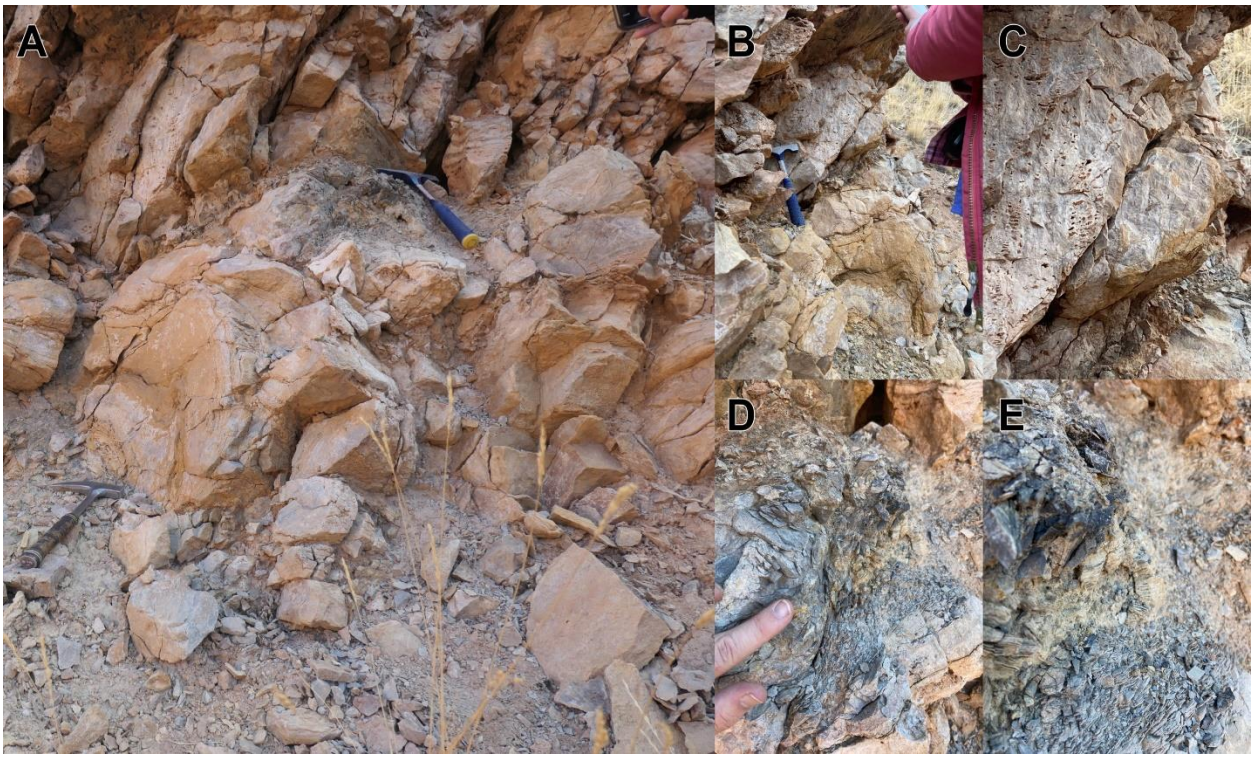

Figure 17: Zebra limestone outcrop B – internal features, folds, zebras, inclusions
A) Folding of the base of the Zebra limestone outcrop with hammer located on top of folded shale. B) Core of fold below of rock hammer with well-developed Zebra texture to the right of the hammer. C) Zebra limestone layers with vugs. D and E) Fold in green carbonate rock (core) and shale.

Another interesting observation is that the Zebra banding is continuous in the direction of the fold axis, but discontinuous perpendicular to it (Figure 18). At the center of the outcrop, where no further folds are evident, the Zebra pattern is most regular, like the Zebra limestone outcrop A. From bottom to top, the Zebra pattern becomes less distinct and is lost at the very top within a thick band of a dark limestone measuring 15 cm, (Figure 15C, Figure 19). Moving laterally at the top of the outcrop to the east toward Zebra limestone outcrop A, the Zebra pattern reemerges as banding that slightly varies in thickness from 0.5 cm alternating bands at the center to 1 cm alternating bands (Figure 15D). This pattern remains discernible for distances of 1-1.5 m.

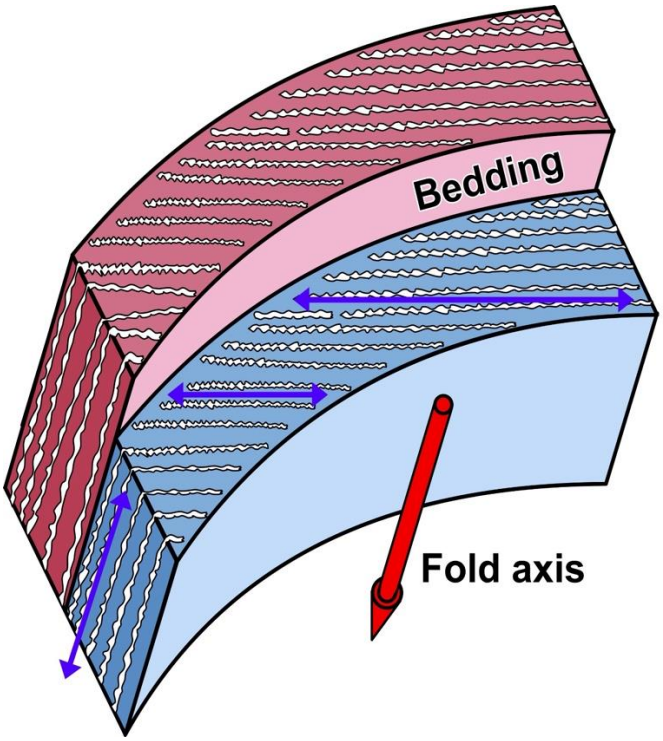

Figure 18: Sketch illustrating relationship between Zebra limestone fabric and folded bedding
Zebra fabrics do not crosscut bedding planes. Within the bedding planes, Zebra texture is truncated at bedding plane (horizontal long and short blue arrows), but continuous within bedding (tilted blue arrow) subparallel to the fold axis.

Zebra limestone outcrop C

Zebra limestone outcrop C measures 2.5 meters in height and stretches 3.2 meters in length (Figure 19). It is located approximately 5 meters to the west of Zebra limestone outcrop C and 4 meters higher in elevation. At the bottom right (west) of the outcrop there is a pine tree rooted in shale, and several smaller pine trees surround the outcrop, while no direct contact to other rock units can be found. This outcrop exhibits a striking array of features with irregular banding, ranging from as thin as 0.5 millimeters (Figure 19E) to as thick as 2-3 cm (Figure 19F), with no clear distribution on the surface. Remarkably, some of these bands can be traced consistently over distances spanning from 30 to 86 cm across the outcrop. Red infills are seen throughout, attributed to oxidation of ferrous iron in calcite crystals (Figure 19F, H). Evidence of folding and brecciation is apparent. Karstification is indicated by the presence of large vugs, some of which are filled with saddle dolomite. At the base of several of the vugs is a fine silty limestone sediment (Figure 19G,

H). Karst formation and subsequent infill post-date folding and brecciation. Unlike the other Zebra outcrops this outcrop is locally petroliferous, which became evident during cutting of rock slabs (Figure 19G).

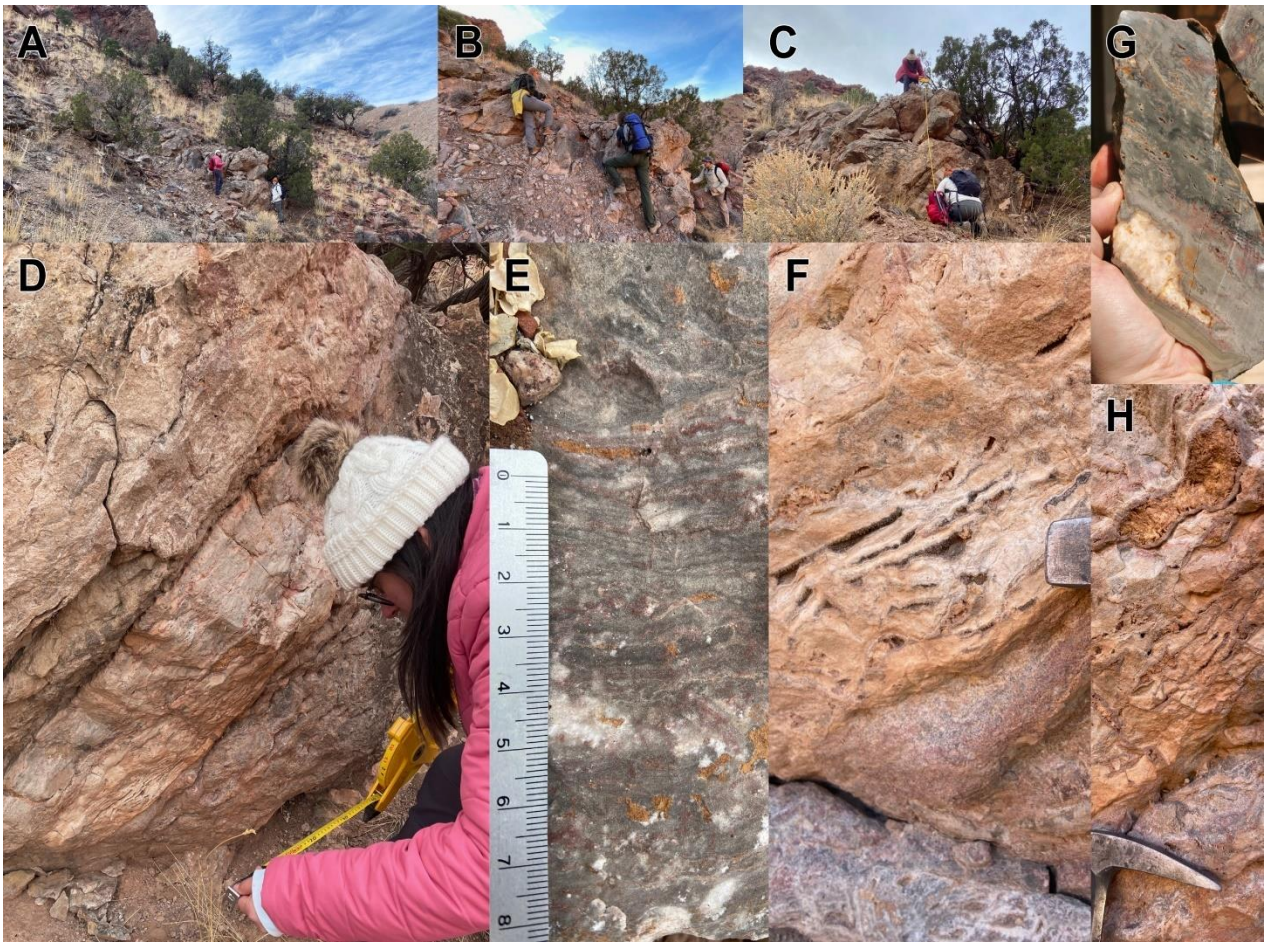

Figure 19: Zebra limestone outcrop C

A) R. Navarrette and P. Salas standing at the outcrop. Note number of pine trees (indicating presence of shale that allows roots to grow). B) R. Navarrette, M. Woelfel, and B. Brunner standing at the outcrop, note the discontinuous nature of apparent bedding. C) R. Navarrette and P. Salas measuring the outcrop, with pine tree growing in shale to the right. D) The base of the outcrop shows brecciated Zebra banding. E) Thin Zebra banding with red discoloration. F) Large vugs in Zebra banding. G) Slab of Zebra rock with zones that indicate presence of dead oil (dark, petroliferous), iron (red discoloration), vug-filling saddle dolomite (white-yellow), and thinly banded green-tan limestone (silt-sized calcite crystals). H) Large vug red/orange filled with saddle dolomite.

Zebra limestone outcrop D

Zebra limestone outcrop D measures 4.3 meters in height, and 4.6 meters in length (Figure 20). This outcrop is located approximately 40 meters east and 7 meters lower in elevation from Zebra outcrop A. Directly underneath this outcrop is shale. Out of the four zebra outcrops this one

is the largest. Banding thickness ranges from 1-2 mm and are seen at that size at the surface of Figure 20B. The right side (west) of Zebra D has a brecciated zone that displays folding (Figure 20C). Zebra limestone is lost at the very top of the outcrop, where it is in contact with a layer of dark petroliferous limestone. The east side of Zebra limestone outcrop is in direct contact with an outcrop I refer to as 'Measles Rock' as it is covered with green specks.

Figure 20: Zebra limestone outcrop D

A) P. Salas and B. Brunner measuring the outcrop which measures from bottom to top 4.6 m. B) B. Brunner using a chisel and hammer to collect a sample that displays banding at its bottom. Note shale (green-gray) below orange-tan Zebra limestone. C) Brecciated Zone. D) Folds in the brecciated zone.

Sandy limestone

The ‘Sandy limestone’ outcrop measures about 1.6 meters in length and 0.8 meters in height (Figure 21). It is located approximately 5 meters east and 20 meters lower in altitude from Zebra Outcrop A. The beds are folded and truncated. Noteworthy characteristics of this outcrop include its sandy texture and distinct lamination, along with its reaction to hydrochloric acid in the field, indicating the presence of calcite cement. There are two prominent bands; the lower band is orange-tan is approximately 10 centimeters wide, the upper band shows a lighter, tan coloration and is roughly 20 centimeters wide. Surrounding the outcrop and directly beneath it lies a bed of shale.

Figure 21: Sandy limestone
Sandy limestone outcrop with orange tan layer at the bottom and light layer on top.

The Sandy limestone turned out to not be of major importance for the outcome of this study. Comparison of thin sections (Figure 22) indicates that it could potentially be correlated to an inclusion that contains non-fossiliferous and mica-bearing sandy limestone found at the Bridge Canyon site to the northeast across the Dolores River (Woelfel, 2023).

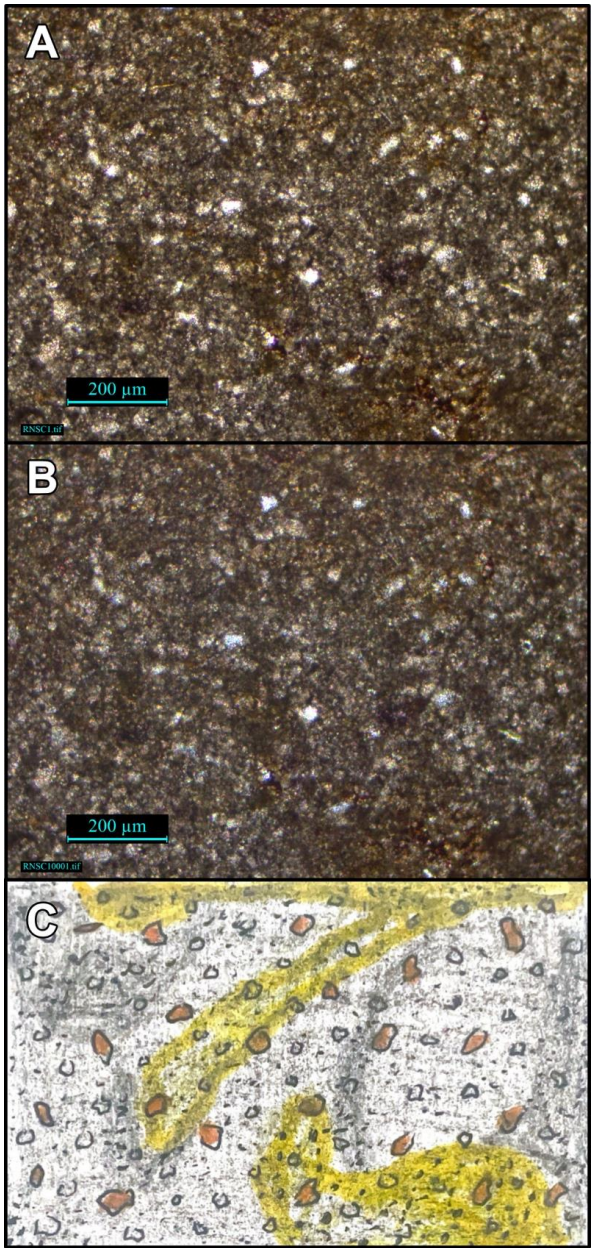

Figure 22: Sandy limestone, RNSC1

A) PPL; B) XPL, C) interpreted. This sample contains a matrix of sparry calcite and micrite with dispersed subrounded quartz crystals (orange). Some areas show presence of dead oil (yellow).

Dolostone 1,2; Questionable Zebra; Dark Limestone, Measles Rock 1,2

Outcrops in proximity to the Zebra limestone outcrops were studied to establish field relationships and assess if they showed any indication of early stages of Zebra limestone formation. Here, the outcrops are briefly described, and their locations are indicated in Figure 13. The Dolostone 1 and 2 outcrops are within the poorly outcropping zone. Dolostone 1 outcrop measures 0.4 meters in height and 8.2 meters in length. It is situated 20 meters east and 5.6 meters higher in elevation from Zebra D. It is a tan sandy dolostone, exhibiting a coarse-grained sand texture with 2-3 cm thick layers. Dolostone 2 outcrop measures 0.15 meters in height and 1 meter in length. It is located about 30 cm below Zebra limestone outcrop B. It rests directly atop a 50-centimeter-thick band of gypsum. This outcrop presents a light gray and fine-crystalline appearance. Questionable Zebra outcrop measures 0.4 meters in height, and 0.6 meters in length. It sits 1 meter above Zebra limestone outcrop C. It consists of a dark limestone outcrop with a few vugs and laminations which was initially interpreted as a potential Zebra limestone (thus its name), now it is considered to represent an early stage of the Zebra limestone formation process. The 'Dark limestone' outcrop measures 1.6 meters in height and 0.84 meters in length. This outcrop is located directly on top of Zebra limestone outcrop D. It is fine-crystalline and slightly petroliferous with massive bedding. The 'Measles Rock 1' outcrop measures 2.6 meters in height and 4.1 meters in length. It is found approximately 6 meters to the east of Zebra D and it consists of coarse crystalline tan dolostone covered in dark green spots (i.e., measles). The 'Measles Rock 2' outcrop measures 1.46 meters in height and 2.2 meters in length. It is located 4.5 meters east and 11 meters higher in elevation from Zebra C. This outcrop has interbedded dolostone and shale. The dolostone is coarse-crystalline and covered in green spots.

Petrography of Zebra limestones

As observed in outcrop and hand samples, Zebra limestone comprises a large variety of fabrics, color, chemical composition, and physical hardness (Figures 14-19, 23). It ranges from regular Zebra banding to cross-cutting relationships, with variations in banding thickness from 0.5 mm to 6 cm banding (Figure 15), vugs ranging from 1-2 mm (Figures 17C, 18H), and a multitude of colors, including white, dark grey, black, orange, red (Figures 14-21). The regular Zebra rocks crumble in one's hand (Figures 23A, B), while the irregular Zebra rocks (Fig. 23C - G) do not.

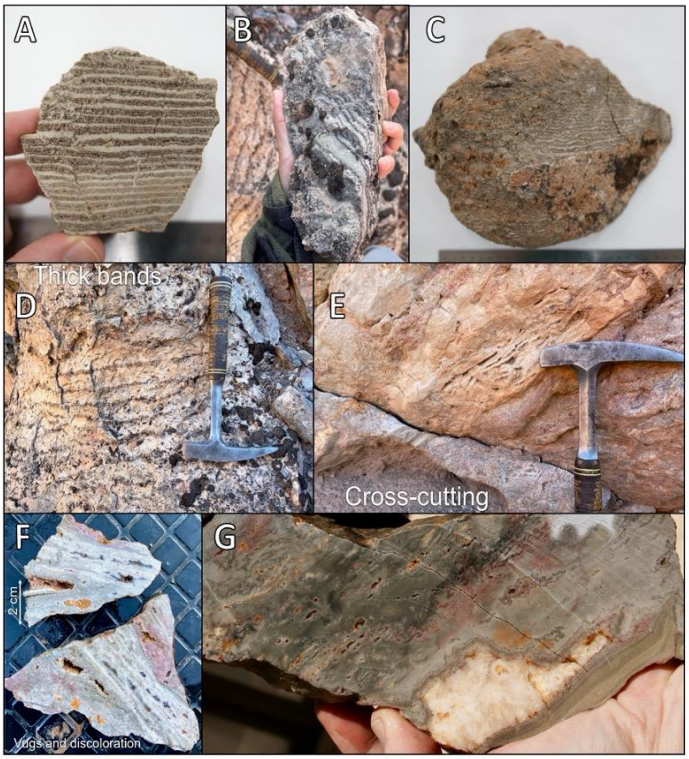

Figure 23: Variety of Zebra limestone in hand sample
In order of increasing variability: A) Regularly banded; B) Straight banded with variable thickness, with thick banding in background of image; C) Regularly banded transitioning into irregular banding, band thickness ~3 mm; D) Thick banded with white bands up to ~4 cm; E) Thick and irregular banding, vuggy and cross-cutting relationships; F) Irregular banding, vuggy, partially massive, red zones appear to contain sands from Chinle Formation; G) Banding barely recognizable, dark zones contain dead oil, vugs filled with white cement, lower right (above hand) shows zone with layered sediment infill.

The most spectacularly irregular sample was found at the base of Zebra limestone outcrop C in contact with a thin layer of shale with an underlaying gypsum layer. It shows a puzzling variety in fabrics, colors, and chemical/mineralogical components: there are some dark colored, petroliferous finely crystalline zones, large calcite-cemented vugs, and what appears to be sedimentary infill (Figure 23G, 24).

Figure 24: 'All-in-one' Zebra limestone

Microscopic analysis of slabs and thin sections of Zebra limestone samples focused on deciphering the genesis of this complex lithology.

Regularly banded Zebra limestone

Zebra limestone outcrop A (Figures 13, 14) is best represented by thin section sample KLGP013A (Figure 25), revealing distinctive alternating bands of micrite and rounded sparry calcite. Varied zones of re-crystallization are evident, ranging from micrite to micro-spar in arbitrary spaces. Notably, dead oil is prominently concentrated along the edges of the sparry

calcite, indicated by yellow stains. This leads to the conclusion that during re-crystallization, oil permeated along crystal boundaries, reaching open pore spaces. There are spots that display more intense calcite (red) and iron (blue) staining. These spots are particularly noticeable within the finer-crystalline areas of the matrix. The blue staining suggests reduced conditions, allowing for the substitution of calcium with ferrous iron (Fe^{2+}), potentially coinciding with the incorporation of magnesium to form dolomite crystals that only display the ferrous iron stain, but not red colors from calcite. In this scenario, the intense red colors might be caused by unmixing of high-magnesium calcite to form low magnesium calcite (more intense red) and ferroan dolomite (blue).

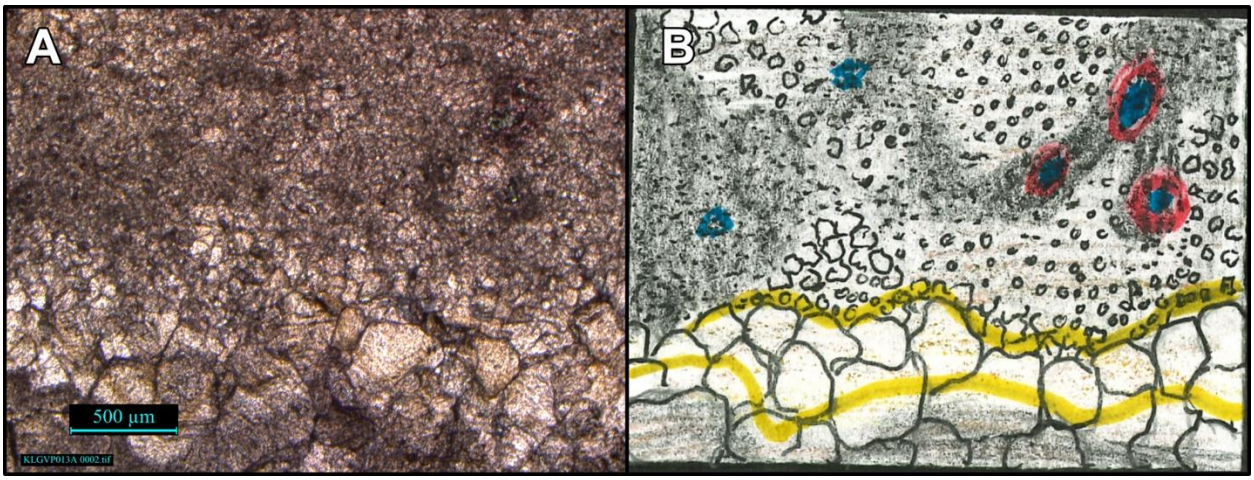

Figure 25: Regularly banded Zebra Limestone from outcrop A, KLGP013A
A) in PPL, B) interpreted. This sample exhibits distinct alternating bands of micrite and rounded sparry calcite. Varied zones of re-crystallization are evident, ranging from micrite to micro-spar. Dead oil is concentrated along the edges of the sparry calcite, indicated in (D) by yellow discoloration. Spots displaying more intense calcite (red) and iron (blue) staining are noticeable within the finer-crystalline areas of the matrix. The blue staining indicates reducing conditions, enabling calcium substitution with ferrous iron and possibly magnesium incorporation to form dolomite crystals. Dolomite only shows the ferrous iron stain, not the red colors typical of calcite. The intense red hues may result from high-magnesium calcite unmixing to low magnesium calcite (more intense red) and ferroan dolomite (blue).

The nearby Zebra limestone outcrop B (Figure 13, 15), which also displays regularly banded Zebra limestone is best represented by thin section sample RNCL1 (Figure 26), showcasing similar alternating bands of micrite and rounded sparry calcite. Unlike the sample from Zebra limestone outcrop A, the micrite in this sample maintains a consistent size throughout. The sparry calcite exhibits dark edges surrounding most crystals. Dead oil is once again observed along

the edges of the sparry calcite, as well as within the dark areas surrounding the crystals, further contributing to the complex geological characteristics of this outcrop. Potentially, some the dark edges can be attributed to the presence of opaque iron oxides, which may have formed at a stage where calcite with ferrous iron was exposed to oxidizing conditions.

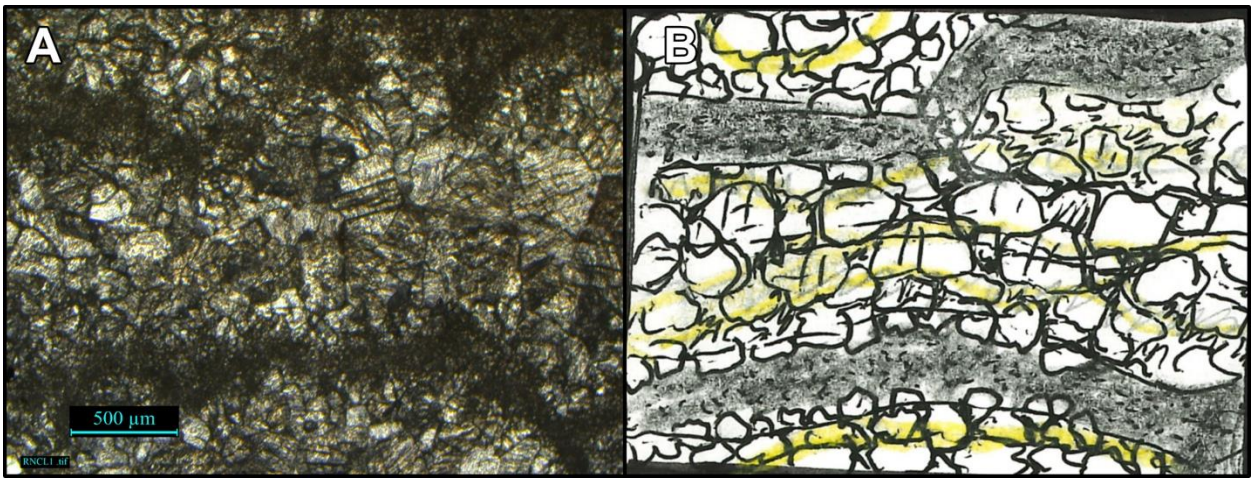

Figure 26: Regularly banded Zebra Limestone from outcrop B, RNCL1
A) in PPL, B) interpreted. Alternating bands of micrite and rounded sparry calcite. The sparry calcite exhibits dark edges surrounding most crystals. Dead oil is observed along the edges of the sparry calcite, as well as within the dark areas surrounding the coarser calcite crystals.

Irregular Zebra Banding

RNSZV (Figure 27), was taken from Zebra limestone outcrop C (Figures 13, 19), showing irregular bands of micrite, elongated angular calcite crystals and rounded sparry calcite. Yellow stains arranged in lines indicate presence of oil along crystal boundaries, coating the surface of the elongated calcite crystals (Figure 22C, E). Zebra banding varies significantly in size and starts to show vuggy and cross cutting relationships.

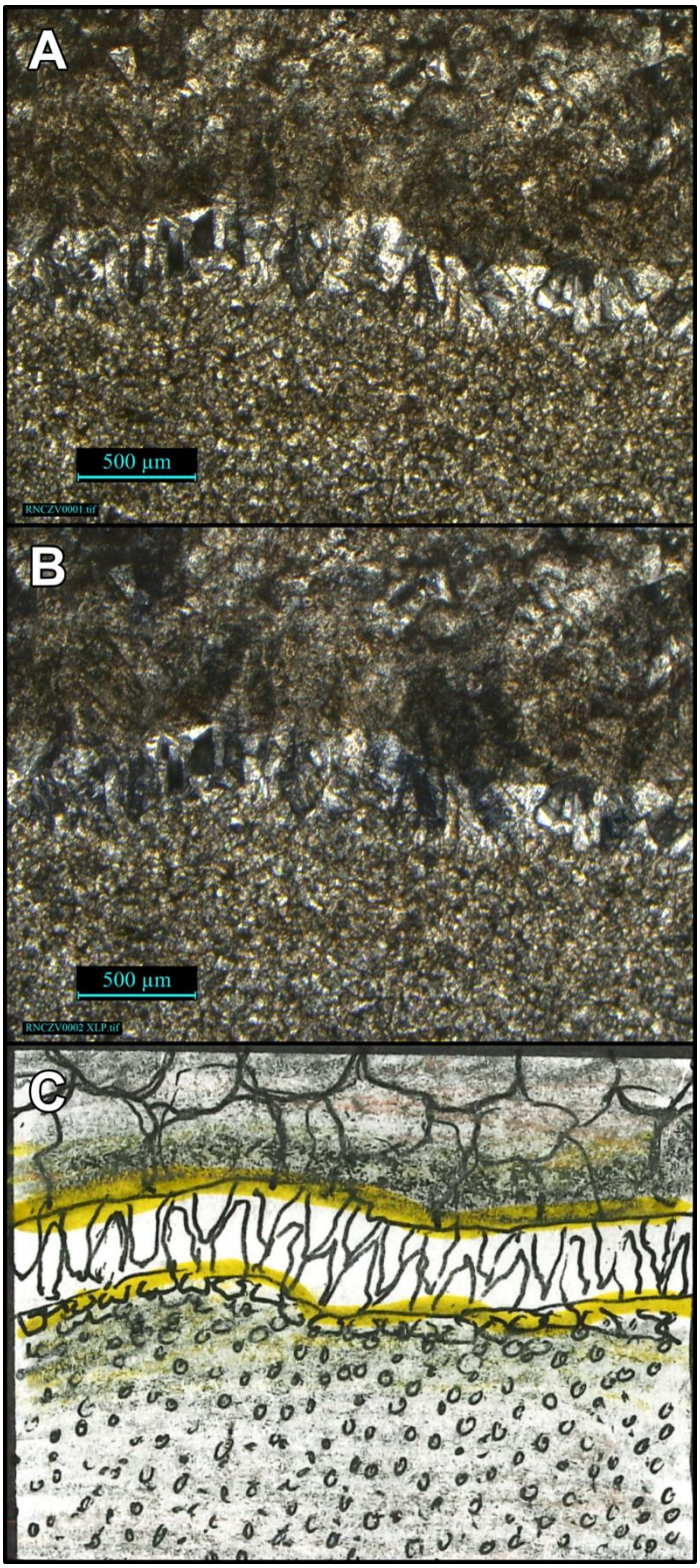

Figure 27: Irregularly banded Zebra from Zebra Limestone C outcrop, RNSZV
A) PPL; B) XPL, C) interpreted. This s sample exhibits irregular bands of micrite alongside elongated angular calcite crystals and rounded sparry calcite. Yellow stains arranged in lines shows the presence of oil along crystal boundaries, coating the surface of the elongated calcite crystals.

Stylolitic New Zebra samples

Both RNNZ 1 and RNNZ 2 (Figure 28), originate from Zebra limestone outcrop D (Figures 13, 20), sharing a common geological history. A general feature is the presence of stylolites containing abundant dead oil and to a lesser extent clay seams. The accumulation of dead oil in stylolites indicates that hydrocarbons moved into clay seams within former (now pressure-dissolved) carbonate layers. In sample RNNZ 1, the presence of subrounded sparite is evident, exhibiting slight differences in crystal size, with slightly larger crystals where stylolites are present. The subrounded shape of the sparite crystals is important because it could indicate rounding due to a later stage of corrosion, for example during oil migration or *in situ* oxidation of hydrocarbons, creating acidity. Additionally, a few quartz grains are observed within the sample, however, differentiating between detrital and authigenic origin was not possible. Sample RNNZ 2 showcases a vug filled with sparry calcite, set against a backdrop of micritic limestone. This matrix also contains a scattering of quartz crystals. The 'Stylolitic New Zebra' samples display both features similar to regularly banded Zebra limestone, as well as the irregular vuggy zebra with dead oil against pushed to the edges of the coarser calcite crystals.

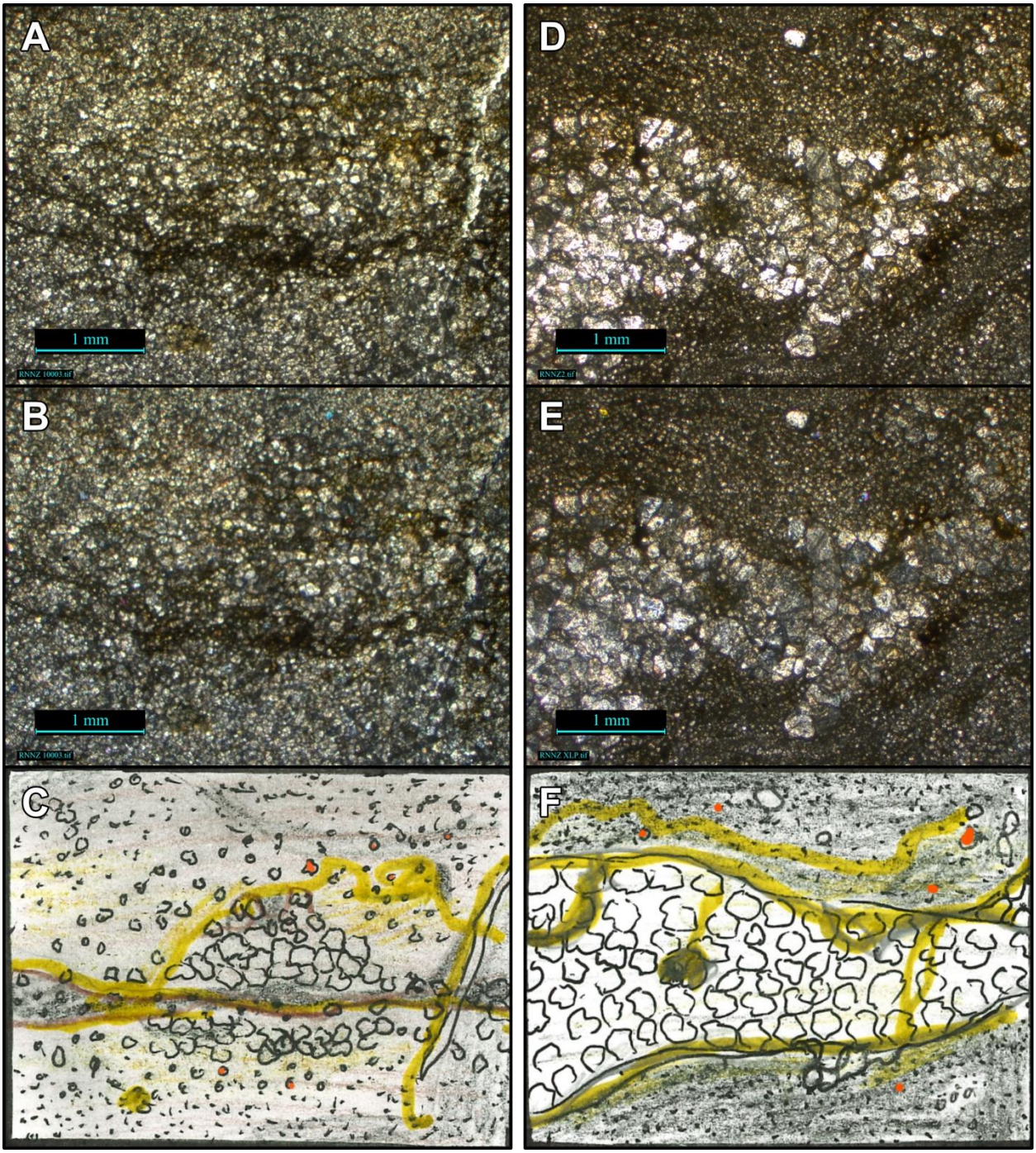

Figure 28: Stylolitic Zebra

Left: Stylolitic New Zebra from Zebra Limestone D outcrop, RNNZ1: A) PPL; B) XPL, C) interpreted. This sample reveals sparite composed of mediumcrystallinecalcite, displaying subtle variations in crystal size. Crystals appear slightly larger in areas where stylolites are present. These stylolites contain dead oil and clay seams. Additionally, a few quartz grains, depicted orange in C, are present.

Right: Vug in Stylolitic New Zebra from Zebra Limestone D outcrop, RNNZ2: D) PPL; E) XPL, F) interpreted. This sample highlights a vug filled with sparry calcite, surrounded by a matrix composed of micritic limestone. Scattered throughout the matrix are quartz crystals. Additionally, dead oil is observed, located at the edges of the coarser calcite crystals.

'All-in-one' Zebra

In the 'All-in-one' Zebra, the presence of separated zones with red discoloration (i.e., iron oxide visible in hand sample and thin section) and blue stains (ferrous iron, Fe^{2+}) indicate the presence of iron (Figure 29). This is confirmed by XRF imagery (see section on XRF results below). The blue color suggests reducing conditions, which may have prevailed during recrystallization and displacement of oil, keeping the environment oxygen-free and reducing ferric iron (Fe^{3+}) to ferrous iron (Fe^{2+}). This phenomenon is particularly evident at the peripheries of the calcite crystals surrounding the large vug filled with saddle dolomite, as observed in samples BC-VZC1 and BC-VZC2 (Figure 29).

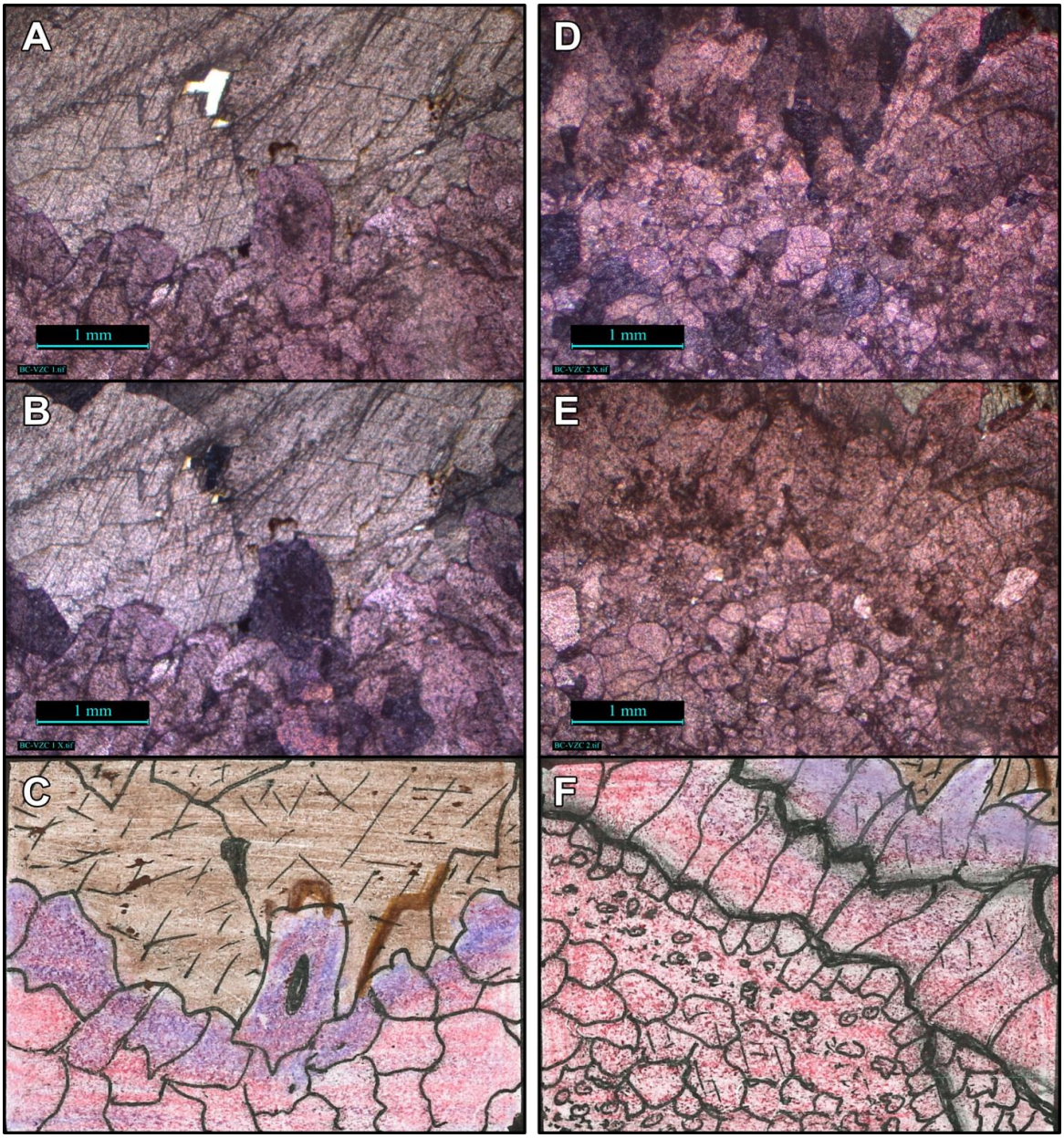

Figure 29: 'All-in-one-Zebra'

Left: Karst Feature in 'All-in-one' Zebra from Zebra Limestone outcrop C, BC-VZC1: A) PPL; B) crossed polarized light (XPL), C) interpreted. This sample shows part of an infilled karst cavity. Distinct zones with red discoloration (iron oxide) and blue stains (ferrous iron, Fe^{2+}) indicate the presence of iron. This is particularly evident at the peripheries of the calcite crystals surrounding saddle dolomite crystals. These dolomite crystals measure 1-2 mm in size. Within the boundary between the dolomite infill and the coating of calcite silt, a few coarse calcite crystals with impurities at the center are observed. These crystals potentially became dislodged from the roof of the karst cavity.
Right: Karst Feature in 'All-in-one' Zebra from Zebra Limestone outcrop C, BC-VZC2: D) PPL; E) XPL, F) interpreted. In this sample, I observe part of an infilled karst cavity. At the right top corner, saddle dolomite is visible with a brown line indicating oil within clay seams around the dolomite crystals. Surrounding the dolomite, subrounded calcite crystals display red discoloration (iron oxide) and blue stains (ferrous iron, Fe^{2+}), indicating the presence of iron. Below these features to the lower left are layers of silt-sized calcite crystals.

In contrast, in samples BC-VZB (Figure 30), the staining appears concentrated in a clay seam within the coarser calcite crystals. Additional evidence for the presence of dead oil is discernible in sample BC-VZB, where the oil has been pushed towards the edges of the finely-crystalline layers, accumulating as coatings on the coarser crystal.

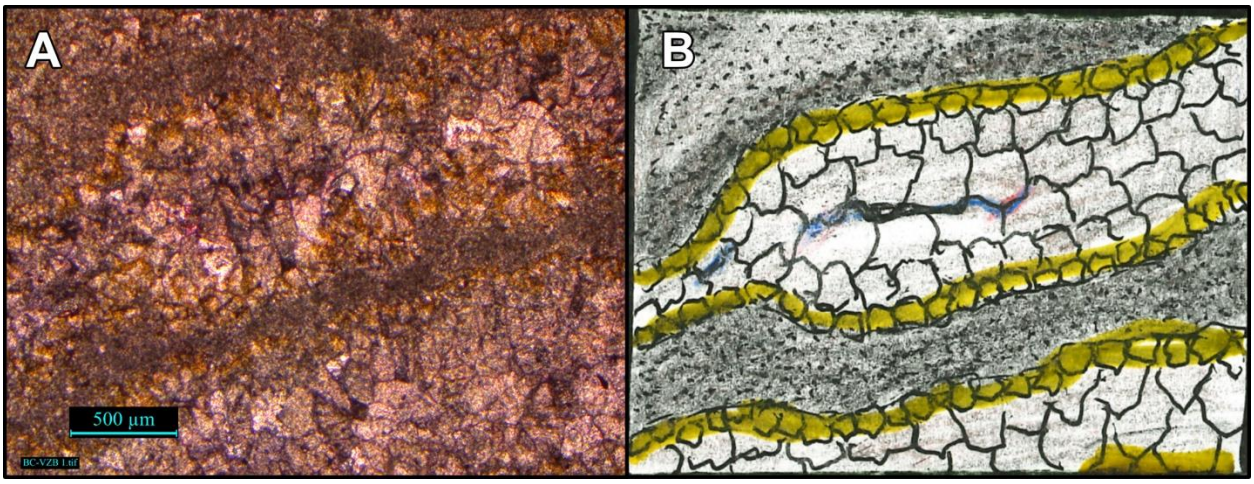

Figure 30: Vuggy Zebra from Zebra Limestone outcrop C, BC-VZB
A) plain polarized light (PPL); B) interpreted. The sample displays alternating bands of micrite with sparry calcite. Notably, dead oil is confined at the edges of the fine-grained layers, accumulating as a coating on the coarser crystalline, highlighted in yellow in (B). The presence of separated zones with red discoloration (iron oxide) and blue stains (ferrous iron, Fe^{2+}) indicate the presence of iron. The staining is concentrated in a clay seam within the coarser calcite crystals.

Karst cavities are most prominently observed in sample BC-VZC1 (Figure 29). They were later infilled by layers of silt-sized calcite crystals (prominently displayed in BC-VZC2, Figure 29), that experienced several stages of cementation and overgrowth followed by saddle dolomite. The saddle dolomite crystals measure 1-2 mm in size. Within the boundary between the dolomite infill and the coating of the calcite silt a few coarse calcite crystals with impurities at the center were identified, similar in appearance to those observed from the 'Questionable Zebra' and 'Dolostone 1 and 2' outcrops (see below). Potentially, these crystals became dislodged from the roof of the karst cavity.

Questionable Zebra sample

Sample RNQZ (Figure 31) was taken from the Questionable Zebra outcrop (Figure 13). It comprises micro-spar to coarse-crystalline calcite which tend to be rounded. Between some of the crystals there are clay seams. These seams host coarser-crystalline calcite, notable for impurities concentrated at their centers. There is the prominent dark brown stain covering most of the coarser crystals, interpreted to represent oil. The boundary for this dark discolored zone does not align with the clay seam but follows a similar trajectory. Correspondingly, on the opposite side of the seam, light brown spots are seen in the finer crystals. These observations can be interpreted as to be caused by oil migrating away from the finer crystals creating the dark brown stained zone, allowing for oxidation of ferrous iron to ferric iron in those finer crystals, creating the light brown iron oxide spots.

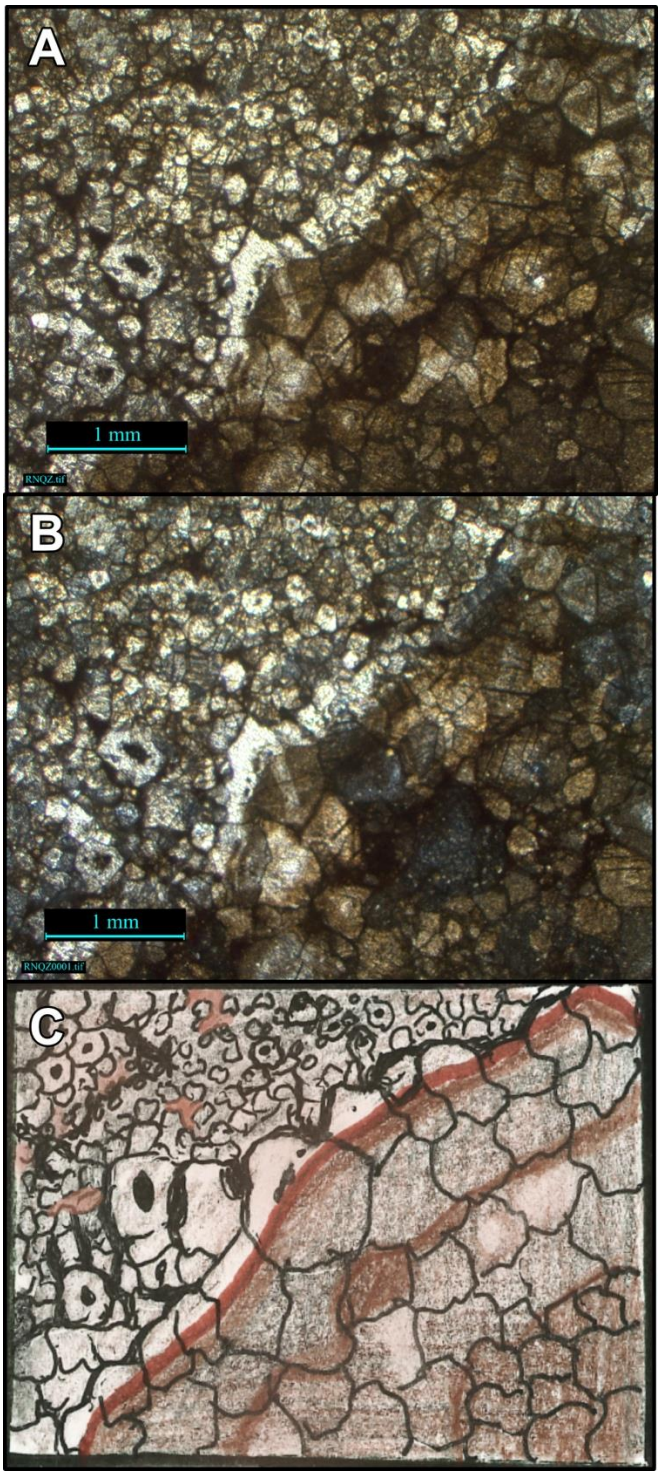

Figure 31: Sample from the 'Questionable Zebra' outcrop, RNQZ

A) PPL; B) XPL, C) interpreted. The sample contains rounded micro-spar to coarse calcite crystals, often with clay seams between them. These seams host coarser calcite crystals with noticeable impurities concentrated at their centers. A dark brown layer of oil covers most of the coarser crystals. There is also a clay seam that doesn't align with the oil but follows a similar path. There are light brown iron oxide spots observed in the finer crystals on the opposite side of the seam.

Petrography of dolostones from poorly outcropping zone

RNSD1 (Figure 32), was obtained from outcrop Dolostone 1 (Figure 13). It displays a microcrystalline dolostone matrix with dispersed subrounded quartz crystals. The sample presents a striking dark brown coating, likely dead oil, that covers approximately 70% of its surface. This coating stands out prominently, creating a stark contrast against the rest of the sample.

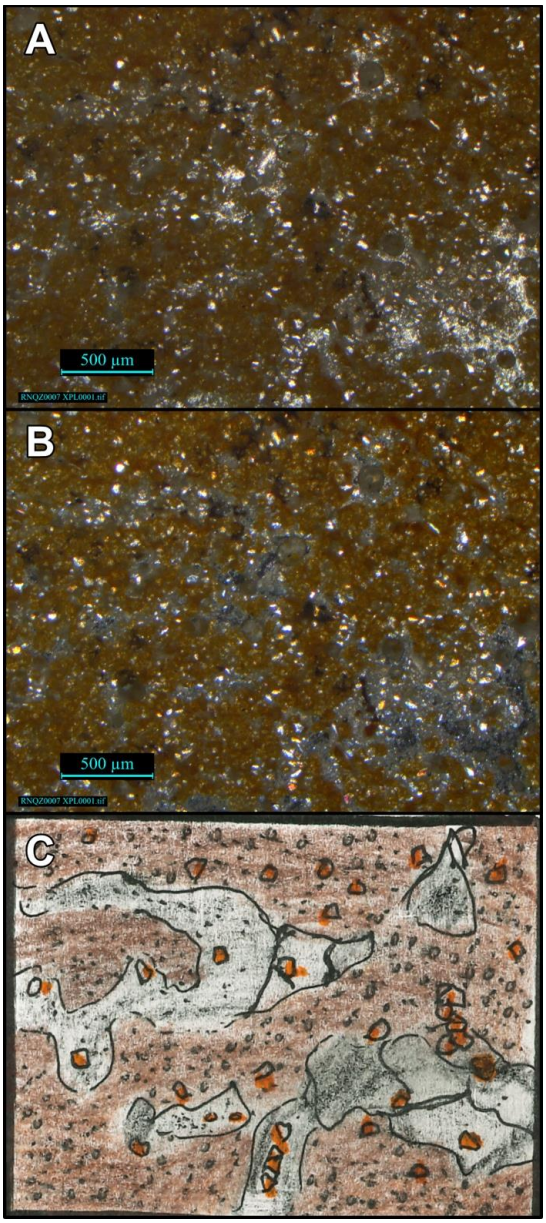

Figure 32: Sample from 'Dolostone 1' outcrop, RNSDL

A) PPL; B) XPL, C) interpreted. The specimen features a microcrystalline dolostone matrix interspersed with subrounded quartz crystals. Notably, a prominent dark brown coating of dead oil covers approximately 70% of its surface.

Sample RNCZDOLO (Figure 33), sourced from Dolostone 2 (Figure 13), showcases a microcrystalline dolostone matrix distinguished by zones containing larger crystals. Scattered throughout the matrix are anhedral pyrite crystals, that form when ferrous iron (Fe^{2+}) comes into contact with sulfide, which is generated by sulfate reduction. The presence of sulfur has been observed through XRD and XRF and extraction of carbonate-associated sulfate (see sections on XRD and XRF below). Moreover, a dark brown layer of dead oil envelopes the entire area of the coarser calcite crystals. In this zone there are areas of lighter coverage, revealing impurities, likely clay minerals, concentrated at the centers of their crystals within an isolated calcite layer in the dolostone. The impurities indicate the onset of the recrystallization process, where coarser calcite crystals develop, trapping accompanied impurities at their cores. The presence of dead oil and pyrite minerals in the dolostones indicates that sulfate reduction took place within those lithologies.

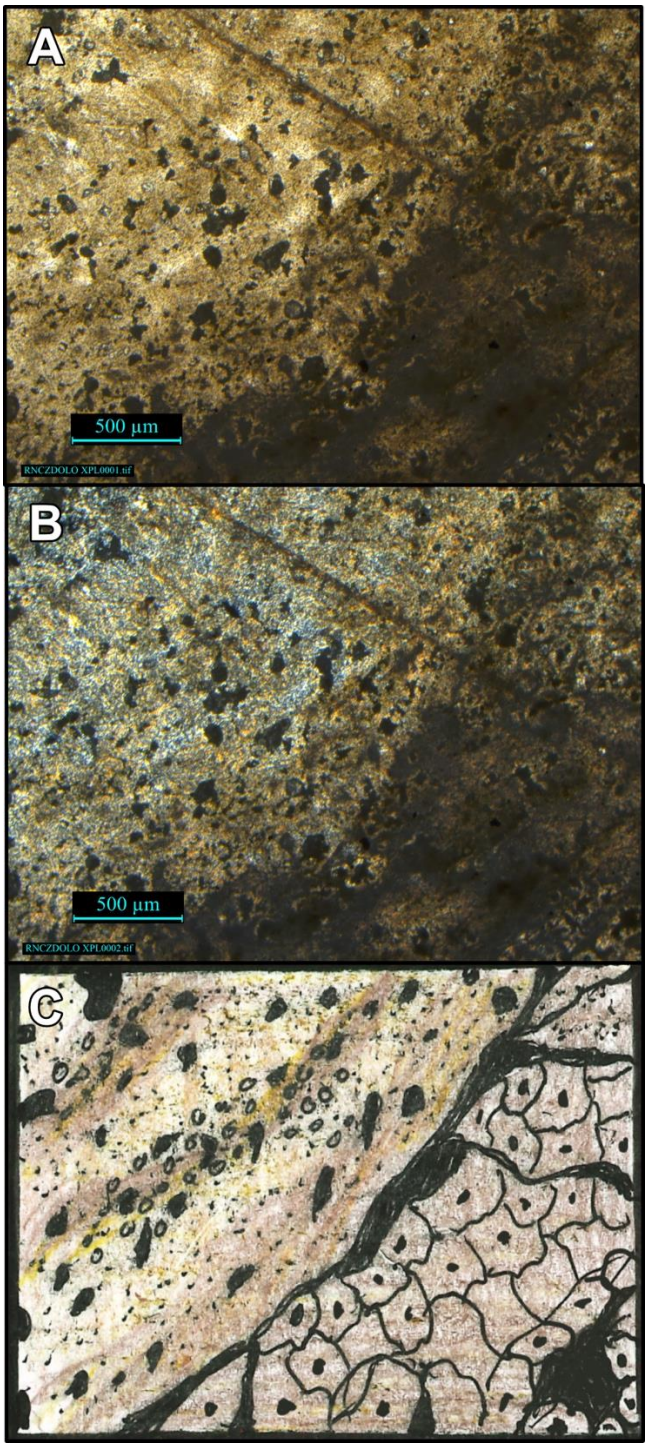

Figure 33: Dolostone with Calcite Layers from Dolostone 2 outcrop, RNCZDOLO
A) PPL; B) XPL, C) interpreted. The microcrystalline dolostone matrix contains zones with larger crystals. Scattered throughout the matrix are anhedral pyrite crystals. Additionally, there is a dark brown layer of dead oil which envelopes the entire area surrounding the coarser calcite crystals. Within this zone, there are areas of lighter coverage, revealing impurities concentrated at the centers within an isolated calcite layer in the dolostone.

Petrography of Dark Limestone

Samples RNDL1 and RNDL2 (Figure 34), were taken from the 'Dark limestone' outcrop (Figure 13). Sample RNDL1 is a micritic limestone, with randomly distributed zones of clusters that display a variety of coarser crystals. There are patches of packed fine calcite crystals, micro spar, and coarse calcite crystals up to a mm in size. A few quartz crystals with orange discoloration are visible throughout the sample. Impurities like those in RNCZDOLO and RNQZ are observed at the center of the finer calcite crystals but only along clay seams in the limestone. The coarser crystals have clear centers more like the calcite crystals in the Zebra patterns. Sample RNDL2 shows fine to coarsely crystalline, rounded sparry calcite with a micritic matrix. The coarse crystals display impurities, likely clay minerals, at their centers. The patterns observed for the samples from the 'Dark limestone' indicate that they represent an early stage of recrystallization after transformation to micritic limestone from microcrystalline dolostone.

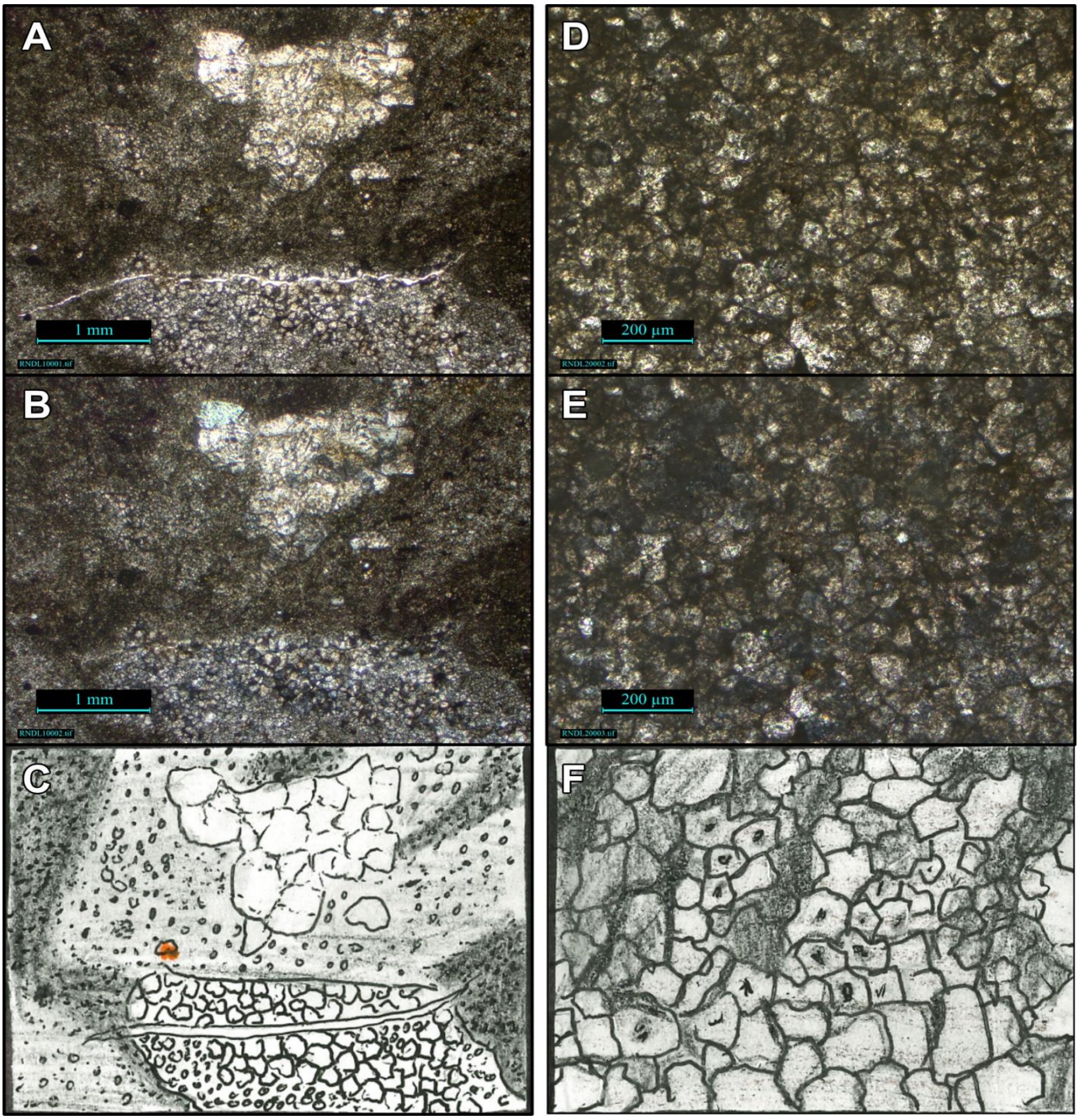

Figure 34: Samples from 'Dark Limestone' outcrop

Left: Limestone with Varying Zones of Crystallization from the Dark Limestone outcrop, RNDL1: A) PPL; B) XPL, C) interpreted. This sample features a micritic limestone matrix with randomly dispersed clusters showcasing a variety of coarser crystals. Among these clusters are patches of densely packed fine-crystalline, micro spar, and coarse calcite crystals measuring up to a millimeter in size. Additionally, scattered throughout the sample, one can observe a few quartz crystals exhibiting orange discoloration.

Right: Limestone from Dark Limestone outcrop, RNDL2: D) PPL; E) XPL, F) interpreted. This sample showcases a range of fine to coarse rounded sparry calcite crystals embedded within a micritic limestone matrix. Throughout the matrix, bands of concentrated clay zones are observed. The coarse crystals exhibit impurities, likely clay minerals, concentrated at their centers.

Petrography of Measles Rock

Sample RNMR1 (Figure 35), originates from outcrop Measles Rock 1 (Figure 13). It consists of a microspar matrix with a zone of coarse calcite crystals that are 1.5-2 mm in size. Surrounding these crystals are clay seams. A distinctive spotted texture, referred to as measles spots, is observed at the top right of the sample. Such spots are characterized by a dark clay rim encircling slightly larger rounded calcite crystals. The appearance of the measles texture may be attributed to an initial stage of recrystallization.

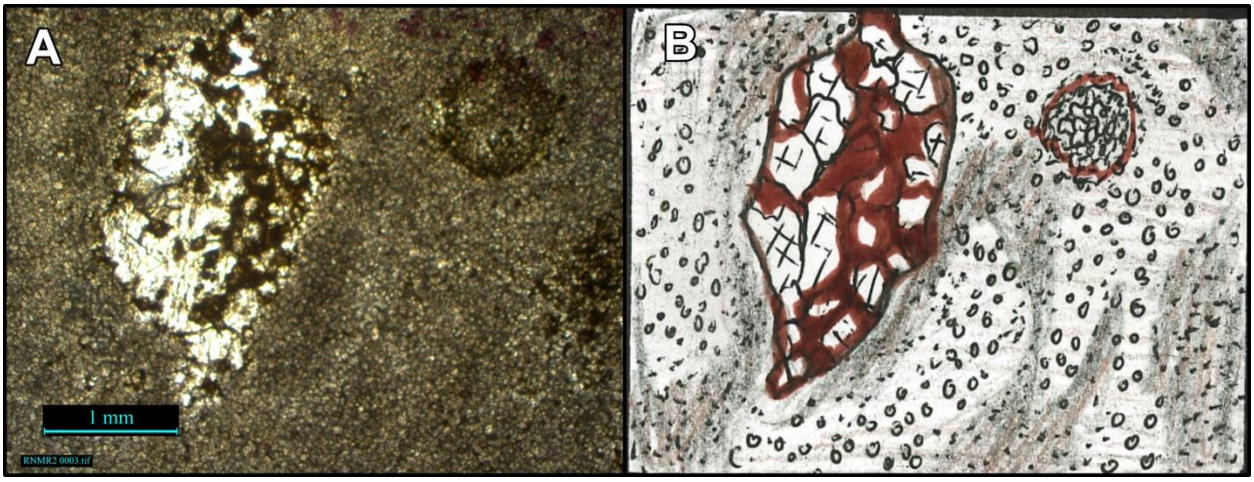

Figure 35: Measels spot from Measles Rock 1 outcrop, RNMR1-2
A) in PPL, B) interpreted. The sample comprises a microsparitic matrix with a zone of coarse calcite crystals (1.5-2 mm) surrounded by clay seams. A distinct spotted texture, referred to as measles spots, is present at the sample's top right, featuring a dark clay rim encircling slightly larger rounded calcite crystals.

Petrography of gypsum caprock

One gypsum caprock sample RNCZGYP (Figure 36), was obtained from the outcrop beneath of Zebra limestone outcrop B, as depicted in Figure 16C. It consists of a gypsum matrix which is host to an array of calcite crystals that vary significantly in size, spanning from fine-crystalline to coarse subhedral crystals. A potential mechanism for the presence of these crystals is gypsum dissolution in presence of carbonate-rich fluids, leading to growth of calcite crystals. While oxidation of organic matter coupled to sulfate reduction is not excluded as potential driver for carbonate formation, there is no dead oil in close vicinity to the gypsum, and there are also no

pyrite crystals that would indicate that such a process took place. An alternative process, driven by anhydrite-gypsum conversion and concomitant increase in carbonate concentrations is proposed in the section on links between anhydrite-gypsum conversion and the carbonic acid system.

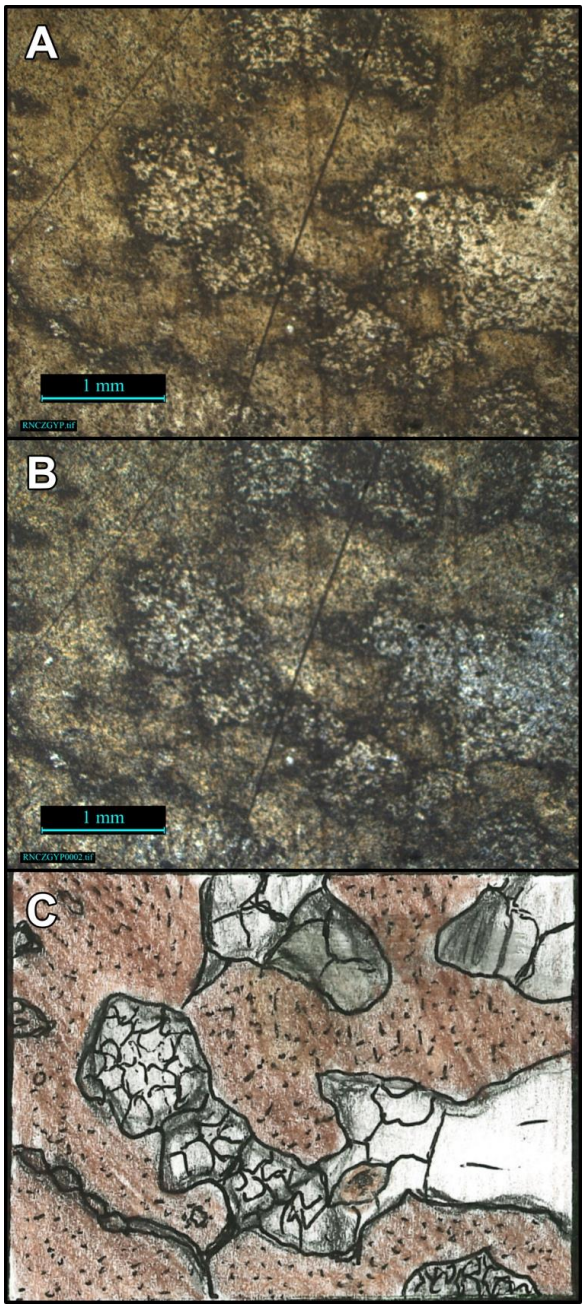

Figure 36: Gypsum with Calcite Crystallization found beneath Zebra Limestone B outcrop, RNCZGYP
A) PPL; B) XPL, C) interpreted. The sample consists of a gypsum matrix hosting an assortment of calcite crystals with significant variation in size, ranging from fine-grained to coarse subangular grains. The calcite zones are encased by clay.

XRD AND CONTENT OF CARBONATE-ASSOCIATED SULFATE IN ZEBRA LIMESTONE

Extracted accessory minerals from Zebra limestone and gypsum predominantly consist of quartz (Figure 37). However, microscopy of the extracted minerals showed that quartz grain shapes from Zebra limestone have a shattered appearance, which is dissimilar to doubly-terminated quartz from gypsum. Thus, the presence of quartz in both lithologies does not unequivocally imply that one replaced the other. Micas (with an optimal match for phengite) was detected in samples of both Zebra limestone and gypsum, and illite was detected in Zebra Limestone only. It is interesting to note that considerable effort has been made into the study of mica such as phengite as a syngenetic product of hydrothermal carbonate rock formation (Park et al., 2020), and of the formation of mica and clay minerals during alkaline diagenesis in reservoirs (Zhu et al., 2015). Presence of mica-like illite (a clay mineral) has been mentioned in a study of clay minerals associated with marine evaporites (Bodine, 1985). Most strikingly, the presence of illite is a marker for oil formation because in shales it forms in the same temperature range as oil is generated, allowing to date oil generation based on potassium-argon (K-Ar) dating of illite (Pevear, 1999). The implication of these findings is that Zebra limestone replaced a precursor rock that experienced temperatures conducive for oil genesis in shales.

oil genesis in shales.

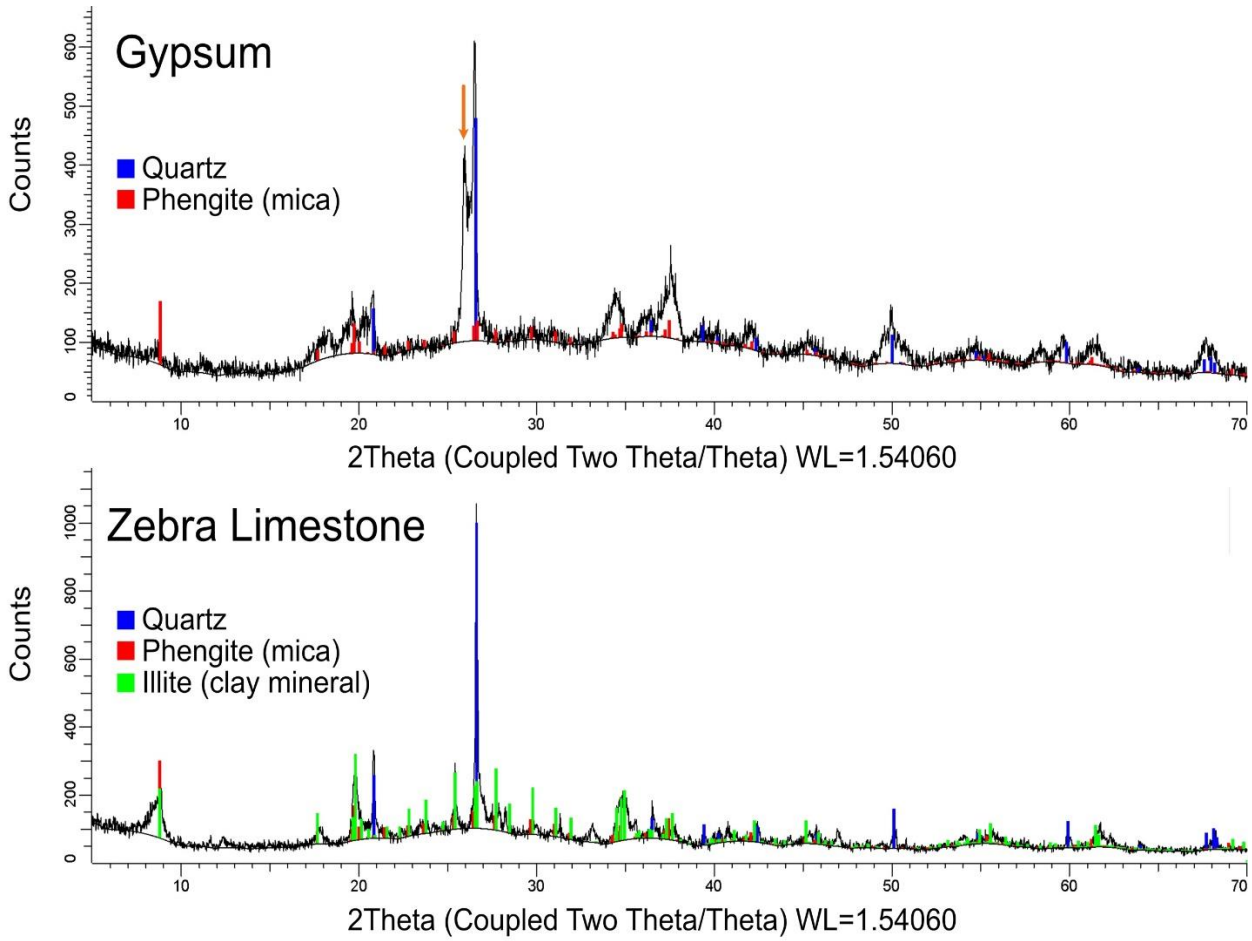

Figure 37: XRD of Zebra limestone and gypsum caprock
Quartz and mica minerals are found both in gypsum and Zebra limestone. Illite, a clay mineral, was only positively identified in Zebra limestone. Gypsum contains a component that I could not identify (orange arrow indicates XRD peak).

During the extraction of accessory minerals, I also determined the sulfate content (CAS) of Zebra limestone samples, finding an average value of 548.6 ppm, which falls in the lower part of the range found by Lerer (2017).

MICRO-XRF

Micro-X-ray fluorescence analysis were performed on a regularly banded Zebra limestone from Zebra limestone outcrop A and the 'All-in-one' Zebra limestone sample from Zebra

limestone outcrop C. As expected, the regularly layered Zebra limestone displays presence of calcium throughout the sample (Figure 38). Iron is present in the coarse-crystalline section of the sample, with a zone that lacks iron and sulfur at the transition from coarse to fine-crystalline (Figure 38D).

Calcium is also present in all parts of the 'All-in-one' Zebra limestone sample (Figure 39). Iron is highly abundant in the saddle dolomite that fills the vug, whereas strontium appears to dominate in the first cement layer that coats the void (Figure 39D, F). The presence of strontium indicates that this layer may originally have been aragonite. Aragonite has been documented to form in karstic systems under vadose (water-undersaturated) conditions (Perrin et al., 2014). The strontium-enriched band is followed by a zone with slightly elevated manganese levels, indicating the incorporation of manganese into carbonate, likely as manganese-II (Mn^{2+}), i.e., in its reduced form. Prevailing reduced conditions are also indicated by the iron in the saddle dolomite, as ferrous iron (Fe^{2+}) can substitute for calcium and magnesium. The zone with silty carbonate particles is characterized by varying element distributions that, except for sulfur, align with the observed layering (Figure 39B, C, E, G, H). Silica is rare, indicating no incorporation of siliciclastics in the rock (Figure 39C, D).

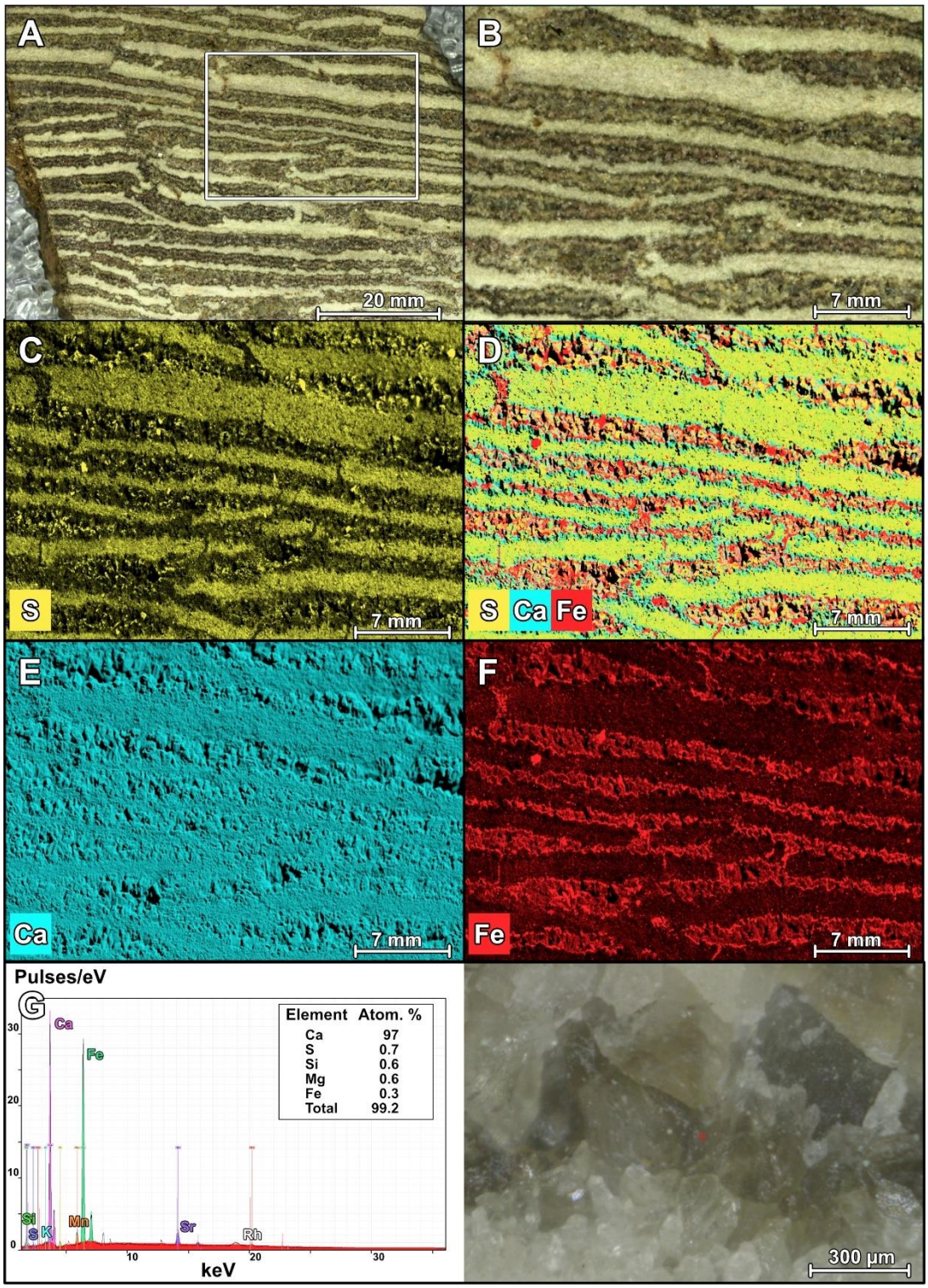

Figure 38: XRF of regularly banded Zebra limestone

Calcium indicated in blue is present in the entire sample. Dominantly iron (Fe) is indicated by red, except in the presence of sulfur (S; likely as carbonate-associated sulfate) whose yellow color results in a green interference color. Green areas correspond to the fine-crystalline (light colored in slab; A) portions of the Zebra limestone, red areas to the coarse crystalline (dark in slab, A) portions. At the margin between coarse and fine-ed zones neither iron (Fe) nor sulfur (S) appear to be present, resulting in a blue rim (presence of calcium, Ca) seen in D.

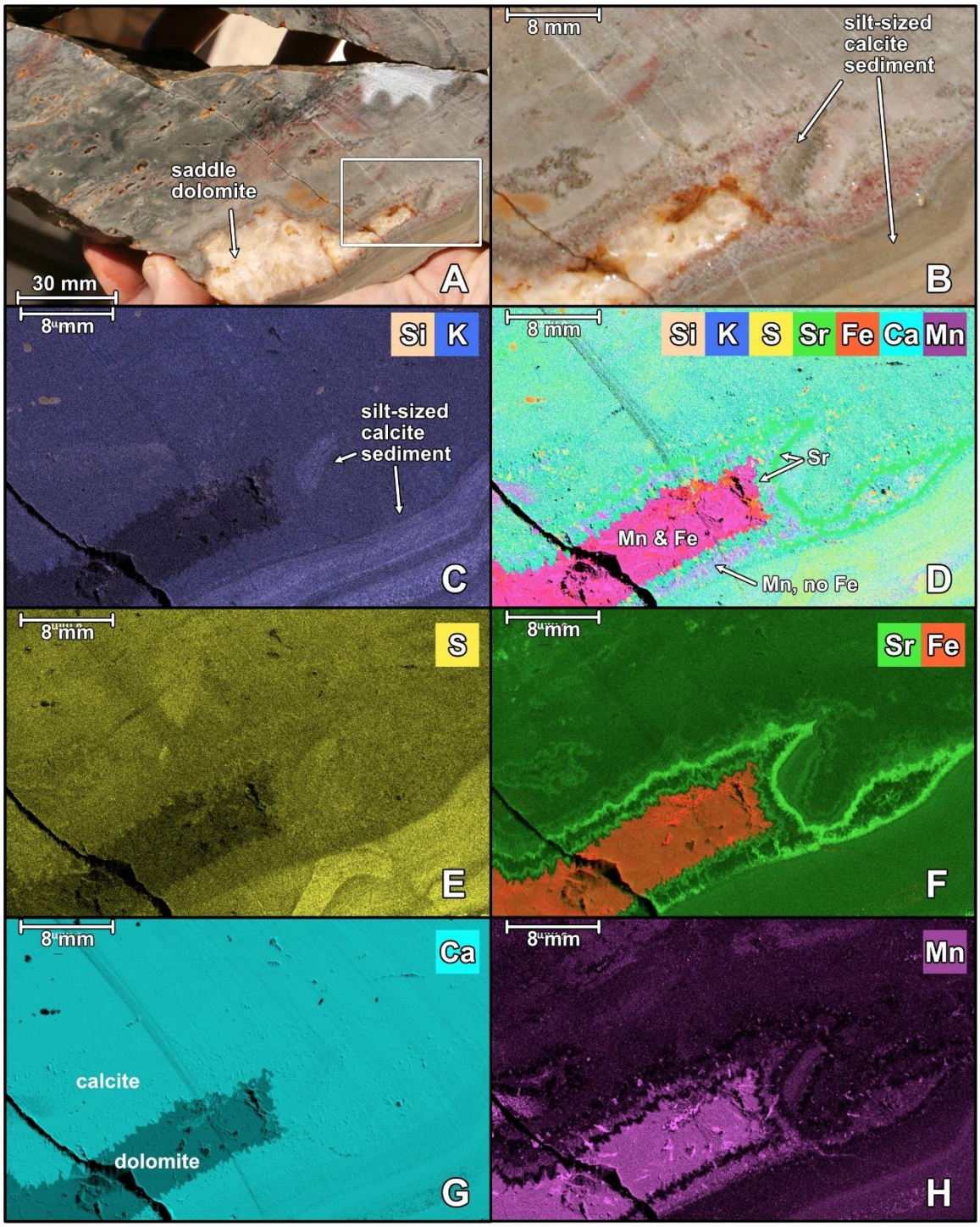

Figure 39: XRF of 'All-in-one' Zebra limestone

Calcium (indicated by blue color) is present throughout the investigated area of the sample. Iron (indicated in red) is highly abundant in the vug, strontium (green) shows up in the first cement layer that coats the void. The strontium-enriched band is followed by a zone with slightly elevated manganese levels (magenta). Silica (light orange) is rare.

Discussion

The discussion follows and addresses the three postulated hypotheses, namely that

- (H1) Zebra limestones at the Bridge Canyon location in Gypsum Valley are the result of a succession of alterations,
- (H2) the inverse dark-light color banding of the Bridge Canyon Zebra limestone is caused by 'self-cleaning' of remineralization, and
- (H3) Zebra limestone genesis is linked to the conversion from anhydrite to gypsum caprock.

WHAT TYPE OF ROCK WAS REPLACED BY ZEBRA LIMESTONE?

For H1 to be supported, Zebra limestone must have replaced a precursor for which reasonable arguments of its existence can be presented. Based on the field relationships it is evident that the Zebra limestone replaced a precursor lithology that was located within, but at the base of the dolostone/dolomudstone/shale zone, just above a band of shale that varies in thickness and is located atop the gypsum caprock. The likely candidate for the replaced rock is dolostone. In the field it was observed that there were petroliferous carbonate rocks (both dolostone and limestone), in the poorly outcropping zone above and sometimes within the Zebra limestones. In this zone there is a distribution of dolostone as the uppermost carbonates, whereas the bottom of the zone (closest to the Zebra fabric) contains exclusively limestones. Moreover, at the top of Zebra B and Zebra D outcrop, there is direct contact between Zebra-textured rocks and dark limestone. In the limestone at the top of Zebra limestone outcrop B, two distinct zebra bands, each approximately 1 mm in size, were observed running along the contact between zebra fabric and the overlying dark limestone (see Figure 40). Thin sections revealed evidence for recrystallization in the limestones,

showing varied grain sizes and distinct zones of recrystallization, indicating a process similar to Ostwald-ripening where larger crystals grow at the expense of smaller crystals (Morse and Casey, 1988).

Figure 40: Zebra limestone interfingering with dark limestone
Direct contact between Zebra-textured rocks and dark limestone. In the limestone at the top of Zebra limestone outcrop B, two distinct zebra bands, each approximately 1 mm in size, were observed running along the contact between Zebra fabric and the overlying dark limestone.

Based on these observations, it is proposed that petroliferous dolostones from the base of the poorly outcropping dolostone/dolomudstone/shale zone are first replaced by calcite, which is progressively overprinted by the Zebra fabric. Alternatively, it is possible that there is an internal stratigraphy to the that zone with petroliferous limestones at its base. It is known that in the Paradox Formation, the black shales can be correlated from an evaporite facies, consisting of 70 to 80 percent halite, into a carbonate facies which is 70 to 80 percent limestone (Hite and Buckner, 1981). 'Salt beds' in the Paradox Formation layered evaporite sequence represent stages in a partial or complete evaporite cyclothem, grading laterally through anhydrite, dolomite, and limestone facies. Depending on its position in the basin, a bed may show a similar vertical transition. As a rule, the limestone and dolomite facies are not present in the cyclothems in the deeper part of the salt basin (Hite, 1960), however the possibility has not been excluded.

WHAT IS THE TEMPORAL RELATIONSHIP BETWEEN OIL GENERATION, OIL MIGRATION AND ZEBRA LIMESTONE FORMATION?

For H1 to be supported, a feasible timeline that accommodates both oil generation, oil migration, and Zebra limestone must be presented. This timeline must reconcile several critical observations:

- Numerous dolostone samples in the poorly outcropping dolostone/dolomudstone/shale zone are petroliferous. If this oil was present in the dolostone that was replaced by Zebra limestone, its fate must be explained.
- Clasts of these dolostones that were incorporated into conglomerates of the Chinle Formation display seepage of oil into the surrounding rock (Labrado, 2021), demonstrating presence of oil in the dolostone clasts prior to the deposition of the Chinle Formation.

- Outcrops of the Chinle Formation located west of the Zebra limestone are fractured and display signs of bleaching, whereas those directly overlying the Zebra limestone do not (Figure 3).
- Vugs in the Zebra limestone do not show coating with dead oil.

The history of hydrocarbon generation and expulsion in the salt anticline province of the Paradox Basin, to which Gypsum Valley belongs, is complex. Onset of hydrocarbon generation was highly variable for the organic-rich source rocks (dolomudstones, often referred to as shales) within the Pennsylvanian strata, but generally started as early as Late Pennsylvanian closest to the Uncompahgre Uplift and migrated progressively westward, with earliest hydrocarbon expulsion starting in the Early Permian but locally possible as late as the Early Cretaceous (Rasmussen and Rasmussen, 2009). Based on oil generation and expulsion modeling by Rasmussen and Rasmussen (2009) for the Andy's Mesa Unit which is located at the north-eastern margin of Big Gypsum Valley, hydrocarbon genesis from the Chimney Rock source interval of the Paradox Formation may have started as early as 270.0 Ma (mid Permian), reaching peak generation and expulsion at 82.8 Ma (Late Cretaceous). This timing allows for hydrocarbon genesis in an interlayered dolostone/dolomudstone/shale package of the layered evaporite sequence, steeping of the dolostone in the oil, mobilization of the package during salt diapirism, and its accretion in the diapir cap prior to the breaching of the salt wall during Moenkopi or Chinle time. From this follows that Zebra limestone likely replaced a petroliferous dolostone. This is supported by observations in hand sample and thin section (see next section discussing H2), but also by the finding of illite, which implies that Zebra limestone replaced a precursor rock that experienced temperatures conducive for oil genesis in shales.

The timing between oil migration and Zebra limestone formation is difficult to constrain. The lack of coating with oil on vug surfaces indicates that after their formation, Zebra limestones were not exposed to oil migration. However, the lack of discoloration/bleaching of the rocks of the Chinle Formation in the burial wedge right above the Zebra limestone outcrops indicates absence of oil after its deposition during the Triassic, while there was oil migration through fractured rocks from the Chinle Formation to the west of the outcrop. Moreover, the observed red colors in some of the Zebra limestones is not caused by admixture of sands from the Chinle Formation, removing another potential constraint. Thus, in principle, it is possible that Zebra limestone formation took place anytime between Late Permian and the most recent exhumation of the diapir in the Quaternary. However, if a link between conversion from anhydrite to gypsum caprock and Zebra limestone genesis (H3) can be established, exhumation of the diapir and intense caprock formation during Moenkopi and/or Chinle time would be likely events to trigger that process.

HOW DOES 'SELF-CLEANING' EXPLAIN THE INVERSE DARK-LIGHT COLOR BANDING OF THE BRIDGE CANYON ZEBRA LIMESTONE?

A key observation made at the onset of this study is that for Zebra textures described in the literature, microcrystalline layers tend to be dark whereas coarse-crystalline layers tend to display light colors. This is inverse to the Zebra limestone fabrics from the study area. Thus, a model for Zebra limestone formation should not only describe a series of plausible replacement and deformation events, but also offer an explanation for the observed inverse color/crystal size pattern. My model suggests that petroliferous micritic dolostone is first replaced by petroliferous microcrystalline limestone, followed by the establishment of the Zebra limestones fabric. During

this second step 'self-cleaning' must be taking place, i.e., material that would result in a dark appearance – here referred to as 'impurities' – of the fine-crystalline portions of the Zebra limestone is removed. Thin section observations provide insight into how this happens, and it turns out that solid impurities behave different from mobile impurities.

Behavior of solid impurities (i.e., clays) during recrystallization

I observe a trend from a high content of impurities in calcite crystals seen in the dolostone samples to the lower content in Zebra limestone grains (Figure 41). For example, in the sample RNCZDOLO from Dolostone 2, impurities dominate the core of crystals which are encased by shale seams (Figure 33). Moving to sample RNDL2 from the Dark limestone there is a noticeable decrease in impurities, with the clay portions becoming concentrated in bands (Figure 34, *right*). This trend is continued in sample RNQZ from the Questionable Zebra outcrop, where clay-seamed stylolites are formed, with calcite crystals that contain some impurities predominantly on one side of the stylolite (Figure 31). On the opposite side of the stylolite, coarse crystals barely contain impurities any longer. The last stage in this succession is exemplified by the classic Zebra limestone, where sample RNCL1 shows no discernable impurities within the calcite crystals, but clay around them (Figure 26).

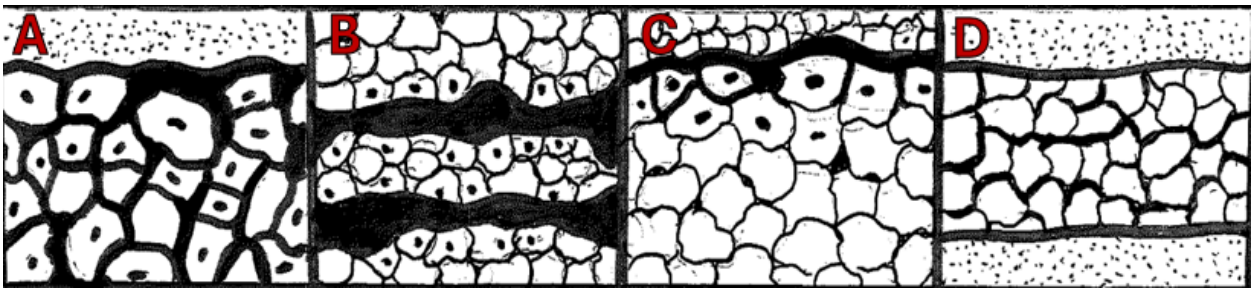

Figure 41: Trend of concentration of impurities
Step one (A), in sample RNCZDOLO impurities dominate the coarse crystals that are incased in shale. Step 2 (B) in sample RNDL2 clay starts to concentrate into bands. The coarse grains along the bands have impurities. Step 3 (C), in sample RNQZ clay filled stylolites are formed, fewer calcite crystals have impurities. Step 4 (D), in sample RNCL1 no impurities are seen in the grains, but there is clay around the coarser calcite crystals.

Behavior of mobile impurities (i.e., oil) during recrystallization

I observe a trend of oil moving away from fine-crystalline samples to space in between coarse crystals. Beginning with sample RNCZDOLO from Dolostone 1, I observe an initial stage where oil is present within the microcrystalline dolostone matrix, albeit more heavily concentrated within the coarse calcite crystals (Figure 33). Moving to sample RNQZ from the Questionable Zebra, I encounter a slightly more advanced stage, where displaced oil begins to occupy the spaces between the coarse crystals. In Zebra limestone D, represented by samples RNNZ1 and RNNZ2, I witness the accumulation of dead oil progressing further into stylolites (Figure A6). Here, the dead oil is observed within seams surrounding the coarser crystals. Lastly, in the classic Zebra limestone, exemplified by sample KLGP013, I reach the stage where oil is confined to narrow zones surrounding the coarse crystals, indicating a significant advancement in the migration process (Figure 25).

Origin of inverse dark-light Zebra banding

In a nutshell, the 'inverse' coloring of the Bridge Canyon Zebra limestones distills down to the observation that the original rock, the petroliferous micritic dolomudstone, contained only small amounts of solid accessory minerals, such as clays, but considerable amounts of mobile oil. During replacement and recrystallization, the clay minerals were concentrated in stylolites, the very same location the oil eventually relocated to, besides residing along crystal boundaries. This led to a self-cleaning of the microcrystalline portion of the Zebra rocks. On a much more coarse-crystalline scale, a similar process can be observed in several centimeter-thick veins in the carbonate caprock at Damon Mound, TX. These veins display a clear, sometimes slightly yellowish color, and contain considerable dead oil – which resides along crystal boundaries

(Labrado, 2021). The reason why the coarse-crystalline bands of the Bridge Canyon Zebra limestones tend to be rather dark finds its cause also in the presence of oil. During growth of the coarse crystals into the forming cavities, the presence of oil maintained a reducing environment, mobilizing ferric iron (Fe^{3+}) and incorporating it as ferrous iron (Fe^{2+}) into the calcite crystals. Later on, upon return to oxidative conditions, this iron became oxidized and formed iron oxides, with a darker color. The process of Zebra limestone formation has an internal and an external driver: internally, recrystallization is driven by the principles of Ostwald-ripening where larger crystals grow at the expense of smaller crystals (Morse and Casey, 1988). From a thermodynamic perspective, this principle is based on the fact that the surface to volume ratio of larger crystals is lower, whereby a crystal surface (essentially a 'defect' in the crystal) is at an energetically higher level than the interior, meaning that recrystallization and crystal growth lowers the overall energy, and thus is happening spontaneously. Unmixing of hydrophobic components of dead oil from the aqueous portion likely also contributes to lowering the overall energy of the system and was facilitated by the mobile nature of these fluids. The external component is stress, which promotes pressure solution (stylolitization) and fluid pressure, which promotes fracturing.

LINKS BETWEEN ANHYDRITE-GYPSUM CONVERSION, THE CARBONIC ACID SYSTEM, AND GENERATION OF ZEBRA LIMESTONE

The observations from Zebra limestone outcrops B and C indicate that the shale interval in between C and the gypsum was thicker than between B and the gypsum. This may also be the case for outcrop A which is in close proximity to B and the gypsum outcrop (Figure 42). The increase in regularity of banding with decreasing shale thickness indicates that potentially, there is a tie between anhydrite-gypsum transformation and Zebra limestone genesis.

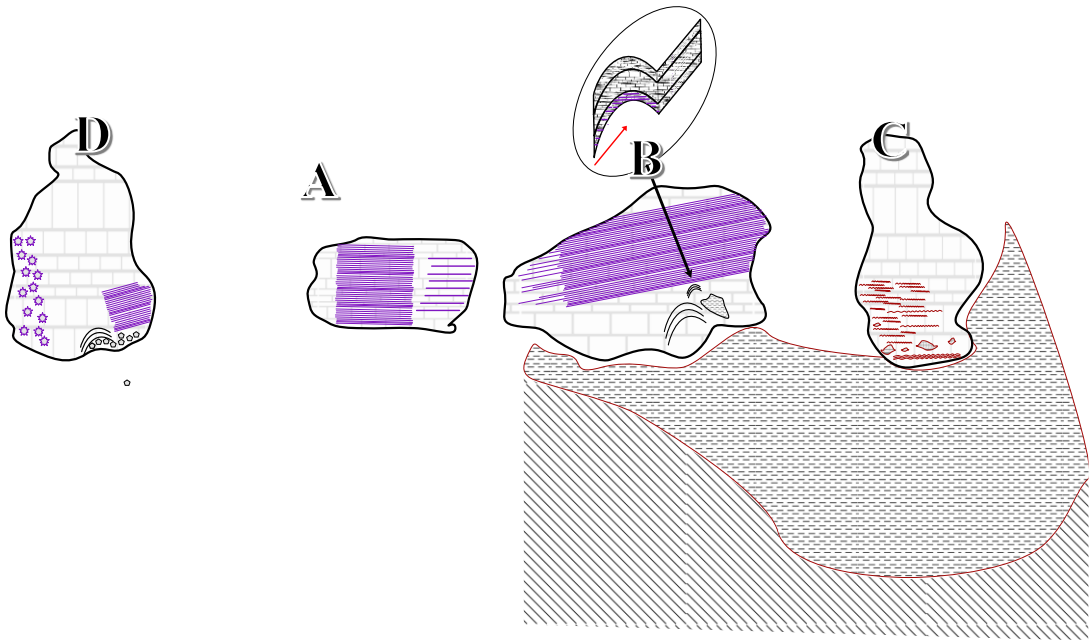

Figure 42: Zebra D, A, B and C fabrics and their proximity to shale
The shale interval (dashed) between Zebra limestone outcrop C and the gypsum (hatched) is thicker than that between Zebra limestone outcrop B and the gypsum. This likely extends to Zebra limestone outcrop A, which is near B. Zebra limestone outcrop D is farther away and the contact to the shale is not as clear. Most regular banding is observed in Zebra limestone outcrop A and B, implying a potential causal relationship between proximity of the limestone to the gypsum and thickness of the shale layer.

Replacement of evaporite minerals, particularly anhydrite to gypsum has previously been inferred to be associated with Zebra textures (Warren and Kempton, 1997; for a compilation of literature see Wallace and Hood, 2018). So far, no rigorous assessment of the process has been carried out, and most interpretations focused on the consequences of volume changes (i.e., change in pressure) during anhydrite-gypsum (in either direction) conversions. The chemical consequences have not been considered, but they are as fascinating as the intricacies of pressure/volume changes associated with anhydrite-gypsum conversions. Moreover, one aspect cannot be considered without the other because anhydrite-gypsum conversion (i.e., the equilibrium constant for the reaction) is governed by thermodynamics and solely depends on temperature, pressure, and the chemical activity of water. I tackle this topic by first investigating thermodynamic aspects, followed by an assessment of the consequences for the carbonic acid

system and carbonate minerals (calcite and dolomite), and third discussing the implications for pressure and stress. I then synthesize the insights and apply them to the study of Zebra limestone at the Bridge Canyon site.

Equilibrium constants, solubility and activity in anhydrite-gypsum conversion

Conversion of anhydrite to gypsum is described by the following chemical equilibrium equation

$$CaSO_4 + 2H_2O \Leftrightarrow CaSO_4 \cdot 2H_2O, \qquad \textit{Eq. 01}$$

where anhydrite ($CaSO_4$) and water (H_2O) are in equilibrium with gypsum ($CaSO_4 \cdot 2H_2O$). The equilibrium constant for this reaction is written as

$$K_{eq}^{anhydrite \Leftrightarrow gypsum}(P,T) = \frac{\{CaSO_4 \cdot 2H_2O\}}{\{CaSO_4\} \times \{H_2O\}^2}, \qquad \textit{Eq. 02}$$

where the terms in {} brackets refer to the activity of anhydrite, water, and gypsum at chemical equilibrium at a given pressure (P) and temperature (T). Colloquially, activities are sometimes referred as '*actual* concentrations' to express that while a chemical constituent 'A' can be present in a certain quantity (i.e., concentration), typically only a portion of that total presence of A can *actually* interact (i.e., react) with another constituent (e.g., 'B') in the studied system. This is because a significant portion of the constituent is already occupied by the presence of other constituents (e.g. 'C', 'D') that compete for the interaction with A.

An example for the impact of activity is the apparent higher solubility of gypsum in strong brines as compared to seawater, where a sixfold concentrated brine can dissolve more than twice the amount of gypsum at 25 ºC (Shaffer, 1967). The dissolution reaction is described as

$$CaSO_4 \cdot 2H_2O \Leftrightarrow Ca^{2+} + SO_4^{2-} + 2H_2O, \qquad \textit{Eq. 03}$$

where the ionic components of gypsum, calcium cations (Ca^{2+}) and sulfate anions (SO_4^{2-}) go into solution, facilitated by the polar nature of the angular water molecule. The equilibrium constant (i.e., the solubility product Sp_{gypsum}) for this reaction is written as

$$K_{eq^{gypsum \Leftrightarrow dissolved\ gypsum}}(P,T) = Sp_{gypsum}(P,T) = \frac{\{Ca^{2+}\} \times \{SO_4^{2-}\} \times \{H_2O\}^2}{\{CaSO_4 \cdot 2H_2O\}}. \qquad \textit{Eq. 04}$$

The terms in {} brackets refer to the activity of calcium cations, sulfate anions, water, and gypsum at chemical equilibrium (H_2O) at a given pressure (P) and temperature (T). It is critical to note that for any given temperature and pressure, the thermodynamic value of Sp_{gypsum} does not change in the presence of brine, such as elevated concentrations of sodium (Na^+) and chloride (Cl^-). Nevertheless, the observation of Shaffer (1967) holds true: more gypsum can be dissolved in the presence of sodium and chloride ions. Their presence 'distracts' a significant portion of calcium (attracted to chloride) and sulfate (attracted to sodium) in solution, which means that the highly saline solution can hold a much higher total concentration of calcium and sulfate, while their activities remain constant and controlled due to fixed solubility of gypsum (Eq. 04). Colloquially expressed, this means that sodium chloride distracts calcium and sulfate from reacting with each other, preventing the formation of new gypsum. Activities of pure phases (i.e., a region of material that is chemically uniform, physically distinct, and theoretically mechanically separable) are considered to be one (i.e., 100%, for example a pure mineral or pure water). For a more rigorous introduction to the concept of activities in the geological context please refer to designated textbooks (Krauskopf and Bird, 1994; Klein and Philpotts, 2016; Anderson, 2017). Analogous to gypsum, the dissolution reaction for anhydrite is described as

$$CaSO_4 \Leftrightarrow Ca^{2+} + SO_4^{2-}, \qquad \textit{Eq. 05}$$

where the ionic components of gypsum, calcium cations (Ca^{2+}) and sulfate anions (SO_4^{2-}) go into solution, facilitated by the polar nature of the angular water molecule. The equilibrium constant (i.e., the solubility product $Sp_{anhydrite}$) for this reaction is written as

$$K_{eq}^{\text{anhydrite}\Leftrightarrow\text{dissolved anhydrite}}(P,T) = Sp_{\text{anhydrite}}(P,T) = \frac{\{Ca^{2+}\}\times\{SO_4^{2-}\}}{\{CaSO_4\}}. \quad \textit{Eq. 06}$$

Considering anhydrite and gypsum as pure substances (i.e., their activities as one), Eq. 02, Eq. 04 and Eq. 06 become

$$K_{eq}^{\text{anhydrite}\Leftrightarrow\text{gypsum}}(P,T) = \frac{1}{1\times\{H_2O\}^2}, \quad \textit{Eq. 07}$$

$$Sp_{\text{gypsum}}(P,T) = \{Ca^{2+}\}\times\{SO_4^{2-}\}\times\{H_2O\}^2 \text{ and} \quad \textit{Eq. 08}$$

$$Sp_{\text{anhydrite}}(P,T) = \{Ca^{2+}\}\times\{SO_4^{2-}\}. \quad \textit{Eq. 09}$$

Combining Eq. 08 with Eq. 09 yields

$$Sp_{\text{gypsum}}(P,T) = Sp_{\text{anhydrite}}(P,T)\times\{H_2O\}^2 \text{ and} \quad \textit{Eq. 10}$$

solving Eq. 07 and Eq. 10 for the activity of water results in

$$\{H_2O\} = \sqrt{\frac{Sp_{\text{gypsum}}(P,T)}{Sp_{\text{anhydrite}}(P,T)}} = \sqrt{\frac{1}{K_{eq}^{\text{anhydrite}\Leftrightarrow\text{gypsum}}(P,T)}}. \quad \textit{Eq. 11}$$

The importance of this finding is that coexisting gypsum and anhydrite will keep the activity of water constant. For example, at 25 ºC, Sp_{gypsum} is ~$3.1*10^{-5}$, and $Sp_{anhydrite}$ is ~$4.9*10^{-5}$, yielding an activity of water of ~0.8 which is significantly less than the activity of 1 that is usually attributed to water. This not only explains the water-absorbing properties of commercial desiccants such as Drierite™ (calcium sulfate with a cobalt chloride indicator) but highlights that during the conversion of anhydrite to gypsum, the activity of water (i.e., its ability to keep ions in solution by lowering their activity thanks to its polar properties) is significantly lowered. Thus, water is not only removed by the conversion of anhydrite to gypsum (Eq. 01) yielding higher concentrations of dissolved constituents, but simultaneously, the activity of the remaining water is lowered,

further increasing the activity of the ions in solution and thus their propensity to react with other constituents, both ionic and solid.

Consequences for the carbonic acid system and carbonate minerals

Abiotic reactions involving carbonates and its two most common carbonate minerals, calcite ($CaCO_3$) and dolomite ($CaMg(CO_3)_2$) can be described by four equations. The first equation describes the speciation of inorganic carbon in an aqueous environment that allows for the presence of a gas phase (water vapor and carbon dioxide).

$$CO_{2(g)} + H_2O \Leftrightarrow CO_{2(aq)} + H_2O \Leftrightarrow H_2CO_3 \Leftrightarrow H^+ + HCO_3^- \Leftrightarrow 2H^+ + CO_3^{2-}\,, \qquad \textit{Eq. 12}$$

where in a fully reversible chain of reactions gaseous carbon dioxide ($CO_{2(g)}$) dissolves in water ($CO_{2(aq)}$), then reacts with water to from carbonic acid (H_2CO_3), which dissociates into an hydrogen cation (H^+, increases acidity, lowers pH) and bicarbonate (HCO_3^-), which further dissociates into another hydrogen cation (resulting in $2H^+$) and a carbonate ion (CO_3^{2-}). The second and third equations describe the dissolution/precipitation of calcite and dolomite at circum-pH-neutral conditions (i.e., bicarbonate being the dominate species in the carbonic acid system).

$$Ca^{2+} + 2HCO_3^- \Leftrightarrow CaCO_3 + CO_{2(g)} + H_2O \text{ and} \qquad \textit{Eq. 13}$$

$$Ca^{2+} + Mg^{2+} + 4HCO_3^- \Leftrightarrow CaMg(CO_3)_2 + 2CO_{2(g)} + 2H_2O\,. \qquad \textit{Eq. 14}$$

The implication of these reactions is that precipitation of calcite or dolomite yields water, which can be used in the conversion of anhydrite to gypsum (Eq. 01), i.e., water removal will drive the formation of the two minerals (an application of Le Chatelier's principle), but also increase the partial pressure of carbon dioxide. The fourth equation considers the reversible conversion of dolomite to calcite

$$Mg^{2+} + 2CaCO_3 \Leftrightarrow Ca^{2+} + CaMg(CO_3)_2\,, \qquad \textit{Eq. 15}$$

which shows that from a thermodynamic perspective, the presence/absence of dolomite relative to calcite (as pure substances with activities of one) depends on the ratio between the activities of calcium and magnesium in solution.

$$K_{eq}^{dolomite \Leftrightarrow calcite}(P,T) = \frac{\{CaMg(CO_3)_2\} \times \{Ca^{2+}\}}{\{CaCO_3\}^2 \times \{Mg^{2+}\}} = \frac{\{Ca^{2+}\}}{\{Mg^{2+}\}} . \quad \textit{Eq. 16}$$

These new insights can now be combined with a scenario in which a sodium bicarbonate ($Na^+ + HCO_3^-$) containing brine that is undersaturated with respect to anhydrite and gypsum comes into contact with the anhydrite cap of a salt diapir. The response of such a system would be the dissolution of anhydrite (Eq. 05) until gypsum saturation is reached (Eq. 04), followed by further conversion of anhydrite to gypsum (Eq. 01) until the activity of water decreases to equilibrium conditions (Eq. 11), inducing the precipitation of calcite and genesis of carbon dioxide (Eq. 13):

$$3CaSO_4 + 2H_2O + 2HCO_3^- + 2Na^+ \Longrightarrow CaCO_3 + CaSO_4 \cdot 2H_2O + 2SO_4^{2-} + Ca^{2+} + 2Na^+ + CO_{2(g)} .$$

Eq. 17

Dissolution of gypsum increases the $\{Ca^{2+}\}/\{Mg^{2+}\}$ ratio because it releases calcium ions and because sulfate complexes magnesium ions, lowering their activity, driving the replacement of dolomite with calcite, according to

$$3CaSO_4 + 2H_2O + 2HCO_3^- + 2Na^+ + CaMg(CO_3)_2 \Longrightarrow 3CaCO_3 + CaSO_4 \cdot 2H_2O + 2SO_4^{2-} + Mg^{2+} + 2Na^+ + CO_{2(g)} .$$

Eq. 18

These considerations demonstrate that the interaction of anhydrite caprock with fluids at the diapir margin will have the tendency to result in the conversion of anhydrite to gypsum, the dissolution of anhydrite/gypsum yielding calcium and sulfate, the precipitation of calcite, and the replacement of dolomite with calcite and yields CO_2 gas.

Implications for pressure, stress and strain and Zebra rock formation

In a spatially-confined system, mineral conversion, dissolution and precipitation, changes in speciation and concomitant changes in occupied volumes result in changes in pressures. While solids experience pressures as tensional (pull), shear (torsional stress is related to shear) and compressional stresses, liquids and gases experience/exert pressures uniformly. High differences between maximum (σ_1) and minimum principal stresses (σ_3) result in high maximum shear stresses ((σ_1 - σ_3)/2), whereby increasing fluid pressure shifts the stress state closer to the failure envelope (Mohr-Coulomb failure envelope, e.g., Yarushina et al., 2018), a concept that finds its application in hydraulic fracking of rocks. Due to the internal geochemical transformations and external forcing (e.g., drape-folding from diapir crest into a flanking position; Giles et al., 2012) salt diapir caprock systems are likely to experience rock deformation (folding and faulting) as well as pressure-induced mineral dissolution and the formation of stylolites. A critical component when considering such systems is the openness or closedness of the system in regard to fluids and gasses. An open system may favor mineral dissolution (reducing stress by volume decrease) whereas a closed system may result in the formation of fractures (elevating stress by volume increase). While a thorough exploration of these intricacies and their interplay is beyond the scope of this thesis, basic considerations of volume changes during chemical reactions provide critical initial insight. Such volume changes can be assessed by combining properties of constituents to calculate their molecular volume (Table 3).

This information can then be used to calculate relative volume changes for selected reactions. These calculations show that the transformation of anhydrite to gypsum yields a strong increase in occupied solid rock volume, and a minor decrease in total volume, creating a

hypothetical void (Table 4, Figure 43). For anhydrite and gypsum dissolution-driven dedolomitization, a decrease in both total and solid volume result.

Table 3: Assessment of occupied molar volume of constituents at standard conditions (25 ºC, 1 bar)

Constituent	Chemical formula	Molecular weight (g/mol)	Density at standard conditions (g/cm^3)	Volume per mol (cm^3/mol)
Water	H_2O	18	1	18.0
Anhydrite	$CaSO_4$	136	2.98	45.6
Gypsum	$CaSO_4 \cdot 2H_2O$	172	2.31	74.5
Calcite	$CaCO_3$	100	2.71	36.9
Dolomite	$CaMg(CO_3)_2$	184	2.84	64.8

Table 4: Mineral transformations and impact on volume (25 ºC, 1 bar)

Reaction	Chemical equation	Reactant volume normalized to mol Ca (cm^3/mol)	Water (vol %)	Anhydrite (vol %)	Gypsum (vol %)	Calcite (vol %)	Dolomite (vol %)	Product volume normalized to mol Ca (cm^3/mol)	Total relative volume change (vol %)	Relative volume change (%) w/o H_2O
Hydration of anhydrite	$CaSO_4+2H_2O \rightarrow CaSO_4 \bullet 2H_2O$	81.6	44	56	91[1]			74.5	-9	63
Anhydrite-dissolution driven dedolomitization	$CaSO_4+CaMg(CO_3)_2 \rightarrow Mg^{2+}+SO_4^{2-}+2CaCO_3$	55.2		41		67[2]	59	36.9	-33	n.a.
Gypsum-dissolution driven dedolomitization	$CaSO_4 \bullet 2H_2O+CaMg(CO_3)_2 \rightarrow Mg^{2+}+SO_4^{2-}+2CaCO_3+2H_2O$	69.6	26		53	53[3]	47	54.9	-21	-47

[1)] Note relative volume increase of solids (gypsum 91% relative to 65% for anhydrite)

[2)] Note relative volume decrease of solids (calcite 67% relative to 100% for combined anhydrite and dolomite)

[3)] Note relative volume decrease in solids (calcite 53% relative to 100% for combined gypsum and dolomite)

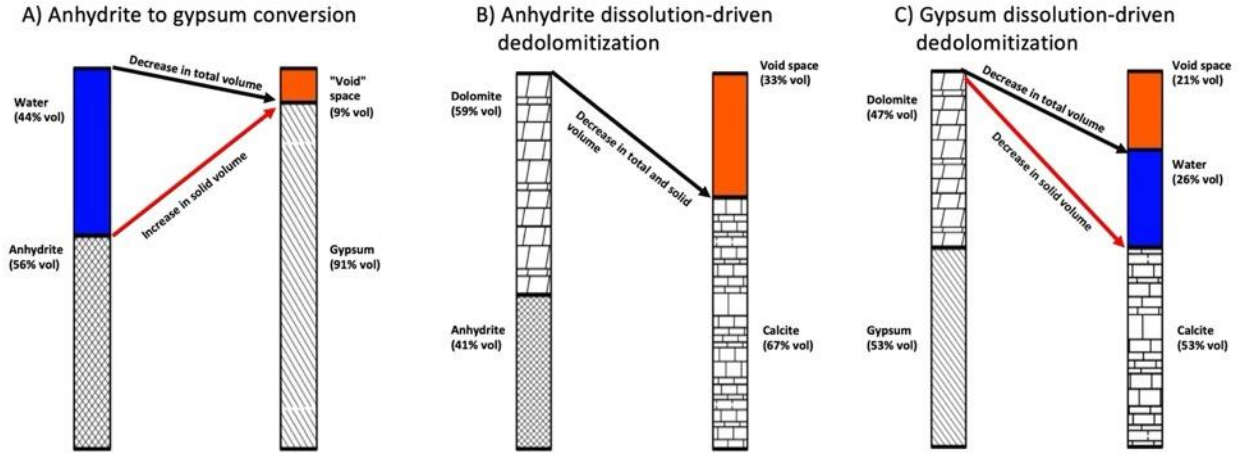

Figure 43: Changes in volume occupied by solids and liquids during mineral transformations
A) Anhydrite to gypsum conversion. B) Anhydrite dissolution-drive dedolomitization. C) Gypsum dissolution-driven dedolomitization.

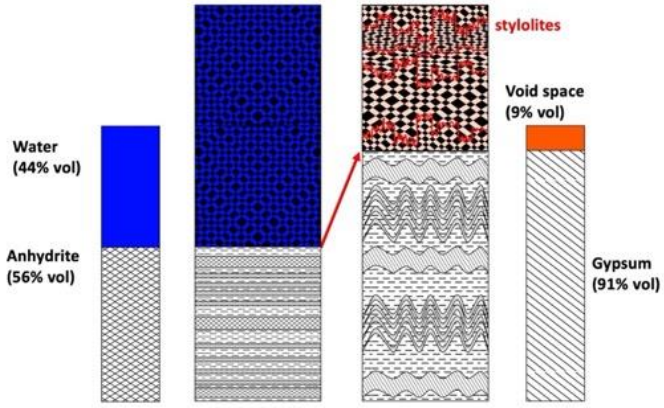

Figure 44: Interpretation of impact of anhydrite-gypsum transformation on structures
A more realistic depiction of the anhydrite-gypsum conversion including a porous rock that holds the water volume, and the impact of volume expansion on this rock. Gypsum will become internally folded, whereas the porous rock will be compacted, develop stylolites and mineral recrystallization is enhanced. A portion of the pore space initially occupied by water will be replaced by carbon dioxide gas.

These observations are critical for the understanding of the observations from the Bridge Canyon site. Conversion of layered anhydrite would have resulted in tight folding of the newly produced gypsum layers, displacing the diapir caprock margin upward (or lower margin downward if salt dissolution provided accommodation). Water would be drained from pore space in the overlying rocks, leaving void space for carbon dioxide produced during calcite precipitation (Eq. 13). The normal stress exerted by the swelling gypsum package may have been accommodated by mineral dissolution and recrystallization and potential formation of stylolites (Figure 44),

supported by the conversion of dolomite to calcite in response to calcium release from anhydrite/gypsum dissolution (Figure 43B, C).

Synthesis of anhydrite-gypsum transformation and Zebra limestone formation

It is plausible that anhydrite-gypsum transformation in the cap of the Gypsum Valley salt wall resulted in the observed features, namely tightly folded gypsum layers and dolostone replaced by Zebra limestone. Such a scenario invokes that at least intermittently, gypsum-undersaturated waters could reach the anhydrite, triggering the onset of a process that leads to gypsum swelling and folding, release of calcium ions that drive conversion of dolostone to limestone, build-up of pressure that favors recrystallization of calcite resulting in a zebra pattern that roughly parallels the margin of the gypsum package (i.e., normal to the stress induced by the swelling of the package due to internal folding), and providing carbon dioxide gas – and a concomitant pressure increase – that may have aided in the opening of void space that ultimately was occupied by the calcite cements that form the second type of Zebra banding. However, opening of pore space for the latter process and potential pressure dissolution driving calcite recrystallization are difficult to reconcile as simultaneously occurring processes. Instead, I propose that these processes alternate, and that this alternation causes the Zebra pattern. The anhydrite-gypsum transformation leads to solid volume expansion, closing fluid pathways that deliver water to the system and driving pressure-induced calcite recrystallization following the principles of Ostwald-ripening where larger crystals grow at the expense of smaller crystals (Morse and Casey, 1988). In the newly closed system water consumption by the anhydrite-gypsum conversion lowers the activity of water, inducing calcite precipitation and generation of carbon dioxide, resulting in an increase hydrostatic pressure, void formation, and ultimately re-opening of fluid pathways into the system, introducing new water that re-starts the cycle. This could result in a ‘lid on pan with boiling water’ situation, in which pressure

build-up creates repeated cycles of fracturing, mineral replacement and void formation, followed by cementation and sealing. Similar scenarios have been postulated previously in the discussion of Zebra patterns in caprock (Figure 45; Hallager et al., 1990; Brunner et al., 2019). The insights gained here corroborate those concepts and could point to commonalities in the mechanism for Zebra rocks at salt-diapir associated MVT type ore deposits.

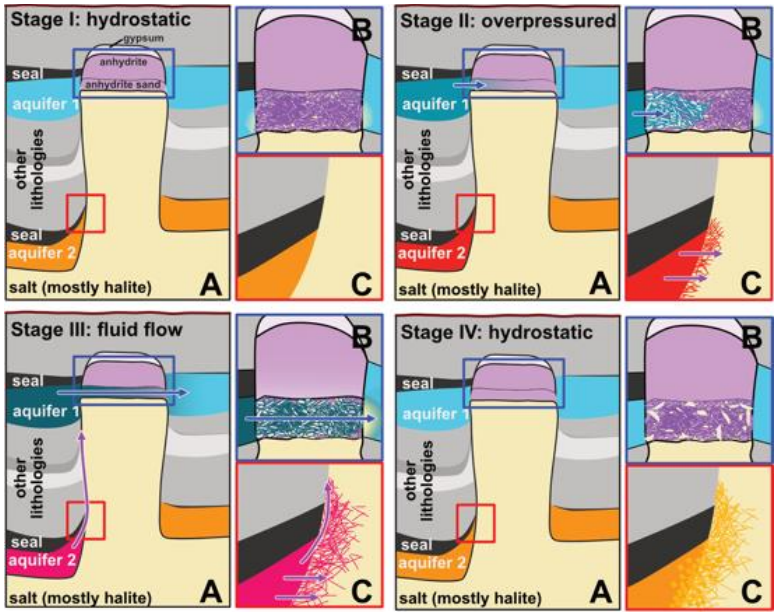

Figure 45: 'Lid on pan with boiling water' model: Four stages of fluid flow
Stage I and IV: hydrostatic regime; Stage II: overpressured aquifer 2 regime; Stage III: fluid flow regime with pressure reduction; A: overview of salt wall; B: caprock-salt contact; C: formation of fluid pathways at depth due to pressure increase. In regard to caprock formation and transformation events, the proposed episodic nature of sulfide precipitation during the accretion (underplating) of anhydrite (Hallager et al., 1990, Goldman's katatectic layers 1933, 1952, and the observation of anhydrite dissolution and re-precipitation by Walker, 1976), have a common denominator. They recognize that changes in fluid flow and composition may be responsible for banding of anhydrite caprock, for example, the opening and closure of fluid pathways. A 'lid on pan with boiling water model' consists of phases with fluid pressure build up in deep aquifers, those fluids finding escape pathways upward along the diapir margin, crossflow at the caprock-salt interface, and formation of new minerals that clog pathways, resulting in the next cycle of pressure build up.

Conclusions and Outlook

Genesis of Zebra limestone at the Bridge Canyon site

The formation of Zebra limestone at the Bridge Canyon site and its subsequent alterations are intimately linked to salt tectonics. The deposition of the Paradox Formation layered evaporite sequence included high sea level intervals during which organic rich shales, dolomudstones, and dolostones were deposited in a stagnant ocean margin basin (Hite and Buckner, 1981). Some of these dolostones would eventually become the lithology that was replaced by the Zebra limestones. During burial by younger portions of the Paradox Formation, the Honaker Trail Formation in the Pennsylvanian and the onset of the deposition of the Cutler Group in the Permian, the package of shales, dolomudstones, and dolostones reached temperatures conducive for oil and illite generation and were entrained in salt movement related to passive diapirism and formation of the Gypsum Valley salt wall. By the mid-Triassic (end Moenkopi time), during a time of extensive erosion across the Paradox Basin, the top of the salt diapir started to be exposed or at least came in contact with halite-undersaturated water, resulting in the formation of a caprock consisting both of accreted (underplated) packages of shales, dolomudstones, and dolostones as well as anhydrite caprock. Continued exhumation lowered temperatures and provided fresher, meteoric water to the diapir cap, initiating anhydrite-gypsum conversion. An associated increase in rock volume and release of calcium triggered replacement of dolostone with limestone and stylolitization perpendicular to gypsum expansion, but also build-up of hydrostatic pressure through release of carbon dioxide, favoring fracturing of rocks and void formation. Unlike solid accessories such as clay minerals that are encapsulated when their host rock is replaced, oil originally trapped in the dolostone remained mobile during the replacement with calcite, accumulating at stylolite seams. Those stylolite seams became the focus of fracturing during phases of volume expansion, and were

kept open due to fluid/gas overpressure, allowing for the growth of coarse dog tooth calcite crystals. Thanks to the expelled oil, conditions in those fluids were reducing, allowing for the mobility of reduced iron. Today, the light bands of Zebra limestone coincide with the fine-crystals replacement calcite that succeeded in 'self-cleaning' by expelling the oil, while the coarse-crystalline dark bands owe their color to iron oxides. Cyclic progress of anhydrite-gypsum conversion, pressure build-up and subsequent fracturing with concomitant pressure release and new inflow of meteoric water maintained the process of Zebra limestone formation, resulting in well-developed Zebra textures where the shale layer separating the carbonate rocks and the gypsum unit are thinnest.

During the late Triassic deposition of the Chinle Formation, the cap of the Gypsum Valley salt wall became fully exposed, the dolostone/dolomudstone/shale package was partially eroded with more resistant lithologies becoming embedded in the burial wedge of the Chinle Formation. Potentially, also Zebra limestones shared this fate, however, they are difficult to detect due to pervasive replacement of limestone clasts in conglomerates of the Chinle Formation (Labrado, 2021). The history of Zebra limestone continued to a next stage, in which acid fluids generated large voids. It is likely that these fluids utilized existing Zebra limestone void space. In limestone cave formation and karstification the main drivers are carbon dioxide and sulfuric acid (Havlena et al., 2023). The latter is often attributed to the presence of hydrocarbons that fuel microbial sulfate reduction and genesis of hydrogen sulfide, which is then oxidized to sulfuric acid. At Gypsum Valley, hydrocarbons were readily available as component of Zebra limestone or during hydrocarbon migration that bleached some of the Chinle outcrops to the west of the Zebra limestone outcrops, and there is plentiful sulfate in the form of gypsum. Nevertheless, a connection between the generation of the voids and presence of hydrocarbons remains speculative. Finely

laminated carbonate sediments with silt-sized crystals partially fill the voids and probably coincide with the formation of the karst. At a later stage, the very same voids became part of another fluid flow system, precipitating saddle dolomite (Figure 46).

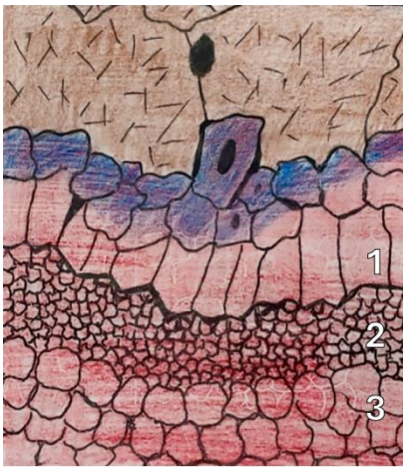

Figure 46: Karst features in 'All in one' Zebra (Outcrop C)
Infilled karst cavity, with saddle dolomite at the top is evident. Adjacent to the dolomite, subrounded calcite crystals exhibit red discoloration (iron oxide) and blue stains (ferrous iron, Fe^{2+}), signifying the presence of iron. Below these features, the karst was previously filled with three layers of finely laminated carbonate sediments, containing varying silt-sized crystals that partially occupy the voids. These sediment layers likely formed simultaneously or shortly after karstification.

IMPLICATIONS FOR THE UNDERSTANDING OF ZEBRA ROCK FORMATION AND FLUID FLOW AT DIAPIR MARGINS

This study proposes that Zebra limestone formation comprises both phases of compression and stylolithization and void formation by extension, driven by an external process (anhydrite-gypsum conversion) that for its continuation in turn depends on fracturing caused by extension for its resupply with meteoric water. While the precise circumstances of this intricate, cyclic relationship likely cannot by applied to other Zebra type rocks, the underlying principle can. It demonstrates a need for external forcing and cyclicity, but also demonstrates that two opposing schools of thought, one emphasizing compression and the other extension, can be reconciled. This work also highlights that to arrive to a satisfactory answer on the topic of Zebra rock formation, field work, petrography, structural analysis, geochemistry and thermodynamics must be combined.

Moreover, it is also shown that counter-intuitive patterns, such as the apparently reversed color banding of Zebra limestone can provide new insights into a seemingly well-studied topic.

Caprock of salt diapir is accepted as one of the best archives of the temperature and fluid history linked to salt tectonics, but if it would need one example for why this is the case, Zebra limestone could serve as such. It not only records the earliest phase of oil generation at that location, but also diapir exhumation, caprock transformation, karstification, and hydrothermal fluid flow – all happening in the critical zone between salt diapir that is considered an almost perfect seal, and outlying strata that may serve as reservoir rocks for hydrocarbons, or the long-term storage of carbon dioxide.

Finally, the proposed process for Zebra limestone genesis has the potential to release carbon dioxide, which would constitute a so far unquantified emission and effectively changes water chemistry. The resulting increase of the relative amount of magnesium and sulfate in solution, which in the effluent may shift the balance toward dolomite precipitation, could thus influence carbonate chemistry downstream of exposed or shallowly buried diapirs.

OUTLOOK/FUTURE WORK

While this project adds new insight into the riddle of Zebra rock formation, it is important to acknowledge it also raises new questions, and that still much work needs to be done.

To better assess a potential link between anhydrite-gypsum conversion and the formation of Zebra fabrics more structural data are needed. While the folding at the base of the Chinle burial wedge has been documented (McFarland, 2016) no systematic analyses of those folds and the folds in carbonates outcrops in the poorly outcropping zone has been carried out. The reason for this is that no systematic pattern was expected for a dolostone/dolomudstone/shale/evaporite unit that was heavily deformed during its transport and accretion and the cap of a salt diapir and then

subsequently experienced further deformation during the emplacement of the Chinle burial wedge. Now, the expected inhomogeneity of structural measurements may be in stark contrast to a set of well-ordered structures caused by the expansion of the underling anhydrite-gypsum caprock, making the effort worthwhile.

Secondly, the proposed mechanism for Zebra limestone is qualitative and has only been assessed at ambient temperature and pressure. Integration into a numerical geochemical reaction-transport model that allows for fractures to develop would provide a critical test for proposed scenario and could serve as a template for other studies investigating Zebra -rock formation. Third, the model proposed here suggest replacement of a microcrystalline dolostone with calcite almost equal in size. Mimetic (grain-by-grain) replacement of aragonite and calcite by dolomite has been reported in the literature (Braithwaite, 1991; Zempolich and Baker, 1993), however, a cursory search of Google Scholar did not yield similar results for the reverse process. Notably, Zebra limestone has previously been mentioned in the context of salt diapirs form the U.S. Gulf Coast (Posey and Kyle, 1988), where there is no evidence for dolostone precursors in the caprock. A more thorough literature study may provide insight on these issues.

Finally, on the larger scale of the understanding of salt tectonics and hydrocarbon genesis in Gypsum Valley and in the Paradox basin, the interpretation of the poorly outcropping dolostone/dolomudstone/shale zone as an inclusion from the layered evaporite sequence that has been accreted in the cap of the salt diapir poses at two challenges. The first challenge is that the very same type of lithology appears to outcrop below the Chinle burial wedge along the northern salt wall flank from almost Hamm Canyon all the way to the Nubbin site, covering a distance of ~12 km (Brunner et al., 2019). This continuity has been used as an argument this cannot be a ‘typical’ inclusion that should be deformed to a degree that such a continuity is not given. The

second challenge is that for hydrocarbons (and illite) to be present in the dolostone, a certain temperature threshold (burial) must be reached, but the same rock package must also be allowed to travel with the salt to the diapir top, removing it from the heat source – a scenario that is further complicated by the fact that salt effectively conducts heat, which like a chimney has both a cooling (at depth) and heating effect (near surface). In other words: the Gypsum Valley salt wall will continue to provide curious minds with exciting riddles.

References

Anderson, G., 2017, Thermodynamics of Natural Systems: Theory and Applications in Geochemistry and Environmental Science: Cambridge, Cambridge University Press, doi:10.1017/9781316796856.

Anikina, E.Yu., and Bortnikov, N.S., 2020, Banded and Rhythmically Zoned Carbonate Veins of the Ag–Pb–Zn Prognoz Depozit (Sakha–Yakutia, Russia): A Result of Self-Organizing Processes: Doklady Earth Sciences, v. 495, p. 894–900, doi:10.1134/S1028334X2012003X.

Bao, H., 2006, Purifying Barite for Oxygen Isotope Measurement by Dissolution and Reprecipitation in a Chelating Solution: Analytical Chemistry, v. 78, p. 304–309, doi:10.1021/ac051568z.

Beales, F.W., and Hardy, J.L., 1980, Criteria for the recognition of diverse dolomite types with an emphasis on studies on host rocks for Mississippi Valley Type ore deposits: SEPM Special Publication, v. 28, p. 197–213.

Bejaoui, J., Bouhlel, S., Sellami, A., and Braham, A., 2014, Geology, mineralogy and fluid inclusion study of Oued Jebs Pb–Zn–Sr deposit; comparison with the Bou Grine deposit (diapirs zone, Tunisian atlas): Arabian Journal of Geosciences, v. 7, p. 2483–2497, doi:10.1007/s12517-013-0942-1.

Bodine, M., 1985, Clay Mineralogy of Insoluble Residues in Marine Evaporites, in p. 133–156, https://pubs.er.usgs.gov/publication/70012897 (accessed December 2020).

Bouhlel, S., Garnit, H., Leach, D.L., Lehmann, B., van den Kerkhof, A., Beaudoin, G., and Schmidt, S., 2024, The Bougrine Zn-Pb deposit, the largest salt diapir-related Mississippi

Valley-type deposit in the Eastern Maghreb salt diapir province, Tunisia: Ore Geology Reviews, v. 164, p. 105825, doi:10.1016/j.oregeorev.2023.105825.

Bouhlel, S., Johnson, C.A., and Leach, D.L., 2007, The peridiapiric-type Pb-Zn deposit at Fedj el Adoum, Tunisia: geology, petrography, and stable isotopes:

Braithwaite, C.J.R., 1991, Dolomites, a review of origins, geometry and textures: Earth and Environmental Science Transactions of The Royal Society of Edinburgh, v. 82, p. 99–112, doi:10.1017/S0263593300007586.

Brunner, B. et al., 2019, Synthesizing old questions with new developments in caprock research: is it time to abandon well-trodden paths? Gulf Coast Section SEPM Publication, v. Perkins-Rosen Research Conference.

Coward, A.J., Slim, A.C., Brugger, J., Wilson, S., Williams, T., Pillans, B., and Maksimenko, A., 2023, Mineralogy and geochemistry of pattern formation in zebra rock from the East Kimberley, Australia: Chemical Geology, v. 622, p. 121336, doi:10.1016/j.chemgeo.2023.121336.

Dickson, J. a. D., 1966, Carbonate identification and genesis as revealed by staining: Journal of Sedimentary Research, v. 36, p. 491–505, doi:10.1306/74D714F6-2B21-11D7-8648000102C1865D.

Diehl, S.F., Hofstra, A.H., Koenig, A.E., Emsbo, P., Christiansen, W., and Johnson, C., 2010, Hydrothermal Zebra Dolomite in the Great Basin, Nevada—Attributes and Relation to Paleozoic Stratigraphy, Tectonics, and Ore Deposits: Geosphere, v. 6, p. 663–690, doi:10.1130/GES00530.1.

Dill, H.G., Nolte, N., and Hansen, B.T., 2014, Lithology, mineralogy and geochemical characterizations of sediment-hosted Sr–F deposits in the eastern Neo-Tethyan region – With special reference to evaporation and halokinesis in Tunisia: Journal of African Earth Sciences, v. 92, p. 76–96, doi:10.1016/j.jafrearsci.2014.01.009.

Dunham, R.J., 1962, Classification of Carbonate Rocks According to Depositional Textures: v. 38, p. 108–121.

Escosa, F.O., Rowan, M.G., Giles, K.A., Deatrick, K.T., Mast, A.M., Langford, R.P., Hearon IV, T.E., and Roca, E., 2019, Lateral terminations of salt walls and megaflaps: An example from Gypsum Valley Diapir, Paradox Basin, Colorado, USA: Basin Research, v. 31, p. 191–212, doi:10.1111/bre.12316.

Flügel, E., 2004, 5.1.5 Birdseye, Fenestral Fabrics and Stromatactis, in Microfacies of Carbonate Rocks, Springer, p. 190–197.

Folk, R.L., 1962, Spectral Subdivision of Limestone Types: v. 38, p. 62–84.

Giles, K., Lawton, T.F., Shock, A., Kernen, R., Hearon IV, T.E., and Rowan, M., 2012, A Halokinetic Drape-Fold Model for Caprock in Diapir-Flanking and Subsalt Positions: Search and Discovery Article #40956, p. 29.

Goldman, M.I., 1933, Origin of the anhydrite cap rock of American salt domes: US Government Printing Office.

Goldman, M.I., 1952, Deformation, Metamorphism, and Mineralization in Gypsum-anhydrite Cap Rock Sulphur Salt Dome, Louisiana: Geological Society of America, v. 50.

Hallager, W.S., Ulrich, M.R., Kyle, J.R., Price, P.E., and Gose, W.A., 1990, Evidence for episodic basin dewatering in salt-dome cap rocks: Geology, v. 18, p. 716–719, doi:10.1130/0091-7613(1990)018<0716:EFEBDI>2.3.CO;2.

Havlena, Z.E., Hose, L.D., DuChene, H.R., Baker, G.M., Powell, D., Labrado, A.L., Brunner, B., and Jones, D.S., 2023, Origin and modern microbial ecology of secondary mineral deposits in Lehman Caves, Great Basin National Park, NV, USA: bioRxiv, doi:10.1101/2023.08.15.553329.

Heness, E.A., 2016, Salt tectonic controls on facies and sequence stratigraphy of the Triassic Chinle Formation, Gypsum Valley Salt Wall, Colorado [M.S.]: The University of Texas at El Paso, 156 p., M.S. Thesis, The University of Texas at El Paso.

Hite, R.J., 1960, Stratigraphy of the Saline Facies of the Paradox Member of the Hermosa Formation of Southeastern Utah and Southwestern Colorado: USGS report, p. 17.

Hite, R.J., and Buckner, D.H., 1981, Stratigraphic Correlations, Facies Concepts, and Cyclicity in Pennsylvanian Rocks of the Paradox Basin:, http://archives.datapages.com/data/rmag/ParaBasin81/hite.htm?aoai=bfz8PQ2zNc1v5uYWwJVsmqrdT7CmzwIOajMWZk84VLcwF%2Fj%2Fl6GvbzDUbHYOAQya (accessed February 2021).

Kawahara, H., Yoshida, H., Yamamoto, K., Katsuta, N., Nishimoto, S., Umemura, A., and Kuma, R., 2022, Hydrothermal formation of Fe-oxide bands in zebra rocks from northern Western Australia: Chemical Geology, v. 590, p. 120699, doi:10.1016/j.chemgeo.2021.120699.

Kelka, U., Veveakis, M., Koehn, D., and Beaudoin, N., 2017, Zebra rocks: compaction waves create ore deposits: Scientific Reports, v. 7, p. 14260, doi:10.1038/s41598-017-14541-3.

Klein, C., and Philpotts, A., 2016, Earth Materials: Introduction to Mineralogy and Petrology: Cambridge, Cambridge University Press, doi:10.1017/9781316652909.

Krauskopf, K.B., and Bird, D.K., 1994, Introduction to Geochemistry: McGaw-Hill College, 640 p.

Kukla, P.A., Urai, J., and Strozyk, F., 2019, New Frontiers in Salt Research, in 2019 AAPG Annual Convention and Exhibition, San Antonio, Texas, AAPG, v. Search and Discovery Article #80706, p. 27, doi:10.1306/80706Kukla2019.

Labrado, A.L., 2021, Geological Problems with Microbiological Solutions: Deciphering the Authigenesis of Calcite, Dolomite, and Native Sulfur in Salty Environments [Ph.D.]: The University of Texas at El Paso, 326 p., http://0-search.proquest.com.lib.utep.edu/dissertations-theses/geological-problems-with-microbiological/docview/2546079021/se-2?accountid=7121.

Langford, R.P., Giles, K.A., Rowan, M.G., McFarland, J., Heness, L., Lankford-Bravo, D., Thompson Jobe, J., Soltero, A., and Bailey, C., 2022, Burial wedges—Evidence for prolonged progressive burial of the Paradox Basin salt walls—With a detailed example from Gypsum Valley, Colorado: Basin Research, v. 34, p. 1244–1267, doi:10.1111/bre.12658.

Lerer, K., 2017, Gypsum, Calcite, and Dolomite Caprock Fabrics and Geochemistry from the Gypsum Valley Salt Diapir, Paradox Basin, Southwestern Colorado [M.S.]: The University of Texas at El Paso, 177 p., https://search.proquest.com/docview/2008155128/abstract/3A2E93E346B34F1CPQ/1 (accessed April 2019).

Mack, J., and Endemann, B., 2010, Making carbon dioxide sequestration feasible: Toward federal regulation of CO2 sequestration pipelines: Energy Policy, v. 38, p. 735–743, doi:10.1016/j.enpol.2009.10.018.

Małachowska, A., Łukasik, N., Mioduska, J., and Gębicki, J., 2022, Hydrogen Storage in Geological Formations—The Potential of Salt Caverns: Energies, v. 15, p. 5038, doi:10.3390/en15145038.

Masson-Delmotte, V. et al. (Eds.), 2021, Climate Change 2021: The Physical Science Basis. Contribution of Working Group I to the Sixth Assessment Report of the Intergovernmental Panel on Climate Change: Cambridge, United Kingdom and New York, NY, USA, Cambridge University Press, doi:10.1017/9781009157896.

McFarland, J.C., 2016, Structural and stratigraphic development of a salt-diapir shoulder, Gypsum Valley, Colorado [MS Thesis]: The University of Texas at El Paso, 93 p.

Merino, E., Canals, A., and Fletcher, R.C., 2006, Genesis of self-organized zebra textures in burial dolomites: Displacive veins, induced stress, and dolomitization: Geologica Acta, p. 11.

Morrow, D.W., 2014, Zebra and boxwork fabrics in hydrothermal dolomites of northern Canada: Indicators for dilational fracturing, dissolution or in situ replacement? Sedimentology, v. 61, p. 915–951.

Morse, J.W., and Casey, W.H., 1988, Ostwald processes and mineral paragenesis in sediments: American Journal of Science, v. 288, p. 537–560.

Nuccio, V.F., and Condon, S.M., 1996, Burial and Thermal History of the Paradox Basin, Utah and Colorado, and Petroleum Potential of the Middle Pennsylvanian Paradox Formation: U.S. Geological Survey Bulletin 2000-O, p. 47.

Park, C., Kim, N., Choi, S.-J., and Song, Y., 2020, Mg-Phengite in Carbonate Rock Syngenetically Formed from Hydrothermal Fluid: Micro-Textural Evidence and Mineral Chemistry: Minerals, v. 10, p. 668, doi:10.3390/min10080668.

Perrin, C., Prestimonaco, L., Servelle, G., Tilhac, R., Maury, M., and Cabrol, P., 2014, Aragonite–Calcite Speleothems: Identifying Original and Diagenetic Features: Journal of Sedimentary Research, v. 84, p. 245–269, doi:10.2110/jsr.2014.17.

Pevear, D.R., 1999, Illite and hydrocarbon exploration: Proceedings of the National Academy of Sciences, v. 96, p. 3440–3446, doi:10.1073/pnas.96.7.3440.

Posey, H.H., and Kyle, J.R., 1988, Fluid-rock interactions in the salt dome environment: An introduction and review: Chemical Geology, v. 74, p. 1–24, doi:10.1016/0009-2541(88)90143-X.

Puchtler, H., Meloan, S.N., and Terry, M.S., 1969, On the history and mechanism of Alizarin and Alizarin Red S stains for calcium: Journal of Histochemistry and Cytochemistry, v. 17, p. 110–124, doi:10.1177/17.2.110.

Quijada, I.E., Suarez-Gonzalez, P., Benito, M.I., Lugli, S., and Mas, R., 2014, From carbonate–sulphate interbeds to carbonate breccias: The role of tectonic deformation and diagenetic processes (Cameros Basin, Lower Cretaceous, N Spain): Sedimentary Geology, v. 312, p. 76–93, doi:10.1016/j.sedgeo.2014.07.006.

Ramsay, J.G., 1980, The crack–seal mechanism of rock deformation: Nature, v. 284, p. 135–139, doi:10.1038/284135a0.

Rasmussen, L., and Rasmussen, D.L., 2009, Burial History Analysis of the Pennsylvanian Petroleum System in the Deep Paradox Basin Fold and Fault Belt, Colorado and Utah: The

Paradox Basin Revisited – New Developments in Petroleum Systems and Basin Analysis, p. 24–94.

Ross Jr, R.J., Jaanusson, V., and Friedman, I., 1975, Lithology and origin of Middle Ordovician calcareous mudmound at Meiklejohn Peak, southern Nevada: U.S. Govt. Print. Off., 871, doi:10.3133/pp871.

Sass-Gustkiewicz, M., and Mochnacka, K., 1994, Genesis of Sphalerite Rhythmites from the Upper-Silesian Zinc-Lead Deposits — A Discussion, in Fontboté, L. and Boni, M. eds., Sediment-Hosted Zn-Pb Ores, Berlin, Heidelberg, Springer, Special Publication of the Society for Geology Applied to Mineral Deposits, p. 219–227, doi:10.1007/978-3-662-03054-7_13.

Stevenson, G.M., and Baars, D.L., 1986, The Paradox: A Pull-Apart Basin of Pennsylvanian Age: Part IV. Southern Rocky Mountains: v. 155, p. 513–539.

Thompson Jobe, J.A., Giles, K.A., Hearon, T.E., Rowan, M.G., Trudgill, B., Gannaway Dalton, C.E., and Jobe, Z.R., 2020, Controls on the structural and stratigraphic evolution of the megaflap-bearing Sinbad Valley salt wall, NE Paradox Basin, SW Colorado: Geosphere, v. 16, p. 297–328, doi:10.1130/GES02089.1.

Trudgill, B.D., 2011, Evolution of salt structures in the northern Paradox Basin: controls on evaporite deposition, salt wall growth and supra-salt stratigraphic architecture: Basin Research, v. 23, p. 208–238, doi:https://doi.org/10.1111/j.1365-2117.2010.00478.x.

Trudgill, B.D., and Arbuckle, W.C., 2009, Reservoir characterization of clastic cycle sequences in the Paradox Formation of the Hermosa Group, Paradox Basin, Utah: Utah Geological Survey, Open-File Report, v. 543, 153 p., doi:10.34191/OFR-543.

Wallace, M.W., and Hood, A. v. S., 2018, Zebra textures in carbonate rocks: Fractures produced by the force of crystallization during mineral replacement: Sedimentary Geology, v. 368, p. 58–67, doi:10.1016/j.sedgeo.2018.03.009.

Walker, C.W., 1976, Origin of Gulf Coast Salt-Dome Cap Rock: Geologic Notes: AAPG Bulletin, v. 60, p. 2162–2166.

Warren, J.K., and Kempton, R.H., 1997, Evaporite Sedimentology and the Origin of Evaporite-Associated Mississippi Valley-Type Sulfides in the Cadjebut Mine Area, Lennard Shelf, Canning Basin, Western Australia, in Montanez, I.P., Gregg, J.M., and Shelton, K.L. eds., Basin-Wide Diagenetic Patterns: Integrated Petrologic, Geochemical, and Hydrologic Considerations, SEPM Society for Sedimentary Geology, v. 57, p. 0, doi:10.2110/pec.97.57.0183.

Woelfel, M.C., 2023, Paradox Diapir Inclusions as a Window Into Diapiric Processes in Proximity to the Uncompahgre Uplift and the Early History of the Paradox Basin, Utah and Colorado [M.S.]: The University of Texas at El Paso, 165 p., https://www.proquest.com/docview/2861041938/abstract/EF844D678201483DPQ/2 (accessed April 2024).

Yarushina, V., Van, N.R., Wangen, M., and Skurtveit, E., 2018, Potential leakage mechanisms and their relevance to CO2 storage site risk assessment and safe operations: FME SUCCESS Synthesis Report, v. 2.

Zempolich, W.G., and Baker, P.A., 1993, Experimental and natural mimetic dolomitization of aragonite ooids: Journal of Sedimentary Research, v. 63, p. 596–606, doi:10.1306/D4267B86-2B26-11D7-8648000102C1865D.

Zhu, H., Zhong, D., Yao, J., Sun, H., Niu, X., Liang, X., You, Y., and Li, X., 2015, Alkaline diagenesis and its effects on reservoir porosity: A case study of Upper Triassic Chang 7 Member tight sandstone in Ordos Basin, NW China: Petroleum Exploration and Development, v. 42, p. 56–65, doi:10.1016/S1876-3804(15)60006-4.

Vita

Rebecca Navarrette was born in the New Mexican town of Santa Fe. While being a New Mexico native, Rebecca considers herself a proud Texan, having rooted most of her life in El Paso, Texas. As the oldest of four, she has a natural disposition to lead and help those around her. After graduating in the top 10% of her class from Horizon High School, Rebecca received the Presidential Scholarship from UTEP thus beginning a journey to receiving her degrees.

Rebecca's undergraduate journey was not linear. After two semesters, life intervened, introducing a new member who later became her biggest motivation. After a 3-year break, with no major in mind, Rebecca decided to finish her degree. Although geology was never a prominent thought, when she discovered the world of rocks and minerals, she never looked back.

During her time at UTEP, Rebecca, received scholarships, grants, and funds from the Lucille T. Stevens Estate Fund, Emil Jay Dittmer Memorial Scholarship, Jim & Karen Handschy scholarship, SWS AAPG, WTGS, SIPES, ITS-SSIRC, empowering her to finish this journey. She also participated in organizing the DEERS annual colloquium as a field trip coordinator, and event planner. Upon undergraduate graduation, Rebecca was named Outstanding Senior for her work ethic in geology. Wanting to push herself even further, Rebecca decided to pursue her Master's in Geological Sciences. In the Fall of 2022, she started the fast-track program, catapulting her into the final steps of her academic voyage. Throughout all this, Rebecca worked full-time, sometimes with two jobs, while finishing her two degrees. She is an unshakable force both professionally and personally. Rebecca's research focused on Zebra limestones in Gypsum Valley, Colorado. She tackled the enigma of Zebra limestone with enthusiasm and grace, showcasing her passion and commitment to advancing our understanding of Zebra rocks.

Contact Information: Rebeccan.136@gmail.com